LYOTROPIC LIQUID CRYSTALLINE (LLC) PHOSPHORIC ACID-10-LAURYL ETHER: MESOPHASES, PROTON CONDUCTIVITY AND SYNTHESIS OF TRANSPARENT MESOPOROUS HYDROXYAPATITE THIN FILMS

A DISSERTION SUBMITTED TO

THE DEPARTMENT OF CHEMISTRY

AND

THE GRADUATE SCHOOL OF ENGINEERING AND SCIENCE

OF

BİLKENT UNIVERSITY

IN PARTIAL FULFILLMENT OF THE REQUIREMENTS

FOR THE DEGREE OF

MASTER OF SCIENCE

By

Ebrima Tunkara

June 2014

I certify that I have read this thesis and have found that it is fully adequate, in scope and in quality, as a thesis for the degree of Master of Science.

_____

Prof. Dr. Ömer Dağ (Advisor)

I certify that I have read this thesis and have found that it is fully adequate, in scope and in quality, as a thesis for the degree of Master of Science.

_____

Assoc. Prof. Dr. Margarita Kantcheva (Examining Committee Member)

I certify that I have read this thesis and have found that it is fully adequate, in scope and in quality, as a thesis for the degree of Master of Science.

_____

Assist. Prof. Dr. Coşkun Kocabaş (Examining Committee Member)

Approved for the Graduate School of Engineering and Science:

_____

Prof. Dr. Levent Onural

Director of the Graduate School

ABSTRACT

LYOTROPIC LIQUID CRYSTALLINE (LLC) PHOSPHORIC ACID-10-LAURYL ETHER: MESOPHASES, PROTON CONDUCTIVITY AND SYNTHESIS OF TRANSPARENT MESOPOROUS HYDROXYAPATITE THIN FILMS

EBRIMA TUNKARA

M.Sc in Chemistry

Supervisor: Prof. Dr. Ömer Dağ

June 2014

Many salts, acids, and bases with low deliquescence relative humidity (DRH) can organize non-ionic surfactants into lyotropic liquid crystalline (LLC) mesophases that form a ready platform for the synthesis of mesoporous materials. In this study, we show that phosphoric acid (H_3PO_4, PA) with low DRH value can also be used as a solvent in assembling non-ionic surfactant ($C_{12}H_{25}(OCH_2CH_2)_{10}OH$, $C_{12}EO_{10}$) into stable LLC mesophases within a broad range of composition (the concentration can be as high as 20 PA/$C_{12}EO_{10}$ mole ratio).

The PA/$C_{12}EO_{10}$ mesophase is bi-continuous cubic phase (V_1) in extremely low concentrations (2 PA/$C_{12}EO_{10}$ mole ratio), 2D/3D hexagonal phases (H_1) at moderate compositions (3 to 5 PA/$C_{12}EO_{10}$ mole ratio) and micelle cubic (I_1) at high, (more than 5) H_3PO_4/$C_{12}EO_{10}$ mole ratios, with a typical unit cell parameter of 127, 55, and 116 Å, respectively. The mesophases of the lower concentrated samples (less than 15 mole ratio) have high thermal stability, with melting points greater than 120 ^oC. However the melting point drops to less than 50 ^oC for extremely high concentrations (more than 17 PA/$C_{12}EO_{10}$ mole ratio). The LLC mesophases were also found to exhibit high proton conductivities (~10^{-3} S/cm) at room temperature. The proton conductivities were even higher (10^{-2} S/cm) at some elevated temperatures and reduced to (10^{-4} S/cm) at temperatures less than 0^oC. The conductivity in the cubic phase is slightly higher. Both the temperature and composition-dependent conductivity obey the most accepted proton conductivity mechanisms: Grotthuss and Vehicle.

We went further to show that the combination of H_3PO_4 and another low DRH species, such as $Ca(NO_3)_2 \cdot 4H_2O$ also form stable mesophases; without precipitating salts, under a wide range of concentration, from 5.3/1 to 13.3/1 precursor to surfactant ratio. High acidity stabilizes both the aqueous solution as well as the LLC phases. The clear solutions obtained from the precursor-surfactant mixtures were spin coated on glass substrates (as thin as a few hundred nanometers) and calcined to form transparent nano-size mesoporous hydroxyapatite (HAp) thin films. The formation of semi-crystalline HAp in our synthetic approach is not a straight forward process; it involves the formation of some intermediate products and also requires a calcination temperature of at least 300 ^oC. The formation, which starts at 300 ^oC, is preceded by the evaporation of nitric acid and excess water molecules to the surrounding. The crystallization continues at 400 ^oC and completes at 500 ^oC, keeping the uniformity, porosity, and transparency of the films. Films of the 5.3/1 ratio,

calcined at 300 ^{o}C have high surface area of up to 96 m^2/g, which dropped down to 20 m^2/g at 500 ^{o}C. The mesopores start collapsing at around 600 ^{o}C. The pore size, pore walls, and the pore volumes were obtained from the N_2 sorption measurements and the values are 22.4 nm, 10 nm, and 0.58 cm^3/g, respectively. We also investigated the effect of precursor concentration on both the pore sizes, as well as the thicknesses of the pore walls. The results showed a reduction of surface area, and also narrower pore size distribution with increasing concentration. Temperature was also observed to have the same effect on crystallinity in all the compositions studied.

All the investigations on these two systems were carried out using XRD (X-ray diffraction), FT-IR (Fourrier Transform Infrared Spectroscopy), Raman spectroscopy, POM (Polarized Light Optical Microscope), N_2-sorption measurements, PEIS (Potentiostatic Electrochemical Impedance Spectroscopy), TEM (Transition Electron Microscopy), SEM (Scanning Electron Microscopy) etc.

Keywords: mesophases, H_3PO_4, proton conductivity, calcium hydroxyapatite, lyotropic liquid crystals, and mesoporous thin films,

ÖZET

LIYOTROPIK SIVI KRİSTALİN (LSK) FOSFORIK ASIT-10-LORIL ETER: ARAFAZLAR, PROTON İLETKENLIK VE ŞEFFAF MEZOGÖZENEKLI HIDROKSIAPATIT İNCE FILMLERIN SENTEZI

EBRIMA TUNKARA

Kimya Bölümü Yüksek Lisans Tezi

Tez Yöneticisi: Prof. Dr. Ömer Dağ

Haziran 2014

Düşük, göreceli nem sulanmaya (GNS) sahip bir çok tuz, asit ve bazlar iyonik olmayan yüzeyaktifleri liyopropik sıvı kristal (LSK) fazlarda organize edebilir, dolayısyla mezogözenekli malzemelerin sentezi için uygun platformlar oluştururlar. Bu çalışmada, düşük GNS li fosforik asitin de (H_3PO_4, PA) çözücü gibi kullanılarak iyonik olmayan yüzeyaktifi ($C_{12}H_{25}(OCH_2CH_2)_{10}OH$, $C_{12}EO_{10}$) geniş bir kompozisyon aralığında ($C_{12}EO_{10}$

da derişim 20 PA/$C_{12}EO_{10}$ mol oranı kadar olabilir) kararlı LSK fazlarında organize edebileceğini gösteriyoruz. Fosforik asitin oluşturduğu arafazların çok düşük derişimler de (2 PA/$C_{12}EO_{10}$ moleranı) sürekli-kubik (V_1), ara derişimlerde (3-5) 2B/3B hekzagonal (H_1) ve yüksek derişimlerde (5 den fazla) misel kübik (I_1) olduğu ve birim hücrelerin ise göreceli olarak 127, 55, 116 Å olduğu belirlendi. Düşük derişimli arafazlar (15 mol oranından daha düşük) yüksek ısıl kararlılığa sahiptir. Erime noktası 120 ^oC den daha yüksektir. Fakat daha yüksek derişimler de (17 mol oranından daha büyük) ise erime noktası 50 ^oC altındadır. Oda sıcaklığında LSK fazların yüksek proton iletkenliğe sahip olduğu da belirlendi (~10^{-3} S/cm). Proton iletkenliği yüksek sıcaklıklarda daha da yüksek iken (10^{-2} S/cm), 0 ^oC nin altında 10^{-4} S/cm in altına düştü. Ayrıca, kübik fazda iletkenliğin biraz daha yüksek olduğu belirlendi. Sıcaklığa ve kompozisyona bağlı iletkenlik ölçüm sonuçları en çok kabul gören Grotthuss ve Vehicle proton iletkenlik mekanizmasına uyduğu belirlendi.

Daha ileri giderek, H_3PO_4 ve diğer bir düşük GNS li (örneğin $Ca(NO_3)_2 \cdot 4H_2O$) tuz ile oluşturduğu karışımın da kararlı arafazlar oluşturduğunu (bu arafazlar da geniş bir PA+tuz/$C_{12}EO_{10}$ mol aralığında, 5.3/1 den 13.3/1, herhangi bir tuz çökmesi olmadı) belirledik. Yüksek asitlik hem sulu çözeltiyi hemde LSK fazları kararlı kıldığı belirlendi. Girdilerden oluşturulan şeffaf çözeltiler döngülü kapla yöntemi ile mikroskop cam yüzeylerine kaplandı (bir kaç yüz nanometre kalınlığında) ve yakılarak şeffaf, nano boyutlu, mezogözenekli hidroksiapatayt (HAp) ince filmlerine dönüştürüldü. Sentez yöntemimizdeki yarı kristalin HAp oluşumu tek aşamalı değildir; yöntem bir kaç ara ürün oluşturur ve en az 300 ^oC ye ihtiyaç vardır. Oluşum 300 ^oC de başlar ve nitrik asit ve su moleküllerinin ortamda uzaklaşması ile sürer. Kristallenme 400 ^oC, de de devam eder ve 500 ^oC de filmlerdeki düzenliliği, gözenekliliği, ve şeffaflığıda koruyarak tamamlanır. 300 ^oC de yakılmış 5.3/1 oranlı numunenin 96 m^2/g olan yüzeyalanının 500 ^oC de 20 m^2/g kadar düştüğü gözlendi. 600 ^oC ise yapı çökmeye başadı. N_2 tutma/bırakma ölçümleri ile gözenek

boyutu, gözenek duvarları, ve gözenek hacmi göreceli olarak 22.4 nm, 10 nm ve 0.58 cm^3/g olarak belirlendi. Derişimin gözenek boyut dağılımına ve duvar kalınlıklarına etkiside gösterildi. Sonuçlar, derişimin arttırılması ile yüzeyalanının düştüğü fakat gözenek dağılımının daha düzenli ve dar olduğunu gösterdi. Bütün kompozisyonlarda sıcaklığın da kristallenmeye bazı etkilerinin olduğu gözlendi.

Her iki system üzerinde çalışmalar XRD (X-ışını krınımı), FT-IR (Fourrier Transform Infrared Spektroskopi), Raman spektroskopi, POM (Polarize Optik Mikroskbu), N_2-tutma/bırakmaölçümleri, PEIS (Potensiostatik Elektrokimyasal Empedans Spektroskopi), TEM (Transmission Elektron Mikroskobi), SEM (Taramalı Elektron Mikroskobi) teknikleri kullanılarak gerçekleştirildi.

Keywords: arafazlar, H_3PO_4, proton iletkenlik, kalsium hydroksiapatit, liyotropik sıvı kristaller, mezogözenekli ince filmler.

ACKNOWLEDGEMENTS

My dreams of being a chemistry graduate turned to reality, courtesy of the Islamic Development Bank (IDB), without whose financial intervention, the long term dream would never have come true. I therefore commence my acknowledgements by expressing sincere gratitude to IDB's scholarship division, through Brother Lakhdar Kadkadi.

My heartfelt appreciation also goes to Professor Dr. Ömer Dağ for not only being my supervisor, but also a friend. He accepted me in his research group when almost everybody rejected me. Since then, he nurtured research skills in me and also challenged me to develop the right mind-set in order to be a successful researcher. He was constantly with me throughout my career as an MSc student in Bilkent University, providing me with the best advice a graduate student could ever wish for. During the two years I spent with him, he was never harsh with me, even though I did many things that could have earned his anger. His formula for correcting wrongs is simply exceptional and worth emulating. His intellectualism, courage, passion, and sense of humour will live long in the minds of all the lives he has touched, especially mine. Without his guidance and persistent help, this dissertation would not have been possible.

I would also like to thank the other two jury members: Assoc. Prof. Margarita Kantcheva and Asst. Prof. Coşkun Kocabaş. Their feedback on the thesis, and the questions they asked during the defense were all paramount as far as the quality of this thesis is concerned. Additional appreciation goes to Margarita Kantcheva for her invaluable support in the interpretation of some of the infra-red data and also for her time in writing recommendation letters for all the PHD scholarships I applied for.

My sincere appreciation also goes to Mr. Oladele Oyelakin, one of the chemistry lecturers at the University of the Gambia chemistry department, where I did my undergraduate studies. When I first met him in 2006, I thought he wasn't the easiest of lecturers in the department, but as I grew up, I realized that the motives for many of his actions were geared towards making us better chemistry students. In fact, it is because of him that, I was able to compete in Bilkent University. I also had the chance to work as a TA under his supervision for two consecutive years (2010 to 2012) and I adored all his teaching and training. I consulted him for advice many times while undertaking this study.

During the tenure of this study, I was blessed with a family in Turkey that did an enormous amount to make me feel at home. When I first met them, I thought it was just a mere coincidence, but as time passed by, I realized that the relationship was destined to be. They

supported me in many aspects, especially when I was so helpless and hopeless in Hacettepe hospital. I therefore owe a depth of gratitude to the entire Aydin family for their support. The two years I have been with them was enough to make me realize how caring and exemplary they are. Their kindness makes me believe that, family isn't always by blood, but through the people in whose kindness one finds sanctuary.

My appreciation also goes to Ian Soulsby for the support he has given me, especially in buying me textbooks and other learning materials. Most of the textbooks I used during the first year of my studies were bought by him. His support was therefore, one of the main reasons behind my successful academic standing in Bilkent University.

Thanks to Mehmet Basaran (Computer Engineering, MSc) too, for designing the template of my thesis, and also for being one of the loyal friends I spent fruitful time with in Bilkent.

I would also like to thank all the present and past members of Dağ's research group: Gözde Barım, Cemal Albayrak, Ezgi Yilmaz, Ahmet Selim Han, Civan Avci, Melih Baci, Zelal Yavuz, and Aykut Aydin. They all contributed immensely to my research during lab meetings and some other discussions. I am most especially thankful to Gözde Barım for being one my best friends in the department. She taught me how to use almost all the instruments in the lab and also supported me in analysing most of my first data.

Among my friends in the chemistry department, I thank Hamidou Keita (Gambian Colleague, MSc), Muazzam Idris (Nigerian, MSc), Sean McWhorter (USA, PHD), Jose Luis Bila (Mozambique, MSc), Hüseyin Alagöz (Turkish, PHD), Rehan Khan (Pakistani, Post Doc.), Jousheed PK (Indian, Post Doc.). I had my best and funniest moments in the department with them. They were all supportive and I must confess that they made me enjoy student life in the chemistry department.

My sincere gratitude also goes to all the members of the Gambian Students' Association in Turkey (AGAST). I met most of them for the first time, when I came to Turkey, but my relationship with them is just uncanny. I received lots of brotherly advice from Muhammed B. Jaiteh, Muhammad Lamin Darboe, Njaw Njie and his family, Ebrima S. Njie, Ebrima Baldeh, Batch Sowe etc. The fruitful discussion and the funny moments we shared together will forever remain in the archives of my memory.

Thanks to the Gambia's deputy ambassador in Turkey, Mr. Serign Modou Njie and his wife for their support. Their residence was my second home, where I ate lots of Gambian meals. Thanks to Madam Isatou Gaye Joof (wife of the former Gambian ambassador) for her support to all Gambian students in Turkey.

To my friends back home in the Gambia, Lamin Ceesay (Farato), Lamin Saho (Tallinding), Samba Bah (UTG), Dawda Kujabi, etc. I thank and salute you all. Your support in helping to process most of the documents I needed from the Gambia was really appreciated.

To my Pakistani friends; Asad Ali, Zulfiqar Ali, Muhamad Maiz Ghauri, Shahid Mahmood, Abdullah Waseem, Abdul Ali Kakar, Shahid Ali Leghari, Ateeq Ul-Rahman, Mehrab Ramzan, Tufail Ahmed etc., thank you for the good humour and great work environment. Special thanks to Prof. Dr. Fakhar Mahmood (Economic department) for the many useful discursions, advices, and for his timely intervention, when I needed him most. Life in Bilkent would have been very difficult for me, if had not met such a nice group of Paksitani students and professor. You have all rendered me enough kindness to remember. I love you all!!

It is also my duty to record my thanks to all my other friends in Bilkent; Sercan Cambolat (International Relations, MSc), Nimet Kaya, Seyffetin Doğru (International Relations, BSc), Kadir Akbudak (PHD, Computer Engineering), Muhittin Çalik (Security), Muhammad Yunus (Nigerian, UNAM), and Adamu Abdullahi (Nigerian, Electrical & Electronic Engineering department). You have all played significant roles in improving my social life in Bilkent. Nimet, was more like a parent to almost everybody in dorm 15. I cherish her kindness and strong feelings for international students.

Finally, I would like to say a big a thank you my beloved family (My Mom in particular) and Mariama Camara, for the support they accorded me throughout my stay in Turkey. Their love for me never fail to falter. I might not have come this far, without their patience, prayers and moral support. This support was the light I always saw when everywhere seemed dark. I am highly indebted to my loving sisters, for always being at my service.

I dedicate this thesis to my loving Mom, and the Aydin family (Ankara, Turkey).

Alhamdulillah!!

TABLE OF CONTENT

LIST OF FIGURES

LIST OF TABLES

CHAPTER 1

1. INTRODUCTION

1.1. Liquid Crystals

Liquid crystals, ordered soft materials, are materials whose features are in the border line between the perfect three-dimensional, long-range positional and orientation order found in solid crystals and the absence of long range order found in isotropic (conventional) liquids and amorphous solids. [1] **Figure 1-1**. For this reason, they can be regarded as intermediate states (mesophases) between the conventional three states of matter.

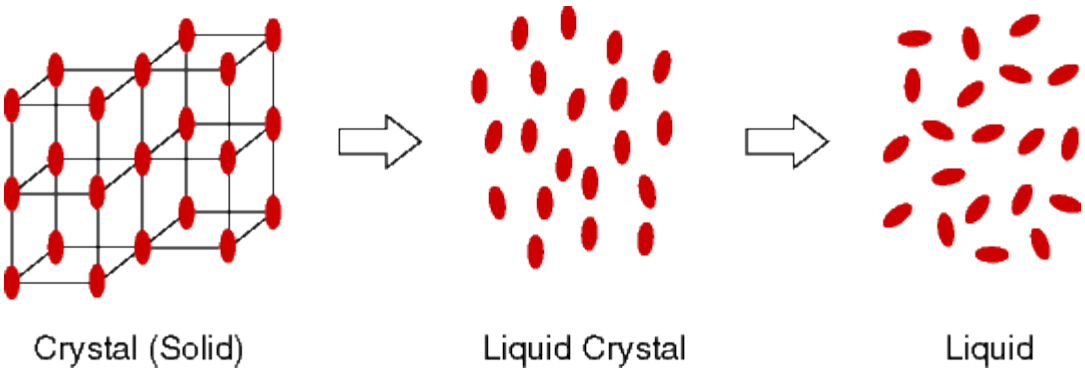

Figure 1-1. Schematic representation of the different states of matter, showing the orientational difference in crystalline solids, liquid crystals, and liquids.

They were discovered in the mid-1850s by Friedrich Reintzer but detailed studies on their structural properties started in the 1950s following publications by G.H Brown and W. G. Shaw. [2] The formation of such materials is aided by the self-assembling of organic amphiphilic molecules when they are exposed to either heat, or solvents. Based on this reason, they are classified into two distinct types: thermotropic (form with the aid of heat) and lyotropic (form with the aid of solvent).

In thermotropic liquid crystals, orientational order arises from the interaction among partially rigid anisotropic molecules [2]. The most outstanding feature for such materials is the tendency of the molecules ‘’mesogens’’ to point along a common axis. This semi ordered nature arising from weak inter-molecular forces among the molecules, limits their translational degree of freedom as compared to liquids, which are completely mobile and solids that have no translational degree of freedom. Thermotropic Liquid crystals are usually formed by single amphiphilic compounds when they are exposed to heat. In such liquid crystals, phase transitions are completely dependent on only heat. [3] They exhibit smectic phases with layered structures or nematic phases (eventually cholesteric) phases. [2] **Figure 1-2** shows the two main liquid crystalline divisions with some schematic representation of the different phases in each of them.

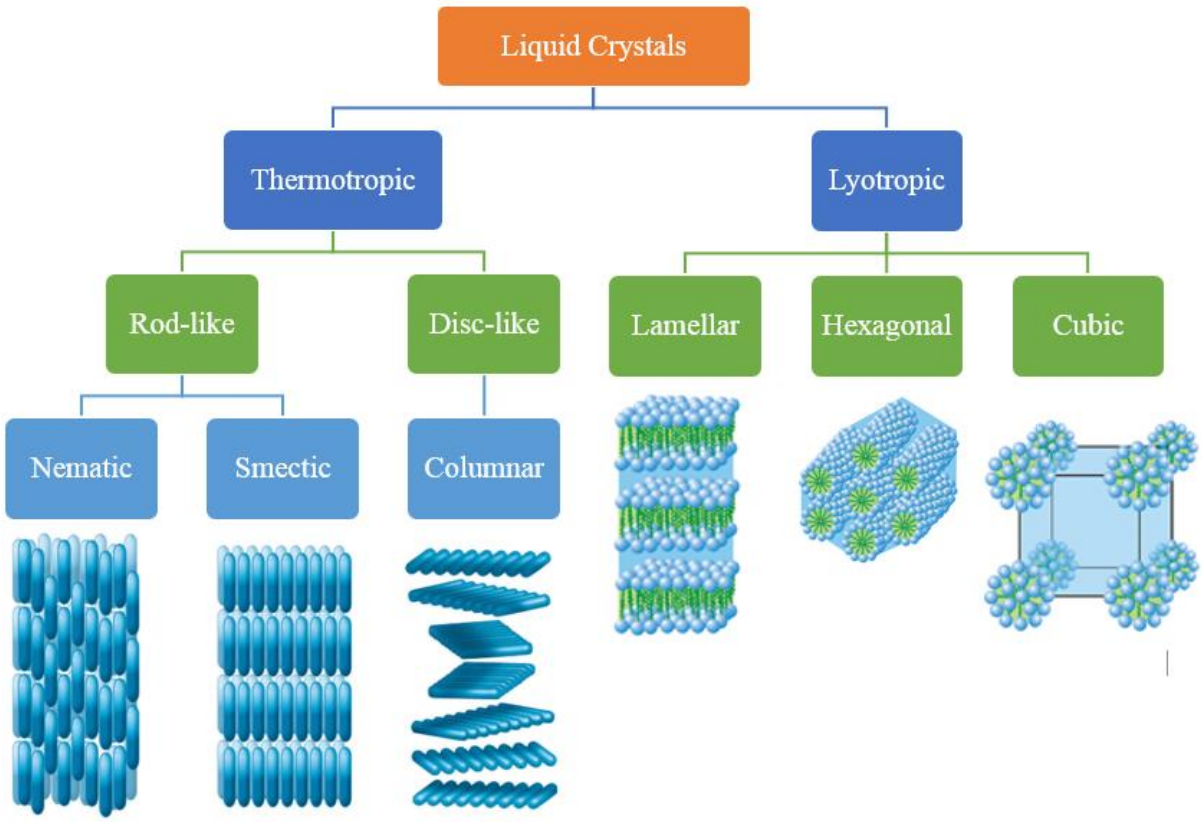

Figure 1-2. A flow chart of the two distinct types of Liquid Crystals with their sub divisions and phases.

Thermotropic liquid crystallinity is more likely to occur in molecules with flat segments, e. g. benzene rings. A fairly good rigid backbone containing double bonds defines the long axis of the molecule. The existence of strong dipoles and easily polarizable groups in the molecule may also be important.

Properties that make liquid crystals different from liquids and solids are: the molecules have anisotropic shape (e. g. are elongated). The formation of ‘’monocrystals’’ (molecular order in one dimension) with the application of ordinary magnetic and/or electric field.

1.2. Lyotropic Liquid Crystals (LLC)

Amphiphilic molecules (surfactants in this case), are surface active agents capable of lowering the surface tension between polar and nonpolar groups in reaction media. As discussed above, these materials spontaneously form aggregations when they are exposed to either aqueous or oily media. At small concentrations in aqueous media, the hydrophilic moieties (head groups) of the surfactant molecules are hydrated in the media while hydrophobic moieties (the non-polar tail group) rest on the surface of the media. As the concentration of the surfactant increases, the continuous segregation between the water-hating and the water-loving moieties results to the formation of thermodynamically stable supramolecular assemblies such as micelles (in aqueous solutions) or micro emulsions (in multicomponent systems with water, oil and often co-surfactant) and as well as kinetically stabilized vesicles. [3] [4] [5] For the case of micelles, the polar head groups of the molecules are on the outside of the micelles and are solvated, whereas the non-polar groups form inner cores and are shielded from the solvent. The exact opposite of this (reverse micelles) is observed when the amphiphilic molecules are exposed to nonpolar (non-aqueous) media. The concentration at which micellization (formation of micelles) occurs, is known as the critical micellar concentration (CMC). The formation of micelles is driven

by hydrophobic effect which acts to squeeze the oil or hydrophobic region out of water. The aggregation numbers in micelles i.e. the number of surfactant molecules in a micellar unit, can be as high as 200 surfactant molecules per micelles, or as low as 50 molecules per micelles. The factors determining such numbers can be the length of the hydrophobic tail, size of the polar head groups, concentration of both surfactant and solvent, temperature and even nature of the surfactant molecule [4]. Salts for example, can affect the CMC especially in ionic surfactants by screening the electrostatic repulsions between the surfactants' head groups and hence lead to the decrease of aggregation number. [5] Above the CMC, the surfactant molecules will further self-aggregate to form mesomorphic phases; phases in between liquids and crystalline materials known as Lyotropic liquid crystals (LLC).

Lyotropic Liquid crystals are a form of liquid crystal in which fluid anisotropy results from the interaction between anisotropic aggregates of amphiphilic molecules. Unlike thermotropic liquid crystals, LLC have wide range of stability with respect to temperature, pressure, and system composition (concentration). [6] When the concentration of the surfactant increases further, the orientation of the micellar units also changes leading to the formation of new phases (increasingly densely packed) such as lamellar **(L_1),** hexagonal **(H_1)**, cubic **(I_α** and **V_1)** etc. in order to accommodate new molecules. In the hexagonal phase, the micelles form rod-like structures of indefinite lengths, in which the rods are separated by water (aqueous) molecules. Further increase in the concentration will eventually lead to a formation of lamellar phase; a phase in which the micelles form stacking layers (hydrophobic tail groups sandwiched between the hydrophilic head groups). Some of these phases are shown in **Figure 1-3.** Other than the concentration of the surfactant, other factors such as the nature of the amphiphilic molecules, temperature, pressure etc. are also known to be affecting the phase transitions of such materials.

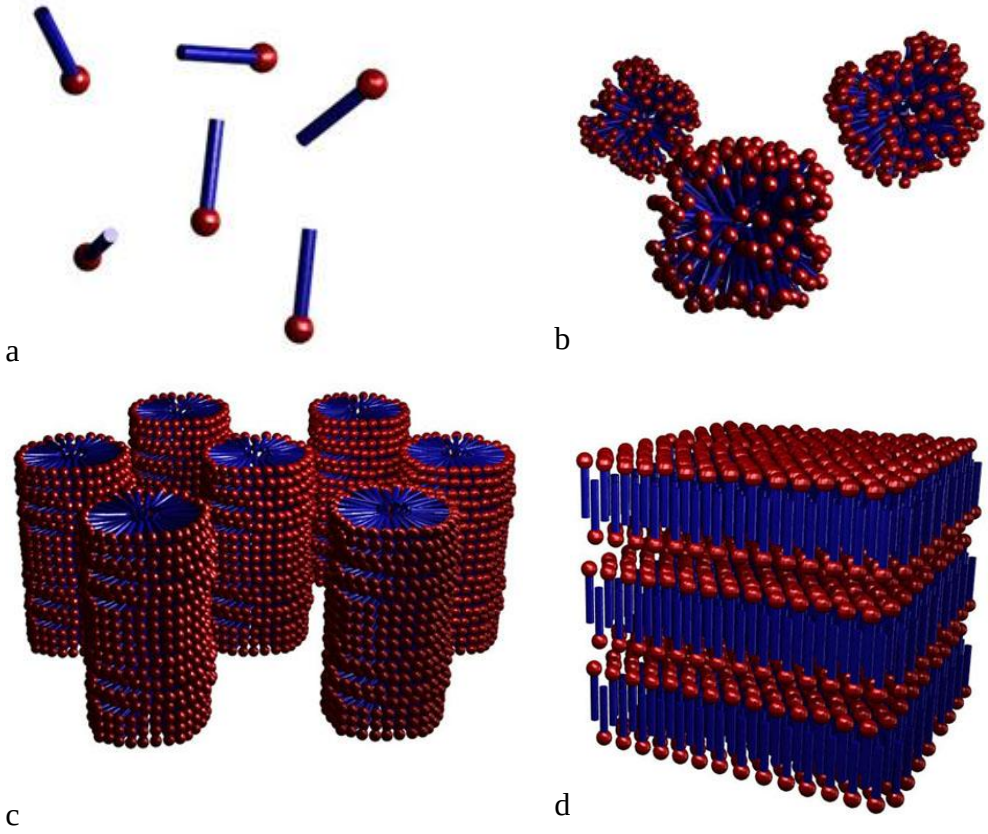

Figure 1-3. Schematic representation of the effect of increasing surfactant concentration on lyotropic liquid crystalline phases. a) Isolated surfactant molecules b) spherical micellar aggregates c) hexagonal phase d) lamellar phase.

Many solvents such as water [7], supercritical carbon dioxide [8], organic compounds [9] ionic liquids [10] and hydrated salts [11] can be used for assembling these amphiphilic molecules into mesophases. Among them, water, and organic compounds such as lipids are the most common ones and were mostly used during the earlier investigations in this field. However, later investigations proved that hydrated salts are the most important ones, because, they assemble larger quantities of metal salt species into ordered mesophases, which could be calcined to obtain mesoporous films. [12]The mesophases obtained from such solvents were also known to possess better thermal stabilities than those prepared from other solvents. [11] This is because of the increased hydrogen bonding interaction between

the coordinated water molecules and the surfactant molecules. More of this has been discussed in detail in the **Chapter 3**

Surfactants are classified into three main categories: cationic, anionic and neutral depending on the charge in the hydrophilic head group of the surfactant. Cationic surfactants have anions as counter ion species, whereas, anionic surfactants have cations as counter ion species. Neutral surfactants, as the name implies, have no charge at all. The Charges on surfactant molecules can sometimes have devastating effects on both the formation and the stability of mesophases. For examples, charged surfactants are more soluble in aqueous media and for that reason, they have higher CMC than neutral surfactants which have lower CMC because of their lower solubility. [13] Neutral surfactants, which form phases via hydrogen bonding, offer numerous advantages such as higher stability (mechanical and thermal), and also gives stronger amphiphilic character [10], which is particularly important for the synthesis of meso-ordered materials.

1.3. Water-surfactant LLC phases.

Mixture of water (as solvent) and surfactants can form stable LLC phases under wide range of temperature and concentration due to the amphiphilic nature of the surfactants. Since water is the most abundant (common) solvent, most of the early day researchers in this field used it as the main solvent in their investigations. The percentage of water to salt that allows the formation of phases in this system is usually 50% w/w. However, other solvents such as oil, ionic liquids, supercritical CO_2, and etc. can be used in large volumes to form stable phases. The mesophases of such systems in non-ionic surfactants can be controlled by the length of the hydrophobic chain as well as the number of the hydrophilic units in the surfactant. To prove this idea, many phase diagrams have already been constructed using various non-ionic surfactants such as poly(ethylene oxide)monalkylether (C_nEO_m) with

various solvents including the aforementioned ones within a wide range of temperature. [14] [15] In most of these studies, both the ethylene oxide (hydrophilic) units and the alkyl (hydrophobic groups) chain lengths were varied in order to monitor the effects each one of them have on the phase transitions of mesophases. [16] The results of these investigations confirmed high dependence of phases on both the two moieties. For example, Tiddy and co-workers [16] found that the cubic phases are dominant in cases were the ethylene oxide groups in the surfactant are more than 8, whereas the lamellar phase prevails more in cases were the ethylene oxide chains are less than 5. The explanation for their result was based on the increase in cross sectional area caused by the increasing number of ethylene oxide units which eventually leads to high interfacial curvatures. In all the phases diagrams constructed so far, it can be seen that increase in temperature leads to phase transitions in the order of $\mathbf{I_1 \rightarrow H_1 \rightarrow V_1 \rightarrow L\alpha}$ because of the decreasing micellar repulsions due to the decrease in the cross sectional area.

1.4. Effect of hydrophilic additives on water-surfactant LLC phases.

Where a salt is to be added to such system, it should always be kept in low concentration in order to avoid disturbance of the LLC phases. Based on these minute quantities, salts are mainly regarded as impurities/additives in such systems. Their presence in mesophases have both physical and chemical effects. Generally, polar solutes cause osmotic dehydration by competing with the surfactant for interaction with water. [17] This interaction favours the formation of ordered phases (gel or crystalline) and the effect may be enhanced if the solute binds to the surfactant head groups, displacing water molecules. However strongly hydrophilic molecules such as certain halides also enhance the interfacial hydration upon binding, and these solutes were therefore known to have opposite effects on lipid polymorphism (LLC phases in biology). [5] From the statements above, it could

be inferred that, other than nature of the surfactant, competition for binding with water molecules among different species in the mesophase is also a main factor affecting the formation and stability of the phases. For this reason, Inoue et al. [18] came up with a statistical thermodynamic model that proposed that, the effect of additives is based on surfactant-water, additive-water, and additive-surfactant interactions. Their investigation was centered on the effect of different additives on the mesophases of heptaethylene glycol dodecyl ether ($C_{12}EO_7$) - water system. They found out that, the increasing concentration of some of the additives such as sugar and glycerol monotonously shrink both the **L*α*** and $\mathbf{H_1}$ mesophase regions to lower temperatures as compared to the pure surfactant-water system. However, urea was found to have an opposing effect on the $\mathbf{H_1}$ phases as compared to the other additives and also causes weakly shrinkage on the **L*α*** phase. This observation was what led to the proposed model.

The effect of other additives such as cationic and anionic species were also well studied. Investigation carried out by Zheng et al. [19] further showed high dependence of phases on the nature of the confined cationic species in metal complexes. The result of their finding showed that, presence of smaller cations causes expansion of the **L*α*** phase as oppose to larger cations. The explanation for this was based on the hydration capabilities of cations of different sizes. Therefore, the stronger a cation's hydration, the more dehydrated the ethylene oxide chain will be, which eventually leads to the increment of the critical parking parameter of the surfactant molecules. Such increment favors the formation of lamellar phase. For this reason, it was observed in their studies that lithium was able to expand the **L*α*** phase due to smaller size and stronger hydration while the larger ions such as cesium have weaker hydration and thus reduced the **L*α*** phase [19].

For the case of anions, their effect on phases is mostly linked to the Hofmeister series shown in **Figure 1-4**. This is a series which categorizes anions as either 'chaotropic' (salting-in)

or ‘kosmotropes’ (salting-out). According to this series, anions on the left side of the series, kosmotropes are more lyotropic and make surfactant molecules more hydrophobic. On the contrary, anions on the right side, chaotropes, are more hydrotropic and make the surfactant molecules more hydrophilic; i.e. they support the formation of stable phases.

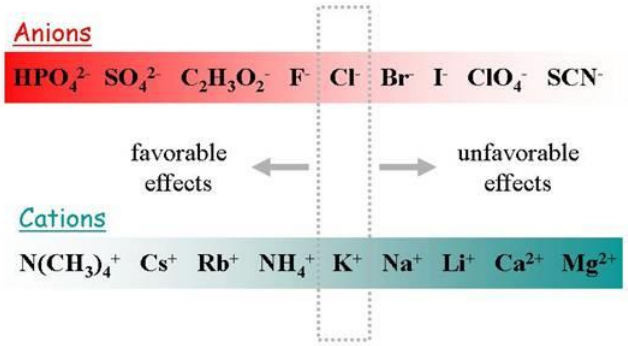

Figure 1-4. Hofmeister series[1]

The phase diagram reported by Inoue and coworkers, [20], showed that anions such as ClO_4^- and I^- reduce **L*α*** phase and expand the $\mathbf{H_1}$ domains of surfactant micelles whereas, anions like Cl^- causes the expansion of the **L*α*** phase and the shrinking of the hexagonal domains [20]. This is because, the ‘chaotropic’ effect of ClO_4^- is stronger than that of I^- and as a result, the hydration of the surfactant in the phase diagram below is much more enhanced by the ClO_4^- than the I^-. This therefore explains why the area of the Lα region becomes much more reduced in ClO_4^-.

[1] Reprinted from http://www.chemistry.sjsu.edu/deggers/Hofmeister.htm

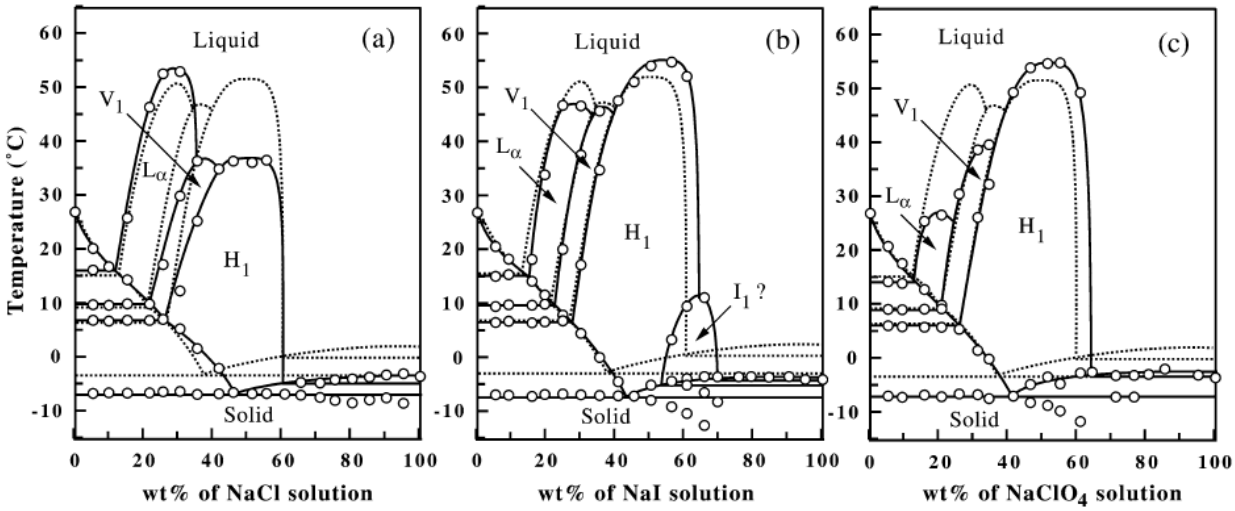

Figure 1-5[2]. Effect of anions on the formation of different phases in the pure water-surfactant system.

1.5. Salt-surfactant LLC materials

The formation of stable mesophases by salts, surfactants and little or no water, was discovered in 2001 [11] . In this new system, formation of mesophases can be either through binary (without additional water) or ternary (with additional water as the third component) depending on the number of components. Although free water, which used to be the main component for the formation of LLC in the water-systems is not necessary, it is still very important that the metal salts are either deliquescence, have water of coordination or hydration sphere. Coordinated water molecules in the metal complexes are enough to effectively assemble the surfactant species into different phases depending on the concentration of the assembling salt. Upon forming such mesophases, ions/salts from the complexes occupy the hydrophilic domains, where they interact through hydrogen bonding with the surfactant molecules and some coordinated water molecules. When salts are confined in such spaces, their physical properties such as solubility and melting points

[2] Reprinted from Inoue, Tohru, Yusuke, Yokoyama, and Li-Qiang Zheng, Hofmeister anion effect on aqueous phase behavior of heptaethylene glycol dodecyl ether. *Journal of Colloid and Interface Science,* vol. 274, p. 349–353, 2004 with permission from American Chemical society.

drastically changes owing to soft confinement effect, which causes the lowering of their melting points and enhancement of their solubility. [21] With these adjustments in their physical properties, they can remain stable as liquid-like in between the hydrophilic domains for many months without recrystallization.

Almost all the first row transition metals (e.g. Mn^{2+},Co^{2+}, Ni^{2+}, Zn^{2+}, etc.) and some of the second row transition metals (e.g. Cd^{2+}), hydrated complexes with low melting point and/or high solubility, e.g. Cl^- and nitrate-containing metal complexes were studied and found to be capable of assembling oligo (ethylene oxide) type surfactants into stable mesophases in the presence of small quantity of water. [11] Later studies by Dag et al. [22] further showed that, the capabilities of such salts in assembling surfactant molecules is not only limited to oligo (ethylene oxide) surfactant, but even Pluronics. Pluronics are triblock copolymers composting of poly (ethylene oxide), poly (propylene oxide), and poly (ethylene oxide) pendant chains. They were investigated and found to be capable of forming phases with Zn^{2+}, Co^{2+}, $Ni^{2+,}$ Cd^{2+} aqua complexes in both the binary and ternary system. [22] The phases formed by these surfactants were 2D hexagonal, 3D hexagonal, cubic and even tetragonal, which was not observed in the ethylene oxide-salt systems.

In addition to the formation of phases, it was also realized that the salt-surfactant ratio in this system can be as high as 6.5 (62.6% w/w) depending on the anionic species on the metal complex. These new discoveries differed from the previous studies in two ways: firstly, the quantity of water which used to be 50% w/w [23] with surfactant mixtures was reduced to a much lower quantity (almost no water in some cases), [24] and secondly, the salt to surfactant ratio which was always kept in low in the water-surfactant system, was also increased to much higher ratios (70% w/w in nonionic surfactants, or 80%w/w in ionic surfactants) [11] [25].

In 2008, Albayrak et al. [26] published the phase diagram of zinc nitrate hexahydrate-surfactant mesophases **(Figure 1-6)** that typically resembles the phase diagram of water-surfactant system. This phase diagram which is universal for all salt-surfactant systems, was constructed within a temperature range of -190 to 100 ^{o}C and a concentration range of

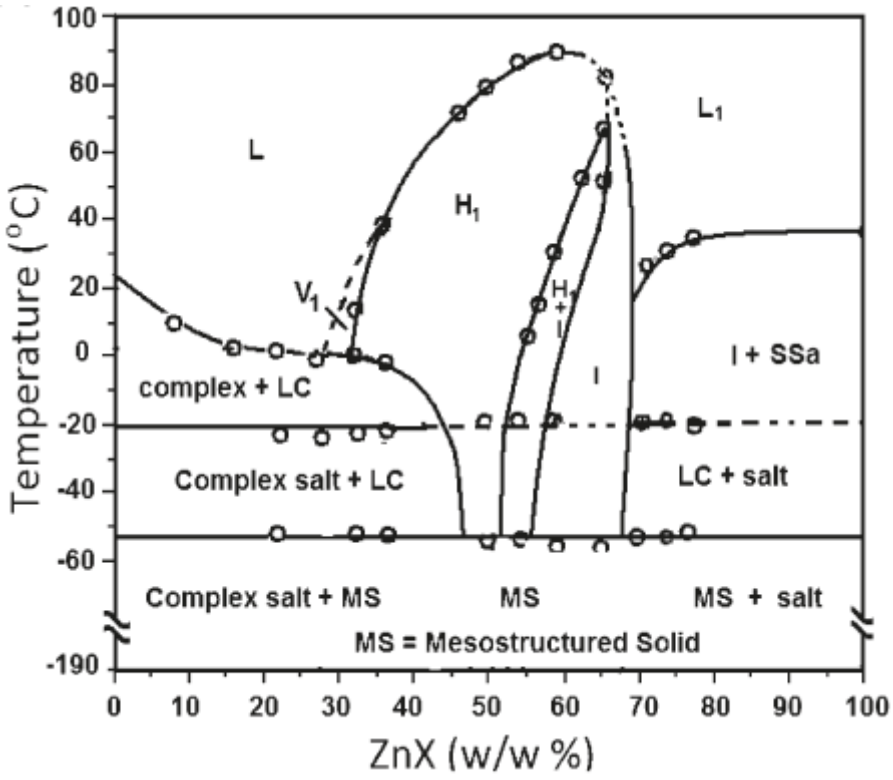

Figure 1-6[3]. Phase diagram of Zinc nitrate hexahydrate showing how the LLC phases change with increasing concentration and temperature.

0 to 100% salt, showed the influence of both salt/surfactant ratio and temperature on the phase transitions of such systems. The letters **H_1**, **L_1**, and **I** in the phase diagram represents hexagonal, lamellar and cubic phases respectively. The transition of phases in

[3] Reprinted from Cemal Albayrak et al. Origin of Lyotropic Liquid crystalline Mesophase Formation and Liquid Crystalline to Mesostructured solid transformation in the Metal Nitrate salt-Surfactant Systems, *Langmuir*, vol. 27, no. 3, pp. 870-873, 2010, with permission from American Chemical Society.

the diagrams provide evidences for the increase of curvature with increasing metal salt concentration.

1.6. **Factors affecting the stability of salt-surfactant liquid crystalline mesophases**

The main factors affecting the formation and the stability of salt-surfactant systems are; deliquescence, melting point and the counterion of the salt [24] [27]. The dependence of phase stability on the anion properties such as solubility is not just a simple direct relation; many major significant factors are inter-connected rather than only one direct relationship. For example, high solubility of metal complexes, which could mostly be guessed from the Hofmeister series of anions does not provide enough details as to whether a particular metal complex containing an anion from the right side of the Hofmeister series will form a more stable phase than another complex formed from an anion on the left side of the series. Investigations showed that, the nitrate-containing complexes, which are expected to be less soluble than the perchlorate-containing complexes on the water-surfactant system can form even more stable phases than the perchlorate's complexes in the salt-surfactant system [24]. This is because of the higher coordination strength in the nitrate complexes which causes reduction of ionic strength in these media and eventually leads to the formation of more stable phases. [24] The presence of M-OH_2 is also vital in this system since the formation of stable phases largely depends on hydrogen bonding networks between the molecules themselves and with the surfactant's ethoxy groups [22]. This simply means that, many salts with anions lacking some of the mentioned features, may still be able form stable phases depending on other parameters, such as their ability to increase the water content of the salt-surfactant mesophases (hygroscopy).

Hygroscopicity, which can be measured by deliquescence relative humidity (DRH) value, is the driving force for many chemicals to self-assemble surfactant into LLC mesophases. In fact, salts are classified into three main categories based on their DRH values. Type I and type II salts, representing salts with low and intermediate DRH values can form stable LLC phases with amphiphilic molecules, whereas, type III salts cannot form phases because of their high DRH values. [27] Type I salts form stables phases in a wider range of concentration than the type II salts, which form stable phases only at very low concentrations.

Salt*	%DRH [25]	Salt*	%DRH [25]
H_2O	100	NaBr	57.0
K_2SO_4	100	NaBr-KBr mixture	56.0
$KClO_3$	98.0	$C_6H_{12}O_6$. $1/2H_2O$	55.0 (27°C)
$CaHPO_4.2H_2O$	97.0	NH,Cl-NaBr misture	54.0
KH_2PO_4	96.6	NaNO,-KBr mixture	54.0
KNO_3	95.0-91.0	$Mg(NO_3)_2.6H_2O$	52.0(24.5°C)
$NH_4H_2PO_4$	93.0	$Ca(NO_3)_2$. $4H_2O$	51.0
$Na_2C_2H_4O_6.2H_2O$	92.0	$NaClO_4$	43-46 [27,28]
$ZnSO_4.7H_2O$	88.5	$K_2CO_3.2H_2O$	43.0
$BaCl_2.2H_2O$	88.0 (24.5°C)	NaI	38.17 [26]
$Na_2CO_3.10H_2O$	87.0	$MgCl_2$. $6H_2O$	33.0
KCl	89.0-84.5	$CaCl_2$. $6H_2O$	31.0
$C_{12}H_{22}O_{17}$	85.0	CH_3COOK	19.0
$(NH_4)SO_4$	83.0-81.1	LiI	17.56 [26]
KBr	79.0	$(CH_3COO)_2Ca$. H_2O	17.0
NH_4Cl	79.3-77.0	LiCl . H_2O	13.0
$CH_3.COONa$	77.0	$LiNO_3$	12.86 [29]
$CO(NH_2)_2$	76.7-76.0	H_3PO_4 . $1/2H_2O$	9.0
NaCl	76.5-75.0	NaOH	6.5
$NaNO_3$	76.0-74.0	LiBr	6.37 [28]
$K_2C_4H_4O_6.1/2H_2O$	75.0	P_2O_5	0.0
$LiClO_4$	~70 [28]		
KI	68.86 [26]		
NH_4NO_3	63.5		

Table 1-1. Room temperature DRH values of some selected chemical species [4]

[4] Reprinted from Dag et al. "Effect of Hygroscopicity of the Metal Salt on the Formation and Air Stability of Lyotropic Liquid Crystalline Mesophases in Hydrated Salt-Surfactant Systems," *Langmuir (SUBMITTED)*, 2013

Table 1-1 above, provides the room temperature DRH values of some salts and other compounds. From this table, it can be seen that both $Ca(NO_3)_2.4H_2O$ and H_3PO_4 have low DRH values, which make them good candidates as non-volatile solvent for assembling non-ionic surfactants. Additionally, some other alkali and alkaline earth metal salts such as $CaCl_2$, $MgCl_2$, LiX (X is Cl^-, Br^-, I^-, NO_3^-) etc. with low DRH values can also be effectively hydrated and dissolved in very small volume of water to form stable mesophases. This therefore shows that deliquescence is the main factor enabling salts without coordinated water molecules to form phases by absorbing water molecules from the environment. Since the presence of water molecules is what facilitates the formation of phases, additional water molecules from deliquescence salts give extra support in keeping the mesophases stable even at extremely high temperature conditions.

1.7. **Application of liquid crystals**

Liquid crystals are advantageous in many applications because of the dynamic nature of their phases. Their electro-optical properties make their phases switchable from one form to another through the application of external stimuli such as thermal treatments and/or electric field. In addition to that, their architecture also makes it possible for the incorporation of both hydrophobic and hydrophilic reagents in separate domains with well-define nanoscale geometries and also offer excellent control over phase geometry and symmetry on the nanometer-scale level via molecular design. [6] These many virtues make them useful in the construction of both biomimetic and non-biological nanostructured organic and inorganic materials. For example, they are found to be applicable in the formation of both 1D & 2D conductive membranes, displays, and also some other photoconductive membranes. [28] [29] [30] Their application as proton membranes is based on confinement effect, which is believed to be capable of enhancing proton transfer

within confined species. [31] Most of the newly immerging anhydrous proton conductive membranes are based on the incorporation of proton conductive materials in channels made from lyotropic liquid crystalline materials. [31] [32]

Additionally, they are very useful in the synthesis of many materials that are found useful in applications, such as drug delivery, [33] pharmacology, [1] and also in the synthesis of many other mesoporous materials for biology applications, catalysis, and also clean energy applications.

1.8. LLC mesophases as templates for the synthesis of porous materials

LLC materials are heavily employed in the synthesis of well-ordered materials, [11] which can be calcined to form mesoporous materials. This method known as liquid crystalline templating (LCT) was discovered by Attard et al. [23] when they successfully synthesized mesoporous silica through the use of LC templating. The method is based on the semi-ordered surfactant molecules in LLC materials, which allows the occupation of salts such as silica, in the hydrophilic domains of the mesophases. Such confinements of inorganic materials may lead to slow heat-independent interfacial reactions among the different confined chemical species (salts, acids, titanic, silica etc.). In some cases, the reactions may also be heat-dependent, depending mostly on the intended product. In either case, the calcination temperatures should be high enough to burn off the surfactant molecules from the mesophases and hence, lead to the formation of mesoporous materials. Many solvents can be used in this synthetic method. However, using salts as solvent will require that the salts are able to cooperatively self-assemble with non-ionic surfactants (such as oligo (ethylene oxides) and pluronics) into stable LLC mesophases [11] [22] thus enabling the reacting ions to occupy the hydrophilic domains. This, therefore, means that hydrated transition metal complexes or highly hydroscopic chemical species are more favorable

chemicals to be used as solvents if binary salt-surfactant system is to be applied in the LCT method.

Since the discovery of LCT, the method has been used in the synthesis of many other mesoporous materials that can have important applications in catalysis, solar cells, conductivity, biological applications etc. Furthermore, it has also been discovered that, this method can be applied in the synthesis of thin films and monoliths. When compared with other methods, this method emerges out to not only been the simplest route of synthesizing mesoporous materials but it is also more advantageous in the production of materials with more uniform pore sizes and also in the production of thin films with higher surface areas, which is important for numerous application.

1.9. Proton conductive materials

As the energy consumption increases with the increasing world population, the need to develop clean, safe and renewable energy sources as alternatives to the highly emissive fossil-based energy source become a major scientific investigation. Currently, most of the scientific research works are centered on improving the efficiency of fuel cells, solar cells, rechargeable batteries and other lesser emissive energy sources. While the fossil based energy source requires no electrolytes, alternative sources such as fuels cells, rechargeable batteries, etc. often require highly conductive electrolytes as media for transportation of charge carriers/ions. The electrolyte plays one of the most important roles in these new technologies and as such, the need to synthesize highly efficient electrolyte materials necessitates many scientific efforts in developing electrolytes that can work in different temperature and humidity conditions.

Electrolytes for solar cells or electrochemical cells such as batteries may be in one of the three forms: solid, liquid or gel depending on where their application is needed. With the exception of anhydrous (solid) electrolytes, gel electrolytes were assumed to be more advantageous [34] than liquid-based electrolytes because of the high leakages associated with liquid electrolytes. Again, because of the well-organized hydrophilic domains (like channels) in gels, they show reasonably high and efficient transportation of ions. [35] Most of the gels associated with fuel cells are either derived from polymers or through the self-assembling of molecules. The LLC gels are usually formed with the aid of surfactant (amphiphilic molecules) as templating agent and solvent(s). The solvent, usually water, plays an important role in enhancing the conductivity of gels. For example, thermotropic liquid crystalline gels (formed without solvents) have relatively lower conductivities; 10^{-6}S/cm when compared to lyotropic liquid crystalline gels 10^{-3} S/cm. [36] In addition to reasonably high conductivity, the LLC gels were also known to be thermally stable; within 83 to 383 K. [37]

Fuel cell is one of the most environmental friendly (low greenhouse-emitting electrochemical energy source), and also the mostly investigated energy systems. It is an electrochemical cell in which electrochemical reactions are characterized by the thermodynamic equilibrium potentials described by the Nernst equation. [38] It works on a simple principle of converting hydrogen, or natural gasses into electricity without causing environment damages. The only liberated product in pure hydrogen-based fuel cells is water and it occurs on the anode while the oxygen reduction reaction occurs in the cathode surface (see the equation below).

$$\mathbf{H_2 + \frac{1}{2}O_2 \rightarrow H_2O \text{ with } \Delta G = -237KJ/mol} \qquad \textbf{Overall reaction} \quad \textbf{Equation 1}$$

For such energy source, anhydrous membranes, permeable to only proton (H^+), with high proton conductivity within a wide range of temperature and humidity conditions, are paramount. The availability of such high-temperature proton conductors will take care of the high rate of evaporation, that usually occur in liquid membranes when they are exposed to high temperature (~100 ^oC) conditions [39], thus leading to a sharp decrease in their conductivities. In addition to that, they are also reckoned to enhance tolerance to CO and H_2S, a quality which increases the possibility for the use of non-precious metals as electrodes, and promote electrode kinetics and ionic conductivity. [40] However, most of the highly conductive electrolytes reported in the literature are either in the liquid or semi-liquid (gel) state. Aqueous LLC membranes were previously reported, but the effect of high temperature on them made them less popular and applicable in fuel cells. [41] [42] Organic proton conductors have shown remarkably interest in fuel cell technology due to their high proton conductivities. [43] For example, perfluorinated sulfonic acid-based polymer membranes such as Nafion exhibit a conductivity as high as 10^{-1} S/cm in the presence of mobile water molecules in the membrane. [44] It maintains good conductivity at moderate temperatures (<80 ^oC). However, its proton conductivity significantly diminishes with high temperatures. [45] Therefore, highly conductive solid/rigidified membranes will be more appreciated in the fuel cell industry because of their high thermal and structural stability even at elevated temperatures. In the literature, very little high-proton-conductive solid/rigid membranes have been reported. One of the recently developed anhydrous membranes was reported by Bartolome et al. [46] through the use of self-assembly of thermotropic LC ionic molecules. The electrolyte was based on the interaction between a zwitterionic thermotropic LC and a nonvolatile acid for the construction of thermally stable proton channels. They anticipated that, the interaction between the two ions may produce mobile ions after the dissociation of the acid, and stabilizes the self-assembled 3D

ion channels. The conductivity reported for this anhydrous membrane was in the order of 10^{-4}S/cm, which is relatively low. In our study, we capitalized on the very powerful, efficient, and environmentally-friendly self-assembly approach [32]. The research was inspired by the highly polarized hydrogen atoms in phosphoric acid molecules that could be interconnected through hydrogen bonding networks when they occupy the hydrophilic domains of LLC. We reckoned that, bringing phosphoric acid molecules in close proximity (confined space) will enhance the formation of extremely viscous and conductive gels. In fact, phosphoric acid in its pure state is among the most promising inorganic proton conductors ($\delta \sim 0.15$ S/cm above T_{melt}=42 ^{o}C) because of its unique proton conduction mechanism. However, its conductivity is limited to certain temperature and humidity conditions. For this reason, most of the present-day researches focused on designing a phosphoric acid-based polymer/composite conducting membranes [47] [48] that can work efficiently in high temperature conditions. The phosphoric acid doped polybenzimidazole (PA/PBI) are presently leading the race, with the one reported by Benicewicz et al. [49] [50] so far having the highest high-temperature proton conductivity value. It was reported to have a room temperature proton conductivity of 0.01 S/cm. Despite the high conductivity of PA/PBI, the significant decrease in the current density arising from the leaching of the phosphoric acid molecules, after hours of being used, limits their application to only short-term applications. [51] To deal with the effect of acid-leaching, it was thought that incorporating the H_3PO_4 molecules in polymer matrices or composites will enhance high acid retention. Qunwei et al. [47] incorporated phosphoric acid molecules inside 3D polymeric framework in order to provide solution to the need for a high- temperature conductive anhydrous molecule. Their composites were reported to poses high acid retention in water-saturated environments, and high conductivity values of 10^{-2} and 10^{-3} S/cm at 183 ^{o}C. A similar research approach conducted by San Ping Jiang et al. [48] also

show conductivity values in the range of 10^{-3} to 10^{-2} S/cm within 80-225 ^{o}C range. The system developed in our research takes care of the acid-leaching observed in polymeric framework systems, because, instead of incorporating the acid molecules in a framework, we formed stable chains through the interaction between the acid molecules in the hydrophilic domains of the mesophase.

Highly conductive LLC phosphoric acid gels were formed through the incorporation of phosphoric acid molecules in between non-ionic ethylene oxide based surfactant micelles. Though not anhydrous, they are still able to exhibit reasonable conductivity within a wide range of temperature conditions (-70 ^{o}C to over 200 ^{o}C) depending on the concentration. The gels are also highly insensitive to water and other environmental fluctuations. More of this will be discussed in chapter 3.

1.9.1. Theories explaining proton conductivity

There exist many theories that explain the concepts behind proton conductivity. Among them, the Grotthuss and the 'Vehicle' mechanisms are so far the most widely accepted explanations. The mechanism of proton conductivity differs from one chemical to the other and is presently the subject of many scientific controversies. For example, the conduction mechanism of water molecules is almost agreed to be through the hopping mechanism, but the conduction mechanism in phosphoric acid and other polymer compounds still remain debatable. In this section, we highlight the most important features of the two most widely accepted mechanisms.

1.9.1.1. Grotthuss Mechanism:

The Grotthuss mechanism shown in **Figure 1-7** is a phenomenon in which protons hop in concerted mechanism from one end of an inter-linked hydrogen bonded molecules to the

other. It involves both formation and breaking of hydrogen bonds. [52] This mechanism explains the abnormally high proton mobility in H_2O, [53] and also explains why ice is more conductive than liquid water since the water molecules in ice are more ordered than those in pure water. The mechanism which is driven by the fluctuations in the second solvation shell of H_3O^+ (reducing the coordination number of a first-solvation-shell of water from four to three [54] [52] [55]), proceed in two stages: in the first stage, a proton (H^+) binds to an oxygen atom located at the free end of a hydrogen bonded water molecules [$H_2O\ldots H^+\ldots OH_2$] or $H_5O_2^+$. This new bond changes the initially neutral H_2O molecule to H_3O^+, which in turn, due to its high acidity, donates its excess proton to the next nearest neighbor water molecule. The process continues on the whole chain and upon reaching the terminal end of the chain, it causes another proton molecule from the terminal end to be liberated; restoring the initial neutral hydrogen bonded chain.

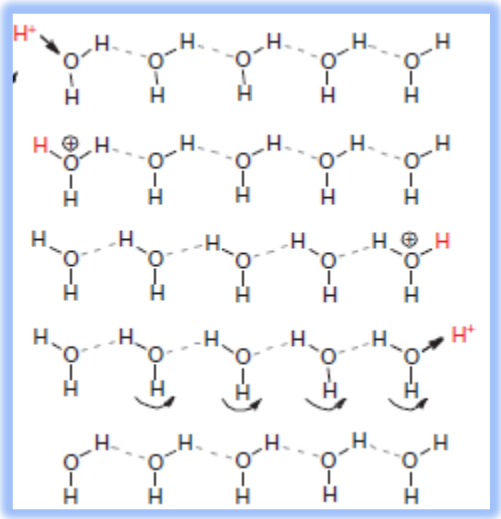

Figure 1-7[5]. Grotthuss mechanism of proton conductivity in water. [46]

[5] Reprinted from L. Xiao, H. Zhang, E. Scanlon, L. Ramanathan, E.-W. Chow, D. Rogers, T. Apple and B. C. Benicewicz, "High-Temperature Polybenzimidazole Fuek Cell Membranes via a Sol-Gel Process," *Chem. Mater*, no. 17, pp. 5328-5333, 2005. With permission from Nature Publishing Group

In the second stage of the mechanism, turn phase, the hydrogen bonded chain rotates either freely or about 110^{o}, [56] [57] restoring the initial configuration of the starting chemical specie.

1.9.1.2. **Vehicle Mechanism**:

This is a newer explanation of conduction mechanism in liquids. Unlike the Grotthuss mechanism, the 'Vehicle' conduction mechanism requires some quantity of water as transporting medium for the free protons. [58] [59] In this mechanism, the liberated protons don't just 'hop' to neighboring hydrogen bonded molecules, but they attach to free water or ammonia molecules to form complexes such H_3O^+ or NH_4^+ ions. These complexes diffuse in opposite direction with the other free water/ammonia molecules. The transporters

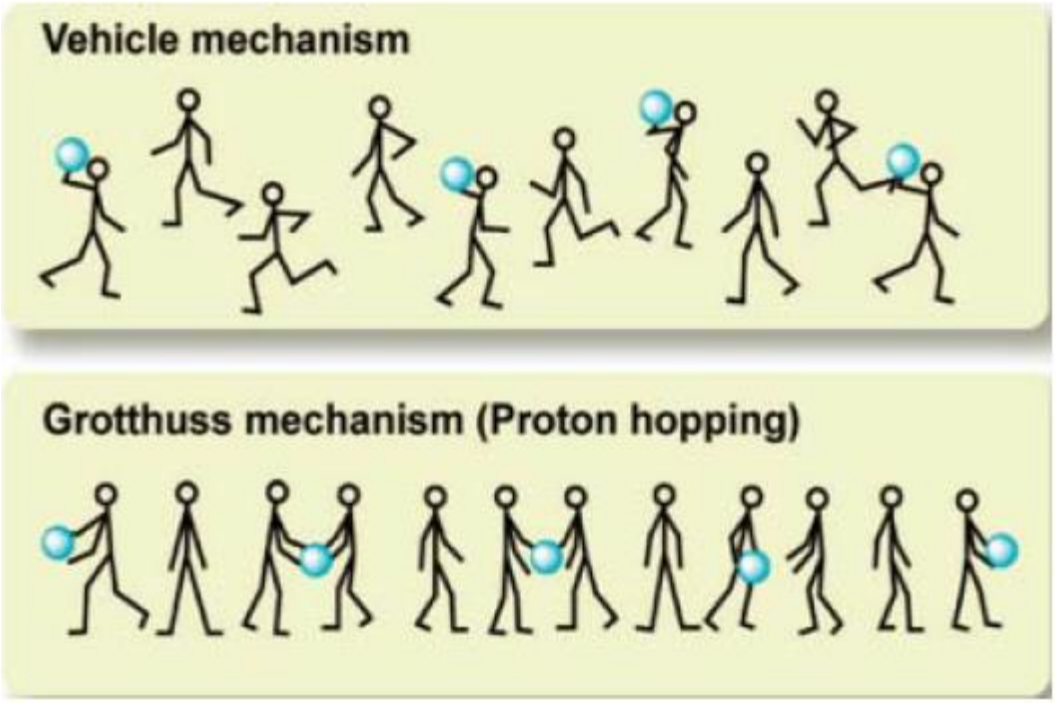

Figure 1-8[6]. Comparison between the two discussed mechanisms. [60]

[6] Reprinted T. U. a. M. Watanabe, Macromolecules in Ionic Liquids: Progress, Challenges, and Opportunities, *Macromolecules*, vol. Vol. 41, no. 11, pp. 3739-3749, 2008. Reprinted with permission from American Chemical Society.

(Vehicles), H_2O, NH_3 etc., in this case, act like Brönsted-Lowry base (proton acceptors) [59] by accepting free protons from the media. While the Grotthuss mechanism involves a ‘’rotation phase’’ of the hydrogen bonded chain, this mechanism did not show correlation between conductivity and the rotation of the Vehicles [59]. The activation energy for this mechanism is relatively higher (0.5-0.9 eV) than the activation energy for the Grotthuss mechanism (0.1-0.4) [58] and it helped to make the extremely large temperature factors observed in neutron and X-Ray diffraction studies understandable. [59] **Figure 1-8** below shows the difference between the two mechanisms explained above. Although the above mentioned theories strongly explained the proton conductivities of aqueous media, the unexpectedly high proton conductivity of neat phosphoric acid still remains unclear. It is however understood that, strong polarizable hydrogen bonds in phosphoric acid produce coupled proton motion and a pronounced protic dielectric response of the medium, leading to the formation of extended, polarized hydrogen-bonded chains, [61] This may therefore, give a clue of why the mobility of protonic charge carriers in phosphoric acid is as high as those in aqueous systems even though phosphoric acid is two orders of magnitude more viscous that water. [62] This conundrum (fast proton mobility in H_3PO_4) raised doubts on whether proton mobility is directly related to the fluidity of a medium. The simulation developed by Klaus-Dieter Kreuer et al. [61] depicted the proton conductivity mechanism of pure phosphoric acid to be somewhat similar to the Grotthuss mechanism. The proposed mechanism, involving creation and migration of protonic charge carriers was driven by the formation of extended, polarizable hydrogen-bonded chains and subsequent solvent reorganization. Their mechanism arises from the combination of strong, polarizable hydrogen bonds and a ‘frustrated’ hydrogen-bond network. In the end, they pictured the proton conductivity of phosphoric acid and phosphate containing compounds to include

four main stages: formation of a contact ion pair ($H_4PO_4^+/H_2PO_4^-$), solvation and the separation of charge carriers, migration and subsequent neutralization.

Besides proton conductivity, the possibility of using LLC phosphoric acid as a precursor in the synthesis of hydroxyapatite (HAp) was also investigated. The next section discusses the features of HAp and also elaborates on some of the reported synthetic methods.

1.10. Mesoporous calcium hydroxyapatite: literature review on the synthetic approaches and applications.

Bone tissue is naturally a two phase organic-inorganic ceramic composite consisting of collagen fibrils, secreted from the osteoblast cells, and an embedded well-ordered inorganic nano-crystalline component. [63] The crystalline component, known as calcium hydroxyapatite (a crystalline form of calcium phosphate) combines with the collagen in order to provide rigidity and mechanical strength to living organisms. This important calcium phosphate mineral is also found in rocks and sea corals. It has the general formula $Ca_{10}(PO_4)_6(OH)_2$ with the mole ratio of calcium to phosphorus always maintained as 1.67. The natural occurring HAp is in the form of nanometre-size crystallites of $Ca_{10}(PO_4)_6OH$ that contain a number of cations and anions impurities. [64] These impurities supress the crystalinity of natural HAp leading to a less crystalline (high surface area) HAp in natural systems. HAp has a hexagonal crystallographic structure (shown in **Figure 1-9 b**) with unit cell parameters of a=b ~ 9.389 Å, c ~ 6.869 Å, $\alpha=\beta= 90^o$ and $\gamma=120^o$ and with a space group of $P6_3/m$. [65] [66] [67] When compared to the alternate calcium phosphate ceramic, HAp was agreed to exhibit a greater stability in aqueous media within a pH range of 4.2-8.0. [64]

The formation of bone itself in natural systems is very complex and requires the presence of collagen protein, HAp, and some other organic and inorganic materials. [68] One of the importance of the collagen protein in bone formation is to dictate the morphology and size

of the HAp crystallites. Therefore, we can safely say that the collagen proteins serves as a template onto which the HAp crystals of well-defined size and shape grow on. The process of formation of bone and the role the collagen proteins plays in directing the nature of the crystalline HAp are outlined in **Figure 1-9 a.**

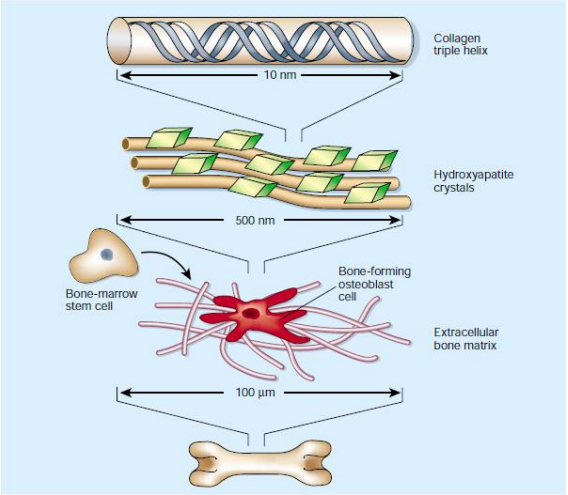

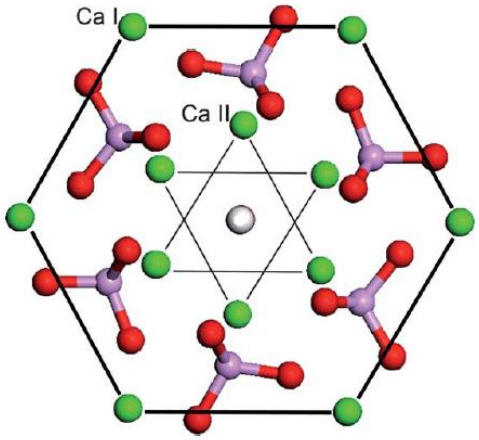

Figure 1-9. Bone formation and crystal structure of HAP.
a) [7] the many scales of organization in natural bone [68] and b) [8] Schematic drawing of the hexagonal building unit projected down the 001 direction. Colour code: White, OH; Green, calcium; Purple, phosphorus; Red, Oxygen. [69]

HAp is one of the most promising materials in bone and tissue engineering because of it osteoconductivity, [70] non-inflammatory, non-toxicity, compatibility and the ability to replace worn-out tissues. [71] [72] These properties makes it a good candidate in drug and protein delivery, [73] templating agent for mesoporous silica synthesis, [74] anti-biotic, [75] anti-cancer drugs, [76] and other medical applications. Matsumato et al., [73] investigated the possibility of using HAp particles as a control released carrier of growth

[7] Reprinted T. A. Taton, "attempts to tailor nanometer-scale objects to mimic and interact wirth natural materials raise the question of how to predict the biological response to these tiny creations," *Nature*, vol. 412, pp. 491-492, 2001. Reprinted with permission from Nature Publishing Group

[8] H. Z. Y. G. Y. W. X. G. Y. L. and F. W. Xiong Lu, "hexagoanl hydroxyapatite formation on TiO2 nanotubes under urea modulation," *CrystEngComm*, no. 13, pp. 3741-3749, 2011. Repinnted with permission from Royal Society of Chemistry.

factors. They first synthesized HAp particles at different temperatures in a wet condition, loaded them with proteins and monitored the releasing of the pre-loaded proteins at different pH solutions. The result showed that the release was higher in more acidic media than in basic or neutral media. They based the protein absorption on the electrostatic interaction between the amino group of the protein and the negative charge site of the HAp crystal. In fact, before the discovery of HAp, metal such as bronze, copper, etc. were used as orthopaedic implants in bones and teeth. [77] However, using such materials as implants resulted to lot of infections in organisms, especially when they corrode inside the bodies of living organisms. For this reason, it was thought that using HAp as filler materials in such coatings or prosthetic implants will help to promote bone ingrowth and at the same time reduce the corrosion of metals. However, its application as filler material for implants is limited to cases where heavy loads are involved because of its brittleness and high modulus limit. [78] Nonetheless, such applications necessitates that, the films are transparent, porous and well attached to the surfaces of the implants.

Its application has gone beyond medical, or pharmaceutical. Recent researches showed that it can also be used as packing media for column chromatography, gas sensors, catalysis, and as a host materials for lasers. [79] [80] The morphology of synthetic HAp, which dictates most of its surface properties such as protein absorption, can also be altered to form HAp with different morphology and properties. [81]

These key attributes, especially in artificial implantations and therapies, led to the development of many synthetic routes in synthesizing HAp that truly mimics the natural form i.e. HAp that will be able to interact with and replace natural biological materials without resulting to complications.

The synthesized HAp comes in two forms; porous or dense, the former been given more attention by many researchers because of the increased surface area it results to. The size

of the pores, which is responsible for the surface area, is one of the most important features to consider when synthesizing this material. This is because, when used as implants, the pour size will affect both the cell growth and bone ingrowth. [78] However the pore size is dependent on pH, [82] synthetic technique, salt-to surfactant ratio, the calcination temperature, [73] the period of calcination, etc. Studies carried out by Matsumato et al., [73] confirmed that calcining at lower temperatures gives HAp particles with higher surface area and higher solubility whereas, calcining at higher temperatures give the opposite.

The synthetic methods are currently grouped into two: solid state and wet synthesis. Solid state methods include sol-gel synthesis, [64] emulsion technique, [83] mixed surfactant-mediated approach, [84] low-temperature hydrothermal process, [85] etc., whereas wet methods include; precipitation, hydrolysis and many others. All these methods focus on synthesising HAp that will exhibit all the features of the naturally-occurring HAp, such as small pore sizes and large pore volume. Tong et al., [86] recently (2013) employed a very neat, cheap, fast, and low energy ultrasound-assisted microwave technique to synthesize nanometer-size HAp particles with pore size of approximately 2-3 nm. Their method was completely surfactant-free and the synthesized HAp particles were highly crystalline and impurity-free. However, the surface areas from their method were only 79.74 and 45.41 m^2/g for the uncalcined and the calcined (500^oC) powders respectively, which is regarded relatively low. These low surface areas in their products portraits the importance of templating agent in the synthesis of mesoporous materials. It also explains why template directing synthesis (sol-gel) is one of the most popular and promising approach in synthesizing mesoporous materials especially HAp. This is because it results to particles with better morphology, and greater adhesion to substrates in the case of thin films. This supramolecular templating technique was successfully developed by Kresge et al. [87] in 1992. They discovered this method while trying to synthesize a silicon-based zeolite

materials. After the discovery of the method, Xinyu Ye et al. [78] were among those that exploited this technique, when they used cetyltrimethyl ammonium bromide (CTAB), a cationic surfactant, to synthesize mesoporous hydroxyapatite thin films of various pore sizes and surface properties. Their study was centred on the influence of the mesopores and pore size on cell attachment and proliferation. However, their research resulted to HAp films with surface area of less than 20 m^2/g. This explains that, even though template-directed synthesis may result to high surface area mesoporous materials, the type of the directing agent plays a more important role. To cater for the effect of the templating agent, Madafumi et al. [88] used a mixed surfactant approach to synthesize HAp powder with record-breaking surface area of 364 m^2/g. Despite the high surface area reported, the numerous expensive precursors used in the synthesis, and the encapsulated calcium stearate (from the templating agent; Tween 60's decomposition) in the HAp core make their synthetic route a less clean approach, because of the difficulty involved in removing all the impurities from the synthesized HAp. These concerns make their method almost inappropriate in HAp applications. Although most of the above stated methods resulted to the synthesis of HAp with uniform pore size and pore distribution, the idea of synthesizing well-ordered HAp with low crystallinity still remains an issue. Low crystallinity is important because, natural hydroxyapatite is not highly crystalline due to the incorporated impurities such as carbonate, sodium and magnesium ions [89] in its structure. Therefore, in order to synthesize an artificial HAp that truly mimics the natural HAp, the degree of crystallinity should not be compromised. Wei Chen et al. [90] capitalized on the rationale that HAp with hexagonal structure and a space group of $P6_3/m$ exhibits anisotropic magnetic properties and therefore the presence of Fe_3O_4 (a magnetic material) nanoparticles can improve the bioactivity, degradation, and crystal orientation of HAp crystals. Their method involves the incorporation of lots of mineral composites such as Mg^{2+}, Na^+, etc. in

order to supress the crystallinity of the HAp particles they intended to synthesize. According to the result they reported, HAp with low crystallinity, high surface wettability, and excellent biocompatibility was obtained. However, the used of Fe_3O_4 and some other minerals in the synthesis process also raised doubt on the impurity level as compared to the natural HAp.

As far as we know, the methods discussed above and some of the other synthetic procedures developed by other researchers still failed to address some key issues that make hydroxyapatite applicable in drug delivery, molecular biology, catalysis, and also as good implant in living organisms. These features include homogeneity of the film on the metal implants, and also the transparency of the films as for the case of microbial applications. Additionally, it can also be seen from the data above that, most of the synthetic techniques reported the synthesis HAp powder rather than films.

The scope of this research ranges from the formation of LLC phosphoric acid proton conductive membranes to the synthesis of high surface area mesoporous hydroxyapatite thin films through the use of LCT synthetic technique. The synthetic method reported in this contribution is a neat LCT- based method that can lead to the synthesis of highly transparent HAp thin films through the use of a non-ionic surfactant; calcium, and phosphorous precursors.

CHAPTER 2

2. EXPERIMENTAL

2.1. Materials

All chemicals were purchased from Sigma Aldrich and used without been stored for long. The concentrations of the PA and calcium nitrate used in the experiment were 85-88% and 99%, respectively. Fresh water obtained from Millipore synergy 185 water purifier was used in the preparation of all samples.

2.2. Sample preparation

2.2.1. Preparation of H_3PO_4 (PA) lyotropic liquid crystalline mesophases:

The LLC phases of these materials were formed in two ways depending on the intended characterization technique to be used. In forming the solution phases for XRD, FT-IR and Raman analysis, known quantities of PA were mixed with 7g of water and 1g of 10-lauryl ether in closed glass vials. The mixtures were stirred with the aid of magnetic stirrers for roughly about 5 hours in order to obtain well homogenized mixtures. This homogenization was shortly followed by spin coatings at reasonable speed (500-700 RPM) on the surfaces of substrates (either glasses or silicon wafers) in order to obtain homogenous films thick enough to be measured by either XRD, Raman, or FT-IR.

The gel phases (for conductivity, POM, isotopization, and DSC analysis) were prepared by adding 1g of 10-lauryl ether to the required quantities of phosphoric acid (exact values shown in **Table 2-1**). The mixtures were made air-tide through the use of teflon tape. All the vials containing different acid-surfactant compositions were put in big beakers and transferred to a shaking water bath. The temperature of the bath was increased above the melting point of the surfactant (40-50 ^{o}C). This process took almost 24 hours and resulted

to the formation of highly viscous gels (with melting points over 100 ^{o}C). **Figure 2-1** below, shows a schematic representation of the two path ways.

Preparation of Different Acid to Surfactant Mole Ratios and their Phases			
Concentration	Mass Of PA (g)	Mass Of Surfactant	Phase
HP2:1	0.368	1.00g	Bicontinuous cubic
HP3:1	0.552	1.00g	2-D Hexagonal
HP4:1	0.736	1.00g	2-D Hexagonal
HP5:1	0.921	1.00g	3-D Hexagonal
HP6:1	1.105	1.00g	Cubic
HP7:1	1.289	1.00g	Cubic
HP8:1	1.473	1.00g	Cubic
HP9:1	1.657	1.00g	Cubic
HP10:1	1.841	1.00g	Cubic
HP11:1	2.025	1.00g	Cubic
HP12:1	2.209	1.00g	Cubic
HP13:1	2.393	1.00g	Cubic
HP14:1	2.577	1.00g	Cubic
HP15:1	2.762	1.00g	Cubic
HP16:1	2.946	1.00g	Cubic
HP17:1	3.129	1.00g	Cubic
HP18:1	3.314	1.00g	Cubic
HP19:1	3.498	1.00g	Cubic
HP20:1	3.682	1.00g	Cubic

Table 2-1. Sample preparation.

2.2.2. Preparation of HAP precursor-surfactant mesophases

2 g of $C_{12}EO_{10}$ surfactant) was added to 7 g grams of water in a pre-cleaned and dried vials. The mixtures were placed on a magnetic stirrer and stirred for 30 minutes for homogenization. This step was followed by the addition of the required masses of calcium nitrate (masses depend on the intended concentration) to the mixture and stirred for another 30 minutes. Finally, the required amount of PA was added to the well homogenized

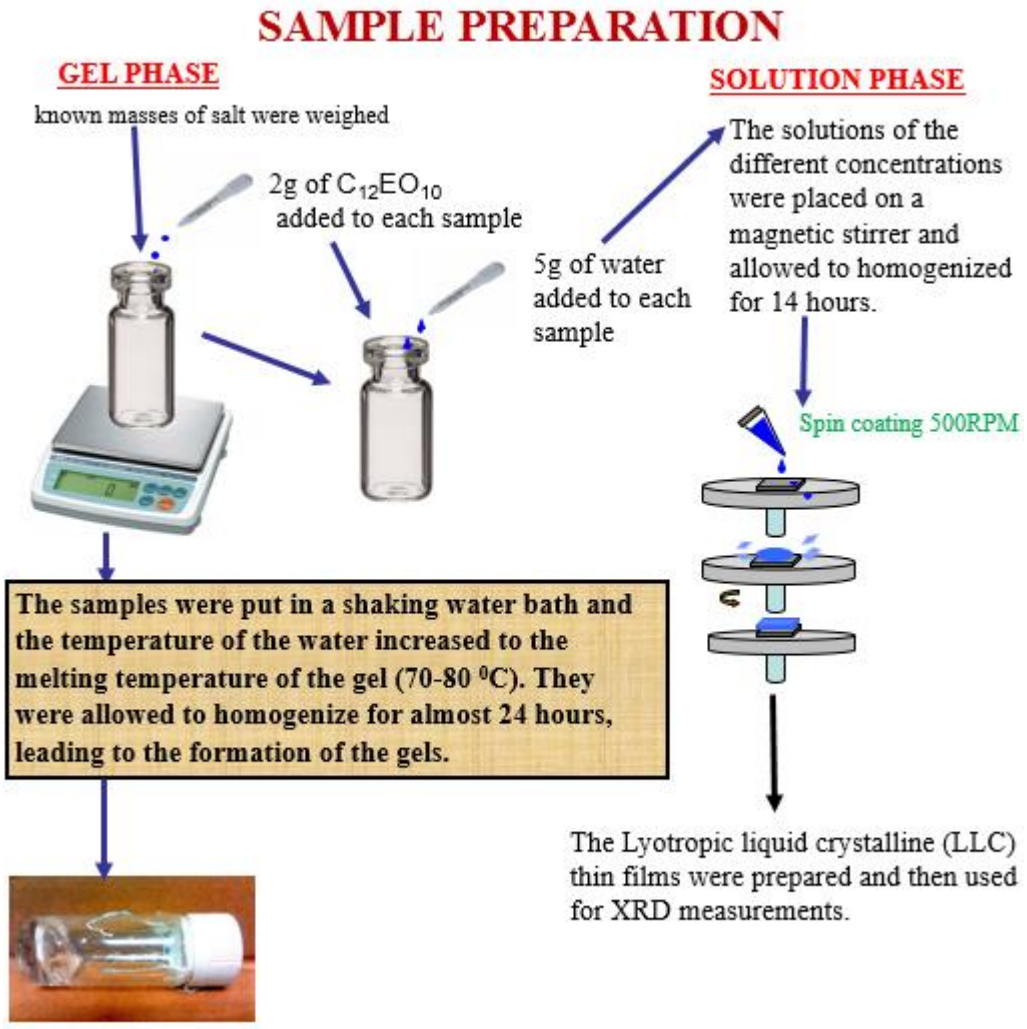

Figure 2-1. Schematic representation of sample preparation.

Preparation of HAp Samples			
Concentrations	Mass of H_3PO_4 (g)	Mass of $Ca(NO_2).4H_2O$(g)	Mass of Surfactants(g)
HAp 5-3	0.552	1.886	2
HAp 6.67-4	0.736	2.514	2
HAp 8.33-5	0.921	3.1425	2
HAp 10-6	1.105	3.499	2
HAp 11.67-7	1.289	4.083	2
HAp 13.33-8	1.473	4.665	2
HAp 15-9	1.657	5.249	2
HAp 16.67-10	1.841	5.833	2

Table 2-2. Masses of HAp precursors used.

mixture in a drop-wise method and stirred for another 2 hours at RT. Table 2-2 shows the masses of each of the precursors used in the synthesis.

2.2.3. Preparation of the HAp and PA thin films

After homogenizing the solutions for about 24 hours, small portions of the clear mixtures were coated on 25 by 75 mm glass slides through the use of a spin coater spinning at a speed of 5000 RPM. This fast spin coating enables the rapid evaporation of excess water from the samples in order to form the LC mesophases. The films were very thin and remained stable under ambient conditions for more than a month (the stability will be discussed in chapters 3).

2.3. Instrumentation

2.3.1. X-Ray Diffraction (XRD)

The XRD patterns of the fresh and aged films of both PA and HAp, and also the powders of HAp were recorded on a Rigaku Miniflex diffractometer using a high power Cu-Kα source operating at 30kV/15mA and a wavelength of 1.5405 Å. For the case of the uncalcined films, the measurements were carried out by spin-coating the solutions on glass substrates while for powder samples, enough samples were collected by scrapping the films coated on glass substrates. In cases of very high intensity diffraction lines, lines capable of inflicting harm on the detector, Cu plate was used as 'block' to reduce the intensity by a factor of ten (10). The measurements for both the films and powder samples were done at scan rate of 1 Θ/min at 0.01 data intervals.

2.3.2. Polarized Optical Microscopy (POM)

The POM images were obtained in transmittance mode by using a ZEISS Axio Scope.A1 polarizing optical microscope. For measuring the isotropization temperatures of the samples, Linkam LTS350 temperature controlling stage was attached to the microscope and the temperature controlled using a LinkamT95-LinkPad temperature programmer attached to the stage. The cooling of the samples was achieved through the help of a liquid N_2 in a dewar connected to the stage and the N_2 level of the environment was controlled with a temperature cooling chamber to make a 100% N_2 environment. The heating and cooling procedures were varied between 1 and 5 degree/ minute and the images of the phase transitions were captured with an inbuilt camera, attached at the top of the microscope.

2.3.3. Fourier Transform - Infrared Spectroscopy (FT-IR)

The FT-IR spectra were recorded using a Bruker Tensor 27 model FTIR spectrometer. A Digi Tect TM DLATGS detector was used with a resolution of 4.0 cm^{-1} in the 400-4000 cm^{-1} range. The spectra were recorded by either spreading the samples on silicon wafers or by using KBr pallets (for the case of powder samples). The FT-IR spectra of the samples were collected using 64, 128, or 256 scans.

2.3.4. Micro-Raman spectroscopy

The micro Raman spectra were recorded on a LabRam confocal Raman microscope with a 300 mm focal length. The spectrometer is equipped with a Ventus LP 532, 50 mW, diode pumped solid-state laser operator at 20 to 34 mW, with a polarization ratio of 100:1, a wavelength of 532.1 nm, and a 1024x256 element CCD camera. The signal collected was transmittance via a fiber optic cable into a spectrometer with 600 g/mm grating. The Raman

spectra were collected by manually placing the probe tip on the desired point of the sample over the glass or silicon wafer.

2.3.5. AC Impedance Spectroscopy

The conductivity measurements were performed by using Gamry G750 potentiostat/galvanostat operating at an AC voltage of 10 mV and within a frequency range of 0.1 to 300 kHz. The cells used in the instrument were all homemade; made from either one or two fluorine doped thin oxide (FTO) coated glass (es) shown in **Figure 2-2**. For the case of the two FTO coated glasses, the cell constants were determined from the cells' dimension, while for the single FTO coated glass, the cell constants were determined by first using a standard solution of KCl with known conductivity value. The construction of these cells will be discussed in **Chapter three**. In the two electrode system, the reference and counter (short cut) electrode were attached to one of the FTO coated glasses while the working electrode was attached to the other. On the other hand, both the short cut electrodes (reference and counter) and the working electrodes were attached to the same FTO; one at either side, for the 'one FTO' system.

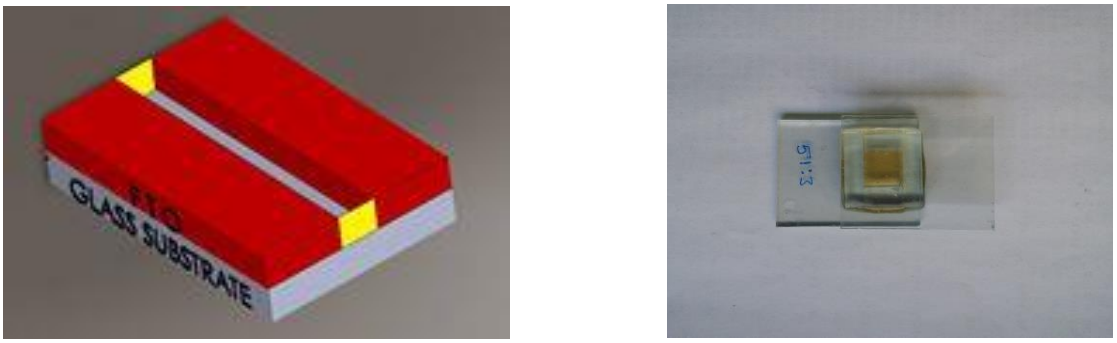

Figure 2-2. Homemade cells used in the conductivity measurements a) a single FTO system in which the gel was placed between the two sides of the FTO separated by strip made by a diamond cutter b) two FTO separated by ordinary glasses of known dimensions.

2.3.6. Scanning Electron Microscopy (SEM)

The SEM images were obtained using ZEISS EVOS-40, operating at 15kV. The samples were first spin coated on glass slides, calcined at the required temperatures, and carefully scraped from glass substrates with clean glasses before been finally placed on the surfaces of aluminium sample holders covered with carbon adhesive tabs.

2.3.7. Transition Electron Microscopy (TEM)

The high resolution transmission electron microscope (HRTEM) images were collected using JEOL JEM 2100F operating at a voltage of 200 kV.

2.3.8. The N_2 (77.4 K sorption measurements)

The gas sorption measurements were carried out using a TriStar 3000 automated gas adsorption analyser (micrometrics) in the relative pressure range, P/P_o, from 0.01 to 0.99 atm. The saturated pressure was measured over 120 minutes intervals. The surface areas of the different samples measured were calculated in the range 0.05 to 0.3 atm relative pressure with 5 points.

CHAPTER 3

3. RESULTS AND DISCUSSIONS

3.1. H_3PO_4- $C_{12}EO_{10}$ lyotropic liquid crystalline system

Many transition metal salts with soluble counterions such as those containing chloride and nitrate are already known to be good solvents in the formation of salt-surfactant mesophases. Studies on these phases showed that weak forces of attraction such as hydrogen bonding are responsible for the high thermal and structural stability arising from phases formed by such salts. However, the idea of using acids, bases, or deliquescence liquids in general as solvents for assembling surfactant molecules have just been briefly reported even though many acids have very low DRH values. This study shows that, phosphoric acid (PA) with three protonic hydrogen atoms attached to highly electronegative oxygen atoms can also be used as solvent in the formation of stable phases. It forms stable phases through the formation of acid-acid, acid-surfactant and or acid-water hydrogen bonded networks. Additionally, all the phases formed by these mixtures were highly conductive owing to the fast proton mobility among the confined PA species in the hydrophilic domains of the mesophases.

3.1.1. LLC mesophases of phosphoric acid

Samples of different acid to surfactant mole ratios were studıed using XRD, FTIR, Raman spectroscopy, etc. The compositions prepaıd range from 2 to 20 PA/$C_{12}EO_{10}$ mole ratio, which is so far the highest ever reported concentration in the literature for the solvent-surfactant system. With the exception of the 2 mole ratio, were leaching of surfactant crystal was observed shortly after the formation of mesophase, because of the inability of the extremely low acid concentration to organize the surfactant molecules, all other

compositions showed high stability. The XRD data of the spin coated films in **Figure 3-1** shows high intensity small angle diffraction lines of both the freshly spin coated samples and the aged samples. A closer look at the diffraction lines shows that, the 2Θ values were not significantly affected by the increasing PA concentration. This observation is in odds

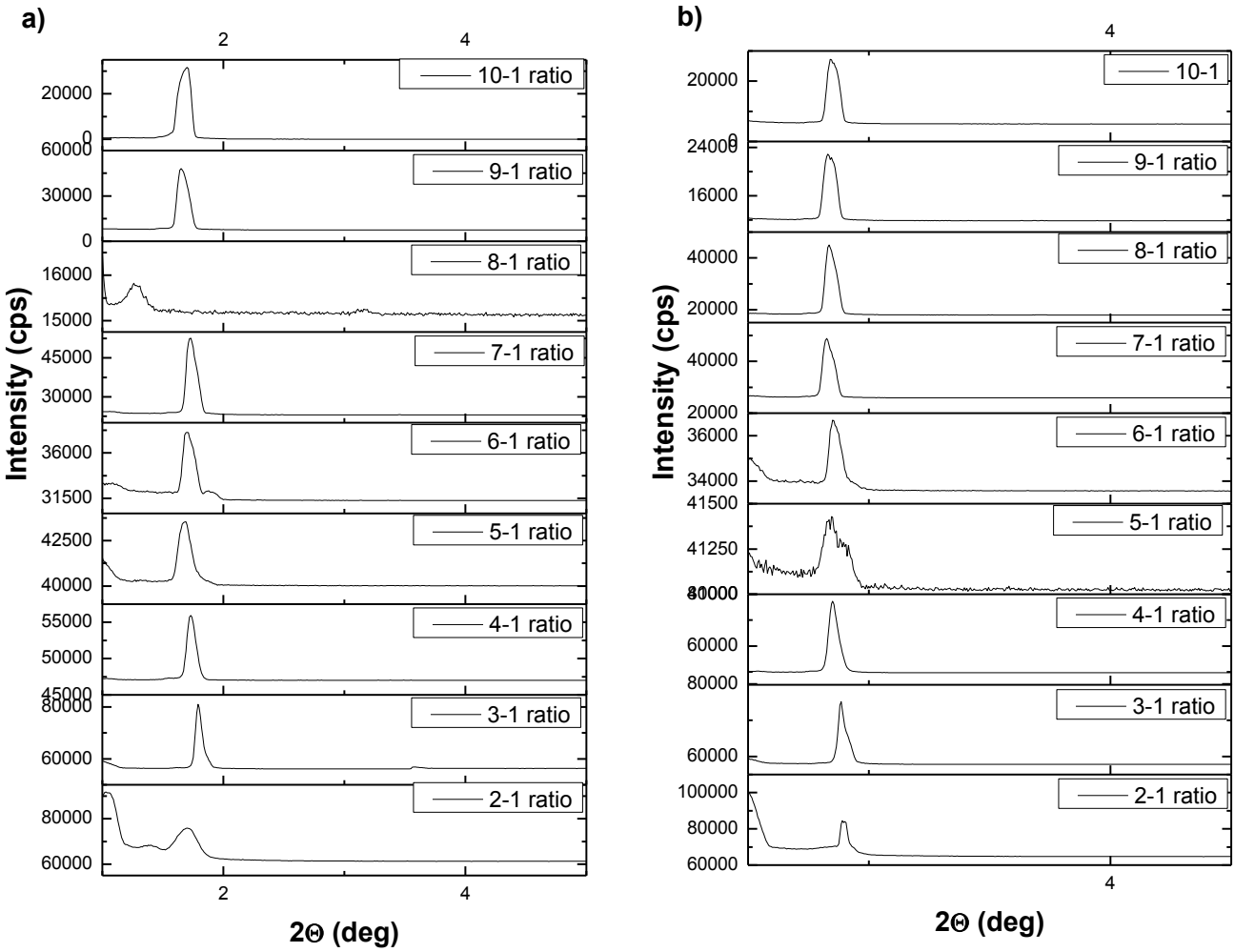

Figure 3-1. XRD patterns of PA-$C_{12}EO_{10}$ between 2 and 10 PA/$C_{12}EO_{10}$ samples a) fresh samples b) aged for 1 week.

with the observed trend in the d-spacing values of most salt-surfactant mesophases, were increase in salt concentrations usually results to increase in the d-spacing values. The explanation for such observation in the salt-surfactant system is based on the expansion of the micellar hydrophilic domains which occurs when more salt molecules are added to the mesophases. With such expansions, the micellar units are pushed further apart causing an

increase in the lattice parameters of the crystalline structures. For the phosphoric acid (PA) case, such changes were not observed. Instead, the aggregation number (AN) in the micelle domains shows a response to the increasing number of PA in the media. We believe that, the AN of the surfactant in the mesophase decreases with increasing PA concentration in the media. This decrease in the AN causes the formation of more micellar units in the mesophases, thus enabling more PA molecules to be incorporated in the meso-structure. Such changes in the AN, prevents the expansion of the hydrophilic domains of the mesophase, which could have been caused by the excessive PA molecules.

The first diffraction lines of each of the studied compositions are highly intense, indicating a long range order in the planes they are originating from. Because of such high intensities, other diffraction lines such as (110), (200), (210) etc. diffraction lines (orientation on the other axis) are heavily overshadowed and thus very hard to observe. The samples were first aged for weeks and later for months but they remained stable in the gel phase and the diffraction lines never fail to appear (shown in the XRD data, Figure 3-1**b** above). This high stability was attributed to both the hygroscopic nature of phosphoric acid and the extensive hydrogen bonding occurring within the phosphoric acid molecules themselves, with water, and also with the surfactant molecules' hydrophilic head groups.

Figure 3-2a shows a schematic representation of the interactions between the highly polarized hydrogen atoms of phosphoric acid and the oxygen atoms of other phosphoric acid molecules. Being a very weak acid in aqueous media, little or no dissociation was expected in the mesophases of the samples. This assumption was proven by the spectroscopic studies of the mesophases (discussed in later sections), which show very similar FT-IR spectra as compared to pure phosphoric acid. In the scheme below, it's

a)

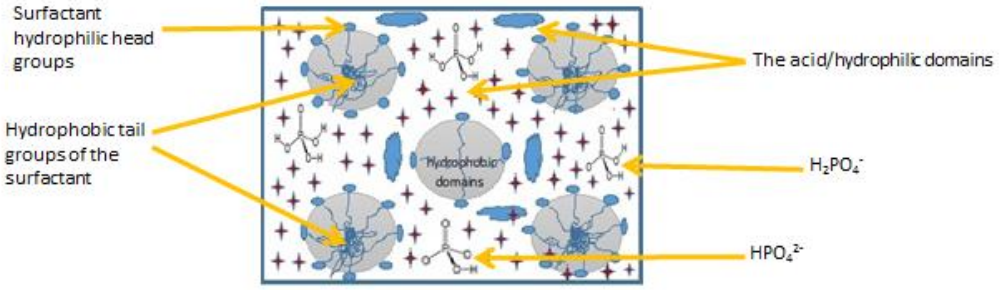

b)

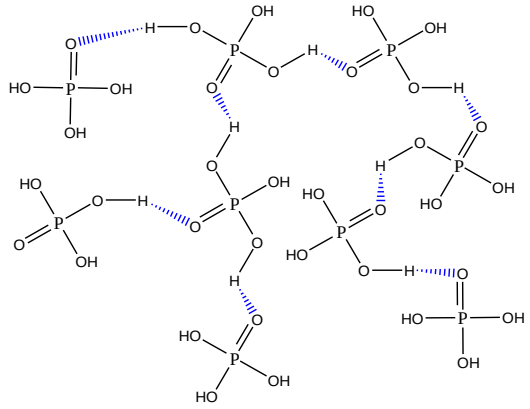

Figure 3-2. a) Schematic representation of the interaction between the surfactants' head groups and the phosphoric acid molecules b) interactions between the acid molecules.

assumed that 99 % of the acid still remain in the pure acid form while small quantity of the acid dissociates into $H_2PO_4^-$, small amount of HPO_4^{2-}, and undetectable amount of PO_4^{3-} ions due to the chemical equilibrium. Based on this, we assumed an infinite chains of hydrogen bonded phosphoric acid molecules between the domains as shown in **Figure 3-2b.**

Samples with acid concentrations higher than 10 mole ratios: from 11 to 30 mole ratios, were also investigated. Their fresh samples shown in **Figure 3-3a** also showed a similar small angle diffraction lines as observed in the lower concentrated samples. Surprisingly,

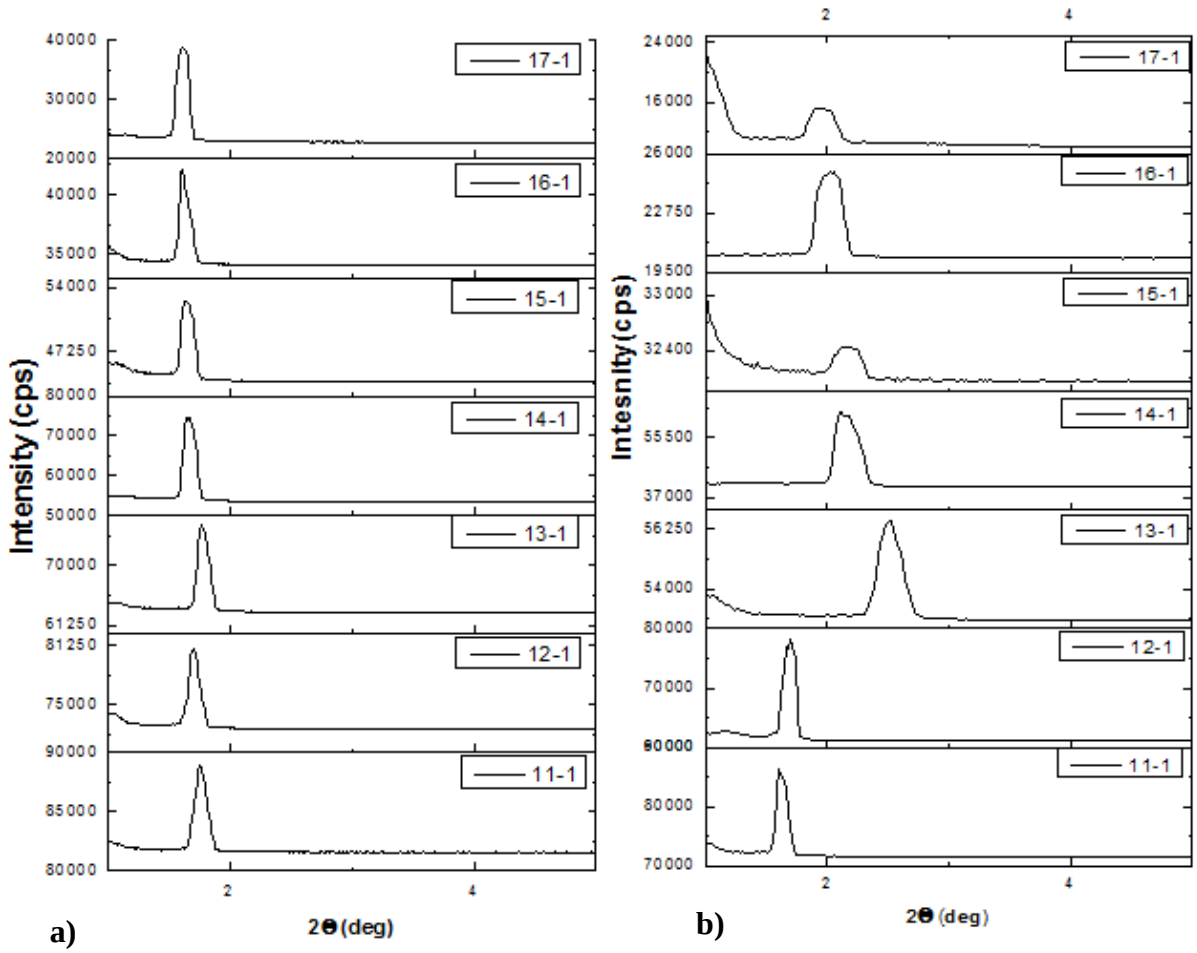

Figure 3-3. High acid to surfactant mole ratios. a) showing the fomation of phases b) the stability of the phases.

the d-spacing values did not also show much changes even though the acid-surfactant concentrations were much higher.

In terms of stability of mesophases, samples from 11 through 13 mole ratios show similar stabilities as observed in the lower-concentrated samples, but samples with higher acid concentrations (from 14 to 30) than the aforementioned ones were not very stable, **Figure 3-3b**. Their stability was affected by the high amount of the acid which makes the LLC phase to exhibit similar behavior as pure H_3PO_4. In such high concentrations, we assumed that the maximum number of micellar units with the lowest possible AN that could be formed by the surfactant have already been exhausted. Therefore, excessively high PA

concentrations changed the chemical properties of the mesophase i.e. the mesophases change from surfactant-dominant phase to acid-dominant phase. This may perhaps be the reason for the humidity-dependent diffraction lines observed in some of the higher concentrated samples. The presence of only one diffraction line in most of the samples makes it impossible to determine the exact crystal structure of the mesophases. Therefore, polarized light optical microscopy (POM) images were also recorded in order to elucidate the phases of some of the compositions.

3.1.2. Phases from the polarized optical microscope (POM) images

As observed from the small angle diffraction patterns of the samples above, all the samples diffract a single line, making it almost impossible to determine the mesostructure of each of the composition. Therefore, one could only confirm the presence of the phases but could hardly say anything regarding the crystal structure of these phases. For this reason, small quantity of each sample was placed on a glass slide and the excess water allowed to evaporate under ambient conditions. This led to the formation of very viscous gels, which could be observed in between the crossed polarizers of a POM. The lower concentrated samples were birefringent and show perfect focal conic fan-like textures, corresponding to 2-D and 3-D hexagonal phases. This texture was observed within a small concentration range: 3, 4, and 5 mole ratios. However, as the concentration of the acid increases, the texture also changes due to the continuous change of phases in the structure in order to accommodate more acid molecules in the hydrophilic domains. At concentrations higher than 5 mole ratio, the phases did not show birefringence between the crossed polarizers. This information suggest that, such samples may possibly be in the cubic phase.

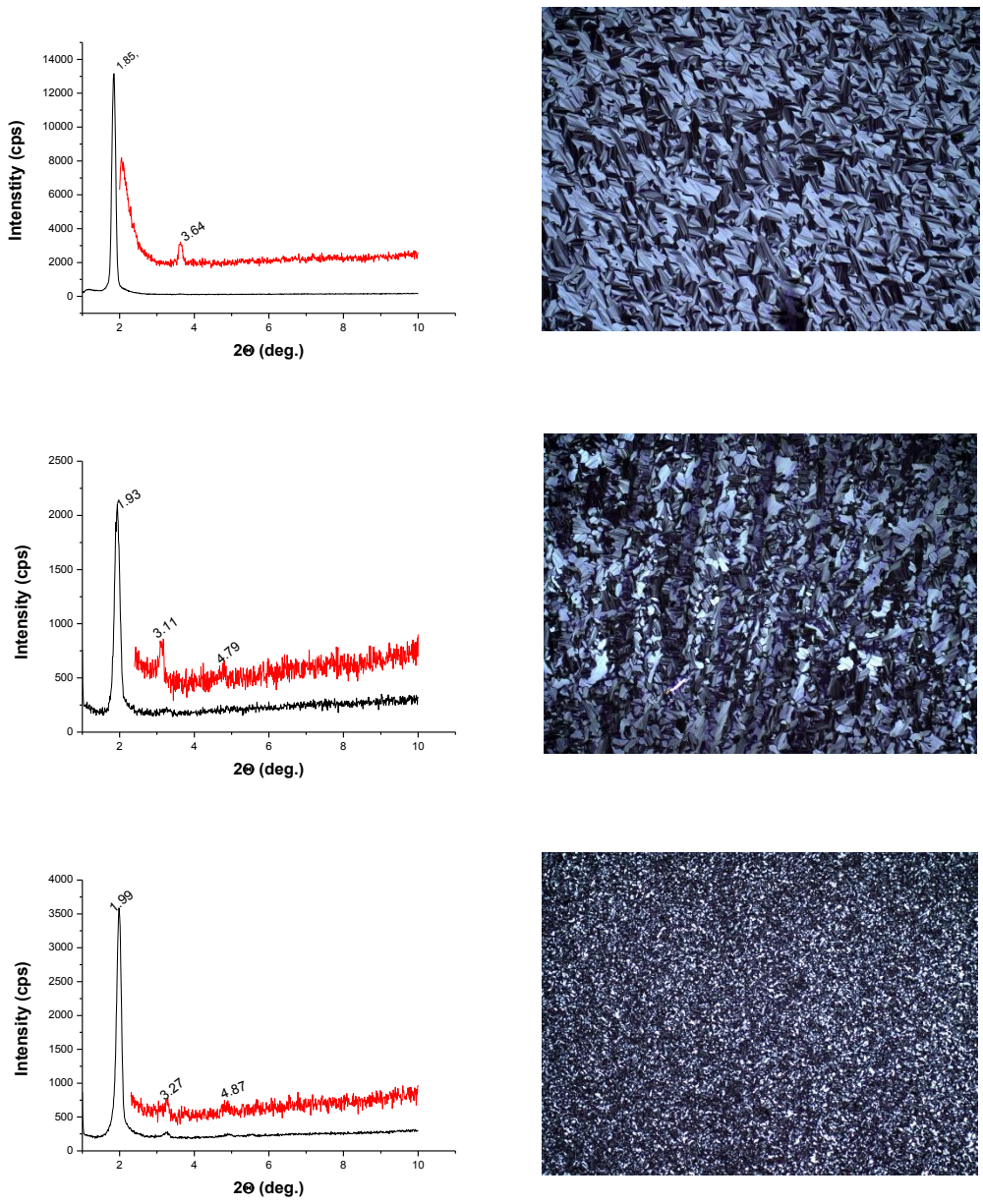

Figure 3-4. The small angle diffraction pattern and POM images of the lower concentrated samples showing 2D and 3D hexagonal phases.

The textures observed in the POM images for the lower concentrated samples prompted the need to re-run the XRD patterns for the 3 through 5 mole ratios. In this time around, large quantities of gel were prepared in a binary system through the help of shaking water bath. The gels were then smoothly smeared on powder XRD sample holders and the data for each of the different compositions were collected by slowly measuring with a scan speed of 0.2 degree per minute, starting from 1.0 degree to 5.0 degree (2Θ values). In many case,

the orientation of the gels on the sample holders were manually destroyed by rubbing clean glass plates over their surfaces. This removes the preferential orientation in one direction and may allow the observation of other diffraction line(s) which could not be detected in the oriented sample. This means that some of the compositions were measured many times. In the 3 PA-$C_{12}EO_{10}$ mole ratio as shown in **Figure 3-4**, very clear diffraction lines can be seen at 1.85 and 3.64^o 2Θ values corresponding to (100) and (200) planes. This data combined with the POM image, confirmed that this sample is in 2- D hexagonal phase. Careful study of the POM and the XRD data of the 5 mole ratio showed that, this composition is in the 3-D hexagonal phase with clearly visible diffraction lines at 1.99, 3.27 and 4.87^o 2Θ values corresponding to the (002), (110), and (300) planes, respectively. Similar to the 5 mole ratio, three distinct diffraction lines were also observed at 1.93, 3.11, and 4.79^o 2Θ values of the 4 mole ratio. The relationship between the successive lines observed in the 4 and 5 ratios were also identical. For examples, dividing the 2Θ of the third peak with that of the first peak in both cases gave approximately 2.45. This may mean that both compositions are in the same phase.

Slow XRD measurements were again performed for the gels assumed to be in the cubic phase. By randomly disturbing the orientations of the gels on the sample holders, we were able to observe different peaks at successive measurements, **Figure 3-5.** Lines from (110), (111), (200), (210) and (211) planes were clearly observed in the 6 mole ratio while, other planes such as (110), (111), (210), (310) and (321) were also observed for the 10 mole ratio. Analysis of these planes confirmed that both of these two compositions are in the cubic phase.

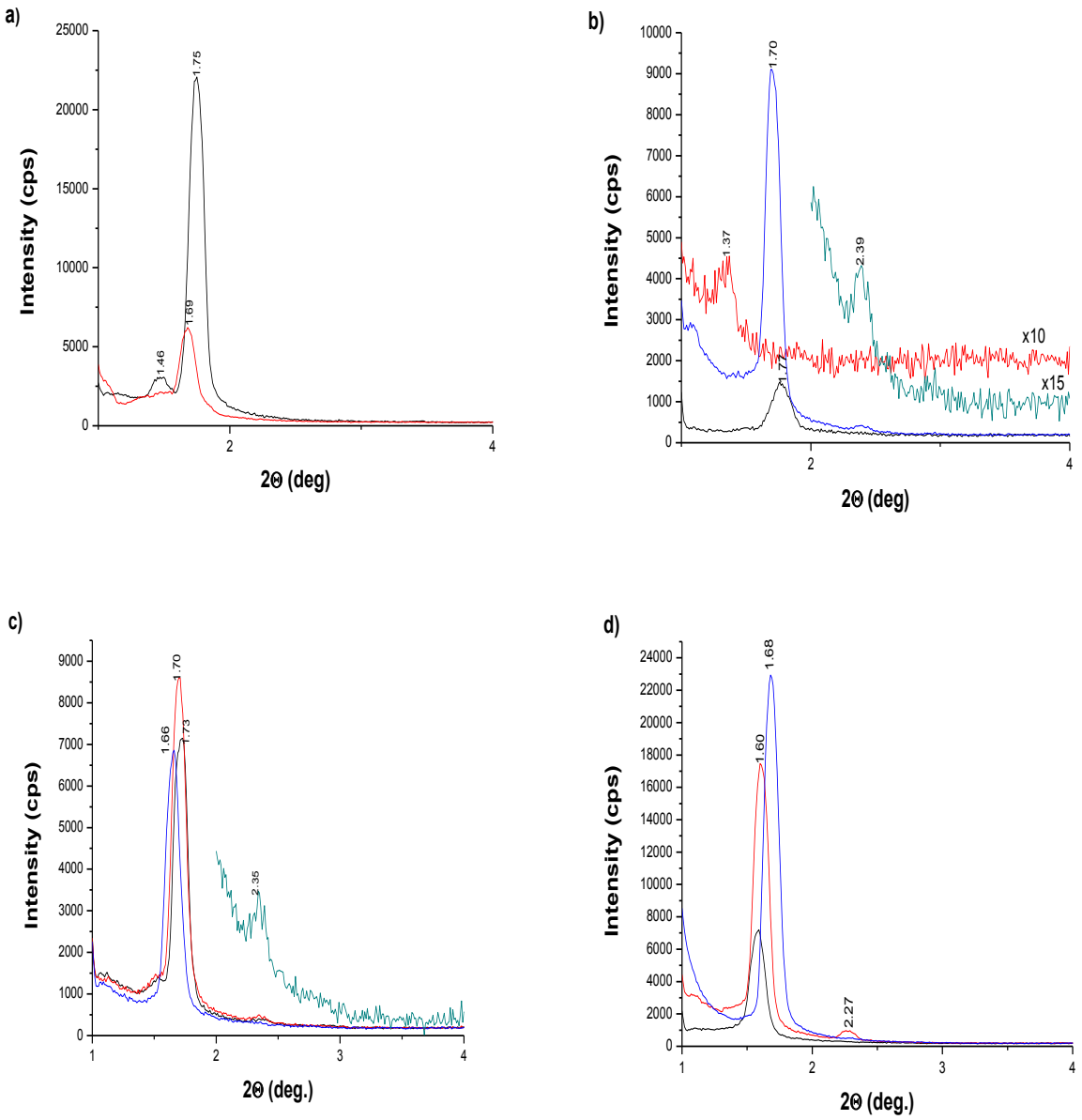

Figure 3-5. XRD data of PA Gels in the cubic phase a) HP 6/1 b) HP 10/1 c) HP 14/1 and d) HP 16/1 ratio.

3.1.3. Spectroscopic studies of pure phosphoric acid

Both FT-IR and Raman data of pure PA were collected and analyzed, as controls for the investigations in the mesophases. **Figure 3-6** is a time-dependent FT-IR behavior of pure phosphoric acid. From this data, it can be clearly seen that pure phosphoric acid gives strong

phosphate absorption peak at 494 cm^{-1}, corresponding to the bending modes of the symmetric and the antisymmetric OPO in H_3PO_4 and $H_2PO_4^{2-}$ respectively. [92] The other sharp peak at 886 cm^{-1} corresponds to both the symmetric mode of PO_2 in $H_2PO_4^{2-}$, and also the antisymmetric stretching mode of $P(OH)_3$) in H_3PO_4. [92] The peak at 995 cm^{-1} belongs to the bending mode of POH in H_3PO_4 and also the antisymmetric stretching mode of $P(OH)_2$ in $H_2PO_4^-$. [92] Another peak, also belonging to the antisymmetric stretching vibrations of PO_2 in $H_2PO_4^{2-}$ was observed at 1130 cm^{-1}. The shoulder at approximately 1238 cm^{-1} corresponds to the stretching mode of P=O of phosphoric acid. [92] The water peaks, as always, show absorption signals at 1642 cm^{-1} and also at 3578 cm^{-1} due to the deformation and antisymmetric stretching modes of O-H groups in water molecules, respectively. The time-dependent measurement also shows increasing absorption with time in the phosphate bending and stretching regions. The two peaks at 995 and 1130 cm^{-1} also became more distinct as the acid absorbs more water from the surrounding. Additionally, the spectra also show the emergence of a new

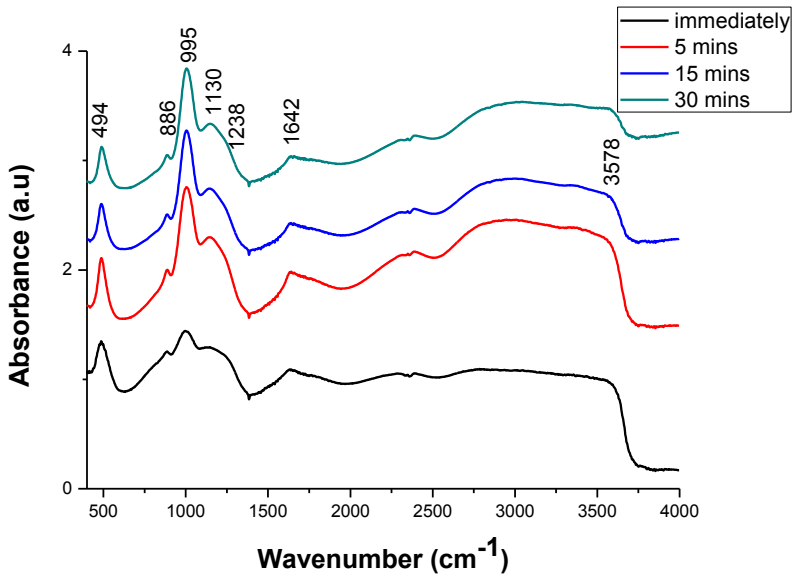

Figure 3-6. Time-dependent FT-IR data of pure phosphoric acid.

broad OH peak at 2373 cm^{-1}, which could also be attributed to the increasing quantity of water in the phosphoric acid sample, causing some little dissociations and hence more hydronium ions (H_3O^+) and hydrogen bonding. Measurements taken after 30 minutes in the time-dependent investigation are not included in these spectra. This is because, after the above stated time, the sample absorbed so much moisture from the atmosphere that it started flowing down the silicon wafer, thus making the signal between 2500 cm^{-1} to 3500 cm^{-1} too noisy.

The Raman data of pure phosphoric acid was also collected and analysed. In the data shown in **Figure 3-7**, the high intensity peak at 899 cm^{-1} corresponds to the antisymmetric

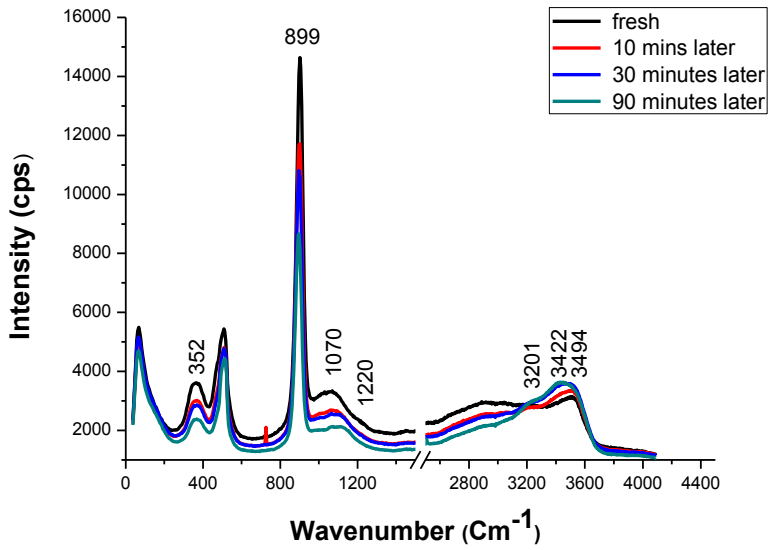

Figure 3-7. Time-dependent Raman spectra of pure phosphoric acid.

stretching mode of the $P(OH)_3$ in pure phosphoric acid. [92] The broad band at around 1070 cm^{-1} corresponds to the symmetric stretching mode of (PO_2) in $H_2PO_4^{2-}$. It is the only band of $H_2PO_4^{2-}$ that does not overlap with the modes of H_3PO_4. [92] The shoulder at around 1220 cm^{-1} most like corresponds to the symmetric stretching of the (P=O) in H_3PO_4 and also the bending (POH) mode in $H_2PO_4^{2-}$. The characteristic water peak at 3494 cm^{-1}

was also observed to shift to low wavenumber (3422 cm^{-1}) due to the increasing quantity of the hydrated water in the acid sample. The other emerging broad peak at 3201 cm^{-1} further shows the increasing quantity of the hydronium ions in the sample.

3.1.4. Spectroscopic study of PA-$C_{12}EO_{10}$ mesophases

Prior knowledge of the spectroscopic behavior of pure phosphoric acid aided us to properly analyze the H_3PO_4 in the mesophases. Similar to the pure phosphoric acid case, both Raman

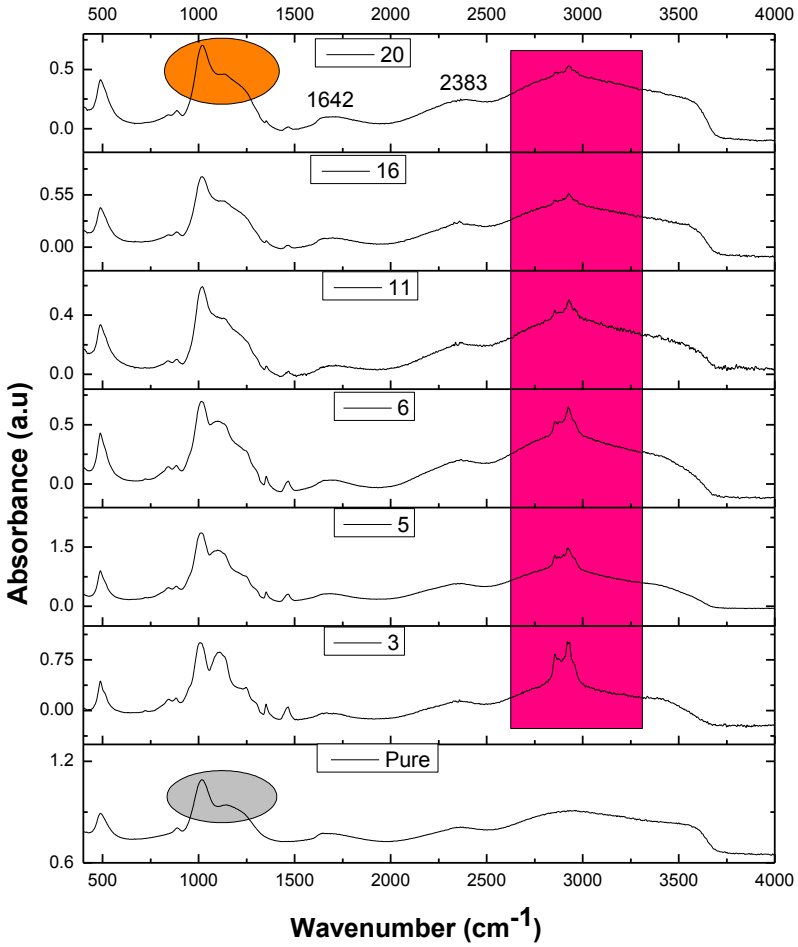

Figure 3-8. FT-IR spectra of the lyotropic liquid crystalline H_3PO_4 with different concentrations (ratios indicated in the upper right of the plots).

and FT-IR spectroscopy were employed in fully accessing the impact of surfactant/hydrogen bonding in the lyotropic liquid crystalline samples. **Figure 3-8** shows red shift in both the bending and the stretching modes of the H_3PO_4 and $H_2PO_4^-$ species. This shows interactions within the species mentioned above, and also with the surfactant's ethoxy groups. However, the bending mode of pure water, which was observed as a sharp peak at 1642 cm^{-1} in the pure phosphoric acid spectra started getting broader and more intense. In addition to that, the broad H_3O^+ peaks which started emerging at around 2383 cm^{-1} in the time-dependent FT-IR studies of the pure PA became more distinct in the LLC phases of the acid. This could perhaps be explained by the extensive hydrogen bonding resulting from the occupancy of the micellar domains of the surfactant by the acid molecules. This confinement effect brings together the acid molecules in close proximity and hence enables the formation of excessive hydrogen bonding between them. It was also observed that the water stretching peak at around 3572 cm^{-1} shifted to lower wavenumbers with increasing concentration of the acid in the mesophases. This also shows enhanced hydrogen bonding of the water species interacting with both PA and surfactant head groups.

3.1.5. The stability of PA-$C_{12}EO_{10}$ mesophases

The LLC gels of different samples were smoothly spread over silicon wafers and their stabilities monitored with time using FT-IR spectroscopy. Each of the gels' stability was monitored for at least a whole week and the results, shown in **Figure** 3-9**,** indicates that, the samples are totally insensitive to atmospheric water/moisture, which is a clear manifestation of the high stability of the gels. However, the stability of the gels decreases with increasing PA concentration. From the FT-IR data, it can be clearly seen that the 4 mole ratio is more stable than the 11 mole ratio, and the 11 mole ratio is more stable than

the 19 mole ratio. It was also realized that samples with lower

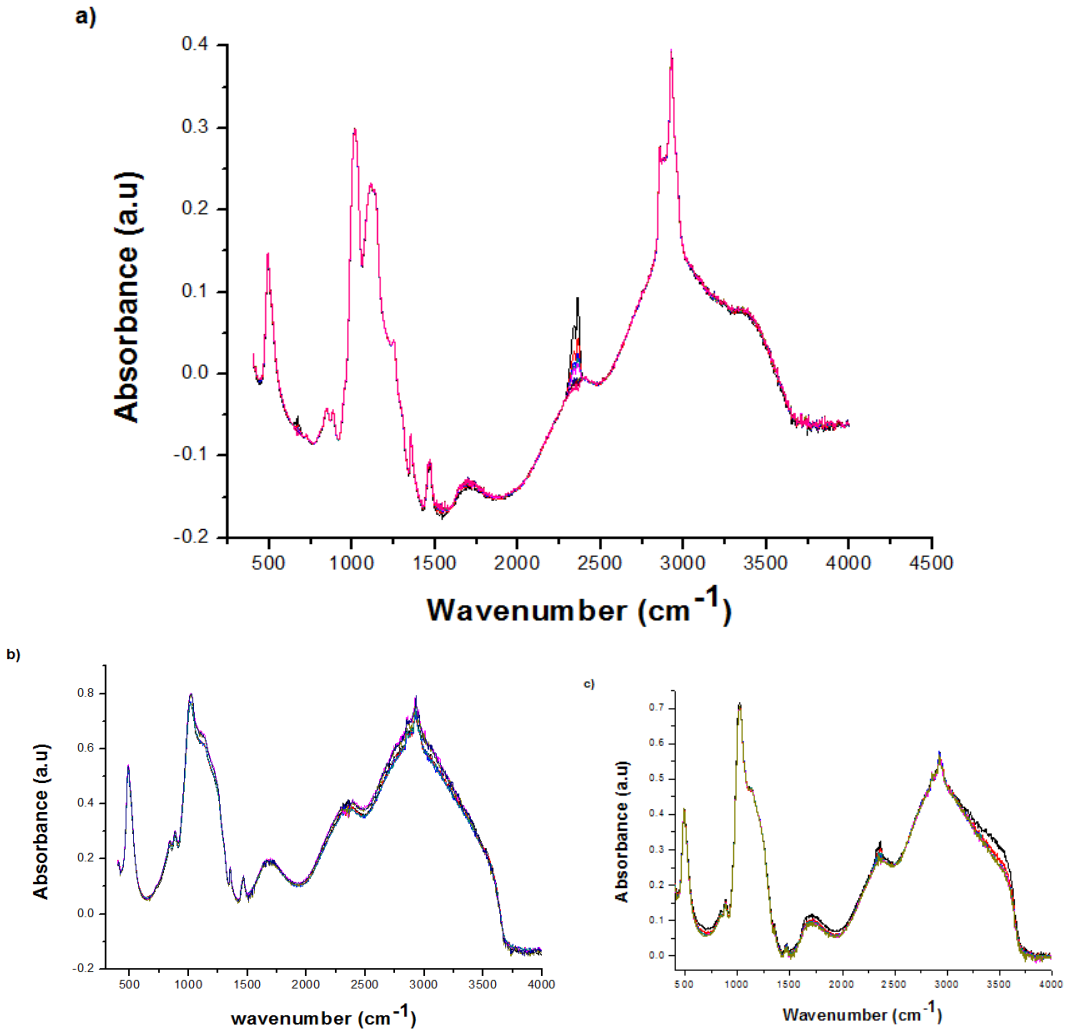

Figure 3-9. The FT-IR spectra showing the stability of gels of different compositions a) 4/1, b) 11/1 and c) 19/1.

acid to surfactant ratios (6 to 15) were highly viscous (viscosity was approximated from the isotropization measurements and will be discussed later), with melting points above 120 ^{o}C whereas, samples with extremely high acid to surfactant ratios (17 to 20) were not very viscous and have melting points of less than 100 ^{o}C. The decrease in isotropic temperatures for the highly concentrated samples was not surprising, since most of them show high resemblance to pure phosphoric acid. Therefore, their high hygroscopic nature will influence the quantity of water they absorbed from the environment. This is what led

to their lower melting points. This data also clearly provide extra evidence that the broad H_2O bending bands at 1632 and the stretching OH band of H_3O^+ at 2383 cm^{-1} increase in intensity as the ratio of acid to surfactant increases.

3.1.6. Isotropization measurement

In measuring the isotropization temperatures of the anisotropic (3 to 5 ratio) samples, small quantities of the LLC phosphoric acid gels that were prepared in a binary system were smeared on ordinary glass slides and covered with much thinner glasses, the edges of which, were sealed with thermoplastic in order to avoid evaporation of water at high temperatures. The samples were then placed on a hot plate attached to POM and the temperature increased or decreased at rates between 2 and 3^o per minute. For the higher concentrated samples, their melting points could not be exactly determined due to the absence of birefringence. However, they could be approximately determined by placing them in an oven and carefully observing the temperature at which melting occurs. **Figure 3-10** shows the thermal behaviors of the 4 mole ratio sample, showing high thermal stability of the gel phase in both high and low temperature regions. This sample melts at 97 ^{o}C as indicated by the disappearance of the texture but the phase failed to collapse even at temperatures below -150^{o}C (not shown in the data). The same analysis was also done for the 3 and 5 PA/$C_{12}EO_{12}$ mole ratios and the whole data tabulated in **Table 3-1**.

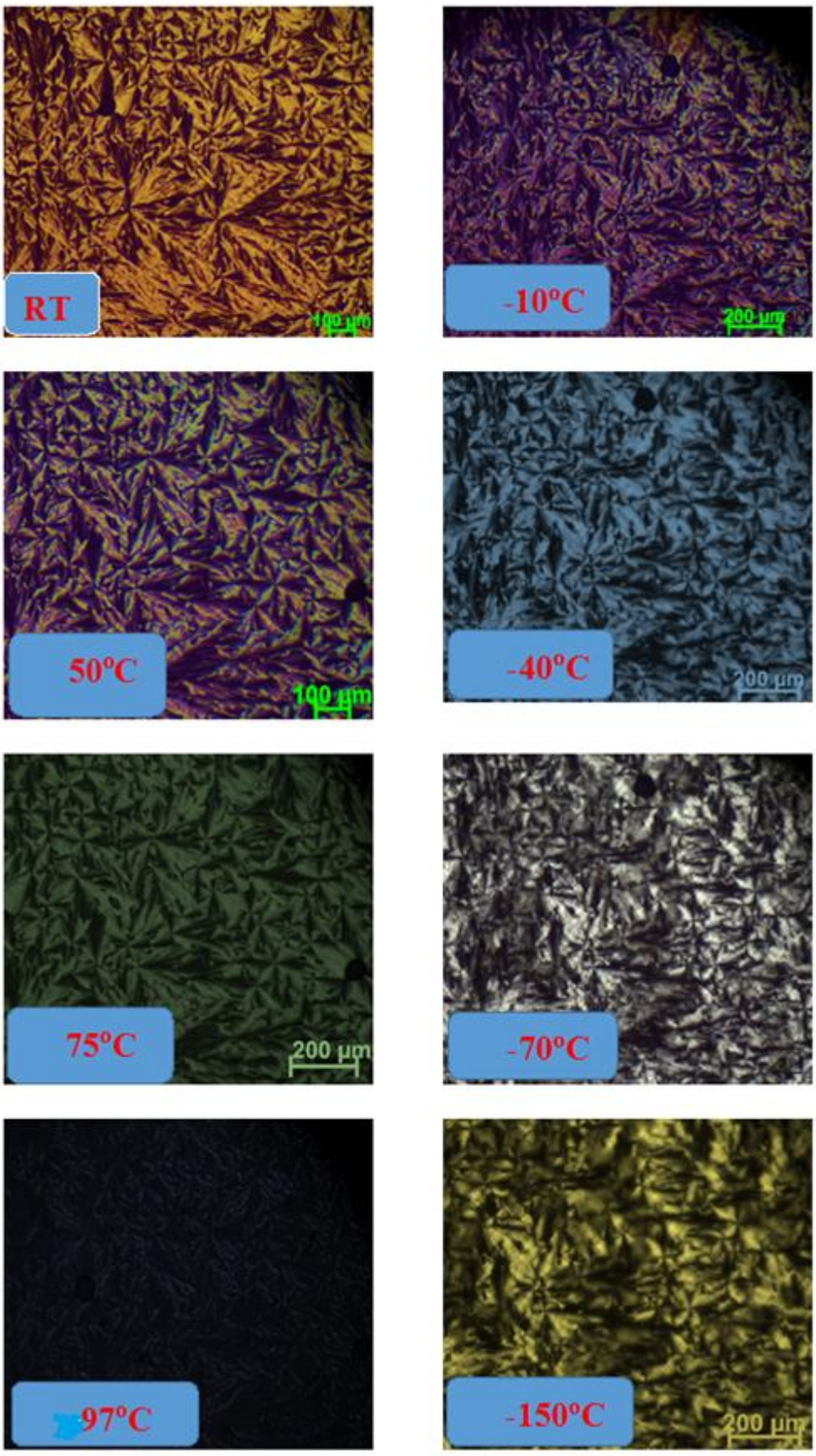

Figure 3-10. The thermal behaviour of the 4 PA/$C_{12}EO_{12}$ mole ratio samples within a wide temperature range.

3.1.7. Conductivity of the H_3PO_4 LLC phases

In this study, we envisioned that sandwiching the acid molecules in between the surfactants' hydrophilic head groups will enhance the formation of macroscopic hydrogen bonded networks, where the transportation of protons can be much easier and efficient. This could be because, the formation of continuous hydrogen bonded acid network will make the conduction mechanism much easier, by further decreasing the intermolecular hydrogen bond lengths in the mesophases.

The electrochemical behaviors were analyzed using Nyquist plots, obtained from a Gamry framework electrochemical device operating at 10 mV AC voltage and between a frequency range of 0.1 Hz to 300 kHz.

Samples for such measurements were either sandwiched in between two FTO coated glasses, or placed in between two sides of an FTO coated glass in which part of the FTO's coating was removed with the help of a diamond cutter. The conductivity in each case was calculated using **equation 2;** where $\boldsymbol{\sigma}$ represents the conductivity, **R** is the resistance

$$\boldsymbol{\sigma = \frac{K}{R}} \qquad \textbf{Equation 2}$$

and **K** is the **cells constants.** The cell constant for the two FTO system was determined from the cell's dimension by using **equation 3,** where **K** represents the cell constant**, L** is the height of the ordinary glasses glued on the FTO**,** and **A,** is the area covered by the glasses on the FTO.

$$\boldsymbol{K = \frac{L}{A}} \qquad \textbf{Equation 3}$$

On the other hand, the cell constant for the 1 FTO system was determined by using standard solution of KCl with known conductivity of $1.413X10^{-3}$ S/cm.

In **Figure 3-11,** it can be clearly seen that, the resistance values decreases with increasing PA concentration. Therefore, the 3 mole ratio (lowest composition) is the most resistive sample and its nyquits plot shows a semicircular arc at the high frequency region of the plot, thus making it difficult to determine its exact resistance. However, we were still able to determine it's ''Real'' resistance by considering its ''imaginary resistance'' value closest to zero. The observed semicircular arc indicates the bulk impedance of the sample, and it decreases with increasing PA concentration and viscosity of the mesophase.

The decrease of bulk resistance with PA concentration can be explained in two ways: Firstly, from a LLC point of view, we already know that increase in concentration induces conformational and phase change (showed in the XRD and POM data). These changes enable the micellar domains to accommodate more acid molecules; thus increasing the number of interacting acid groups in the mesophase. For examples, the 6 mole ratio is in the cubic phase, where more acid molecules interact through hydrogen bonding.

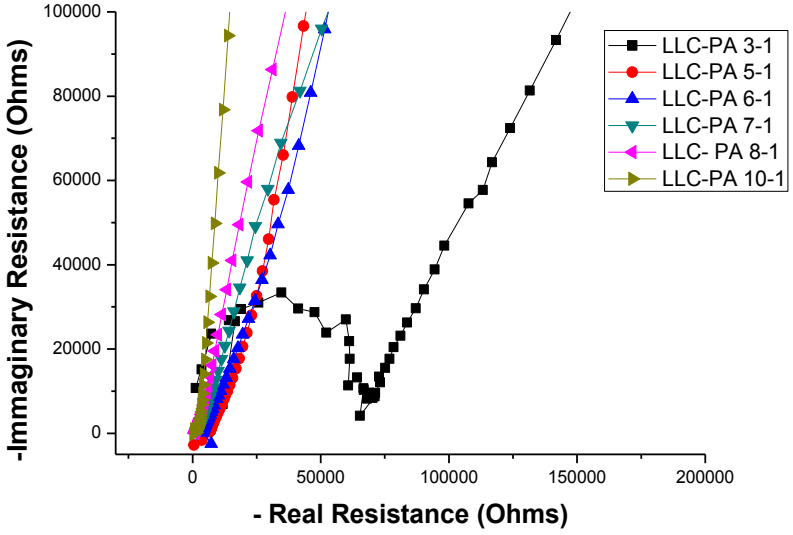

Figure 3-11. A Nyquist plot showing the resistance of different acid-surfactant mole ratios.

Such compact arrangement in the cubic phase decreases the inter-molecular distance between neighbouring phosphoric acid molecules, and hence makes the hopping of protons more feasible. This explanation is quite plausible because it also explains the decreasing trend of resistance with viscosity. Secondly, the trend can also be explained by considering the conduction path ways. In the Grotthuss pathway, conduction is facilitated by the hoping migration of protons; which will require close proximity of the ions involve (the case in relatively high concentration), while in the Vehicle pathway, transportation of proton is not affected by the absence of infinite chain of hydrogen bonded molecules. It only requires 'vehicles' such as water, with high self-diffusion constants to facilitate the protons' mobility [59]. Therefore, if we assume Grotthuss pathway, then the higher concentrated compositions which were apparently more viscous, should definitely be more conductive due to the high confinement effect (explained above).

This observation was completely different from the trend observed in LLC-hydrated metal salts assemblies [34] which portraits indirect correlations between ionic conductivity and viscosity. Dag et al. [34] reported that, the lesser viscous samples are, the more conductive they become because of the high proton or ionic mobility associated with the more liquid-like gels. From these two observations, it can be assumed that while investigations in the LLC hydrated metal salts obeyed the 'Vehicle' mechanism of proton conductivity, our explanation for the lower resistivity in the highly viscous gels is based on the fact that they obey the Grotthuss conduction mechanism.

The isotropization temperatures (viscosity in this case) increase from 3 to 15 mole ratio before finally decreasing at extremely high concentrations. At concentrations above 16, the melting point of the samples started decreasing to values far below 100^{o}C. In these compositions, we assumed that, since the mesophases are in the acid-dominant phase

(shown in both the FT-IR and XRD data), their chemical properties will be very similar to that of pure phosphoric acid molecules. This therefore, induced hygroscopic behavior in the mesophases and led to the adsorption of more atmospheric water, causing the observed relatively low viscosities. This increase in the quantity of water leads to the lowering of the activation energy [42] and at the same time, lowers the glass transition temperature [91] making these samples more conductive. Some water is also necessary for the formation of successive hydrogen-bonded networks for inducing the hopping conduction of protons [44]. However, high quantity of water completely changes the conduction mechanism, from hopping to vehicle. **Figure 3-12** comprises of Nyquist plots of different compositions (11 to 20), showing the effect of increasing quantity of water in the samples. The effects of concentration on conductivity and isotropization temperature are outlined in **Table 3-1.**

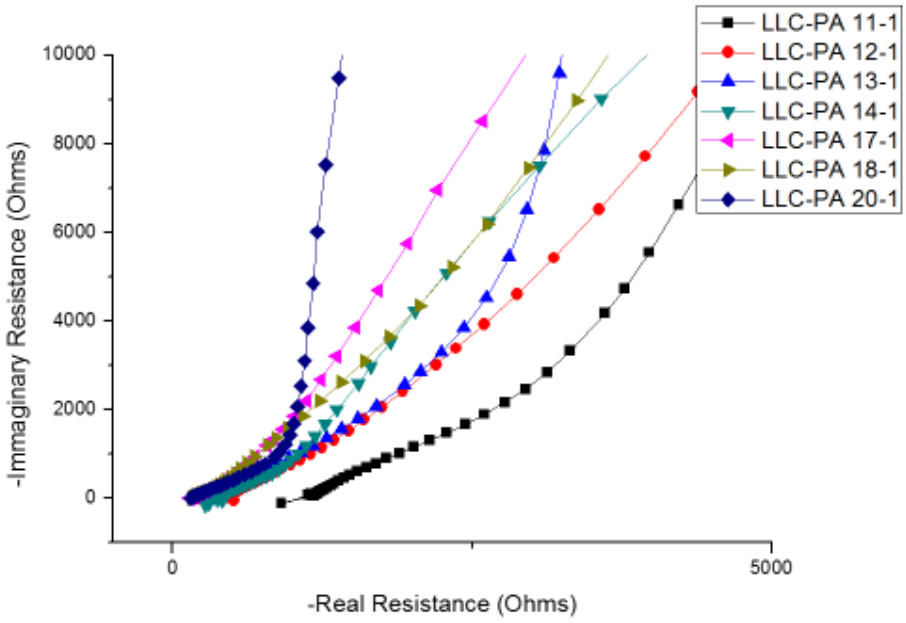

Figure 3-12. Nyquist plots of the higher PA/$C_{12}EO_{10}$ mole ratio. It shows the decreasing trend of the resitances with concentration.

Each of the impedance measurements were performed many times using both approaches (homemade cells), but all of them gave similar conductivity results as shown in the conductivity versus composition plot in **Figure 3-13**.

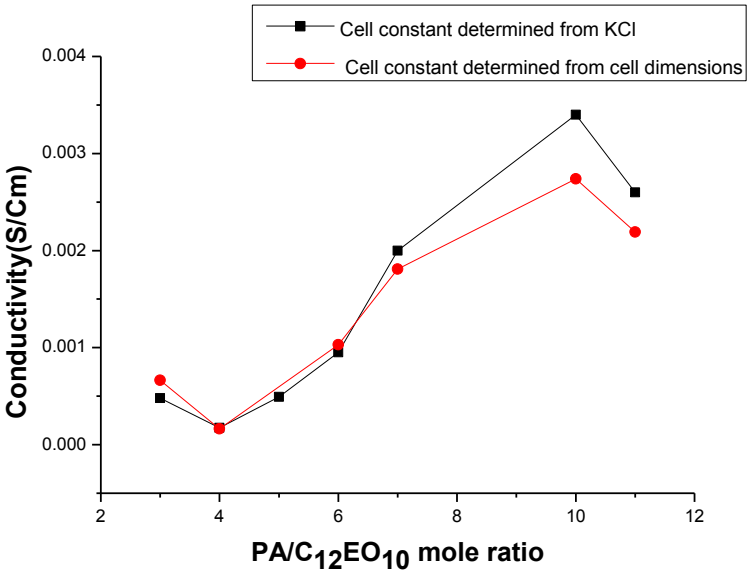

Figure 3-13. Conductivity versus composition plot; comparing the results obtained from two different cells.

PA/$C_{12}E_{10}$ mole ratio	Resistance (ohms)	Cell constant (Cm-1)	Conductivity (*10-4) Scm-1	Melting point
3:1	6528	3.314	4.80	63
4:1	2124	3.719	1.75	97.6
5:1	6770	3.336	4.92	114.4
6:1	3784	3.596	9.50	Above 130
7:1	1957	3.873	19.79	Above 130
8:1	948.8	2.628	27.70	Above 130
10:1	875.1	2.971	33.96	Above 120°C
11:1	1172	3.059	26.04	Above 120°C
12:1	450.5	4.239	94.09	Above 120°C
13:1	335.7	3.606	107.40	Above 120°C
14:1	360	3.762	104.50	Above 120°C
15:1	1389	7.852	56.53	Above 120°C
16:1	450.3	2.695681	57.60	Above 120°C
17:1	146.6	3.0250	206.00	Less than 100°C
18:1	156.1	3.8100	244.00	Less than 100°C
20:1	148.6	3.778	254.00	Less than 100°C

Table 3-1. The resistance, conductivity, and melting points of all the compositions studied. The melting points increases to a certain limit and then start to decrease.

3.1.8. Temperature-dependent conductivity measurements

In addition to determining the room temperature conductivity values, we also investigated the behavior of the gels with increasing/decreasing temperatures. The gel samples were placed on FTO coated glasses before being finally placed on a HTF500 hot plate. The hot plate was connected to two probe Gamry Framework electrochemical device for conductivity measurement. The temperature was slowly increased (3^o per minute) and

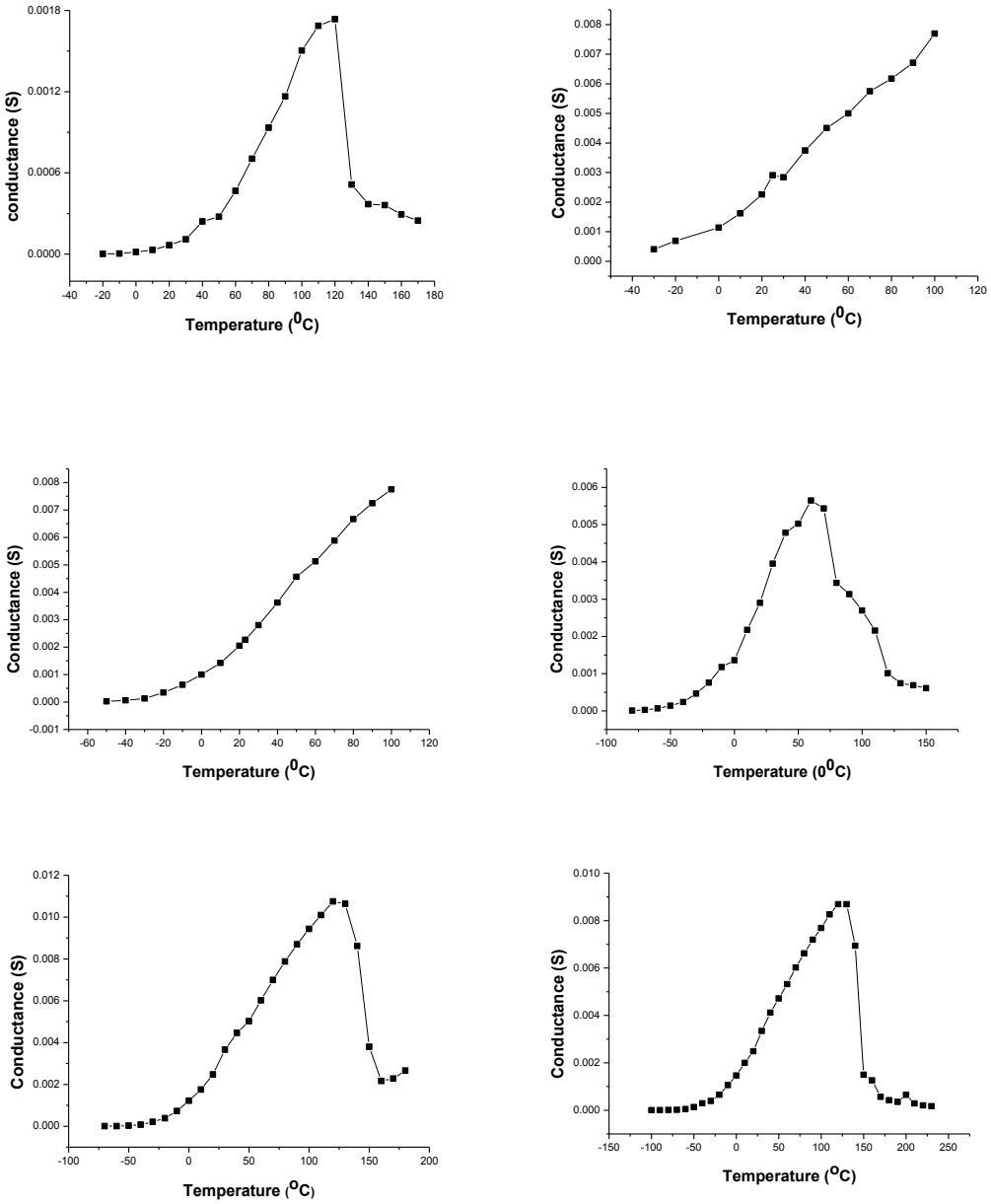

Figure 3-14. Temperature dependent conductivity measurements for some selected compositions; Top; 5 and 10, middle; 11 and 16, and bottom; 18, and 20.

upon arriving at the required temperature, the samples were left there for about 30 minutes for equilibration before measuring their conductivities. The results showed that the gels remained conductive within a wide range of temperature, depending on the compositions. For e.g, the 20 mole ratio has a conductance of 1.36×10^{-4} S/cm at -50^{o}C, which later

increased to $2.5x10^{-3}$ S/cm at 20°C. The bulk resistance values as shown in **Figure 3-14,** decrease with increasing temperature until certain maximum values (above melting points), then start increasing again showing the complete evaporation of water from the samples. In such situations, we assume that all the water content of the sample evaporates to the atmosphere causing the complete collapse of the hydrogen bonded matrix. Therefore, the reason for the rise of resistance at such high temperatures could also be due to the collapse of the mesophase, caused by melting. This behavior was observed in all the compositions but at different temperatures, which led to the conclusion that, the vaporization temperature was affected by the viscosity of the composition. For examples, the more viscous, low concentrated samples remain conductive even at temperatures above 130°C, while the more fluid-like samples were conductive at temperatures just beyond 100°C. In the low temperature regions, it was also realized that the more concentrated (lesser viscous) samples showed reasonable conductivity (7.60×10^{-5} S/cm) even at temperatures below -80°C, while the lesser concentrated samples could only show fair conductivity at temperatures around -30°C.

It is already known that the increase in temperature causes the breakage of hydrogen bonds and at the same time, enhances the conductivity of materials. Therefore, the conductivity of our gels which we assumed to be largely dependent on hydrogen bonded networks may be in odds with this already accepted belief. However, this could be explained when we consider the different conduction mechanisms and the possibility of changing from one mechanism to the other. When the gels completely melt, the decrease in the activation energy coupled with the fast mobility of the 'vehicles'; explained in **chapter 1**, will enhance the proton conductivity even more. Therefore, the 'vehicle' mechanism, which requires higher activation energy will be the preference mode of conduction in such a situation. This is what led to the observed rise in conductivity as a function of temperature

in the viscous gels. This behavior continues until the gel-like liquid start losing water molecules to the atmosphere. Even though the cells were covered with thin glasses to avoid evaporation of water, it is still logical to assume that 99% of the water molecules will evaporate at some elevated temperatures, leading to the complete collapse of the mesophases. This situation is shown in the temperature dependent conductivity plots as a 'V' shape at the higher temperature regions.

On the other hand, when the temperature was reduced to temperatures much lower than $0^{o}C$, the resistance values were observed to sharply increase. One of the factors that might be responsible for this sharp change may be the decrease of the mobility of the carriers at temperatures below the freezing points of the gel. Another convincing explanation can be the formation of cracks resulting from the frozen gels. In either case, semicircular arcs, showing bulk impedance of the sample, were observed in the high frequency regions of all the samples that were completely frozen.

3.1.9. Conductivity behaviour

The AC temperature-dependent conductivity measurement, shows Arrhenius-type plot, **Figure 3-15**. Clearly, the total conductivity increases with both temperature and concentration. The decrease in conductivity at the high temperature regions can be observed at different temperatures for the different compositions. Both linear and non-liner relations can also be observed in the plots. The non-linear jumps observed at the high temperature region could perhaps be due to phase transitions.

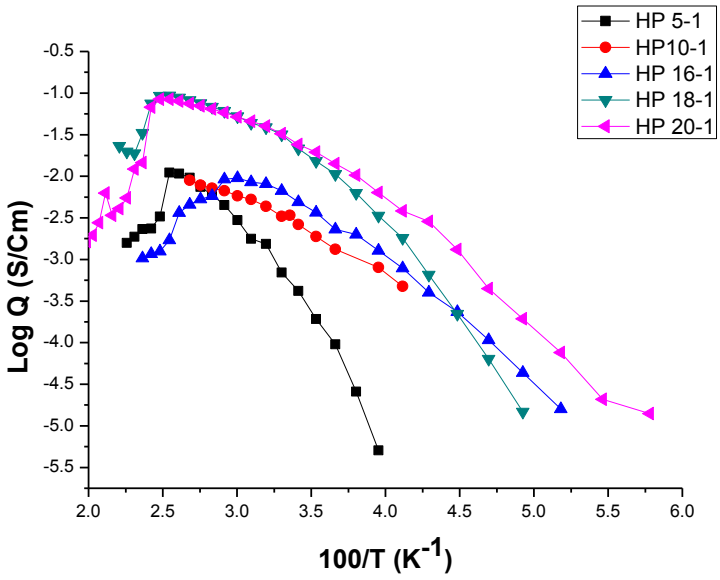

Figure 3-15. Temperature-dependent conductivity plots.

3.2. Synthesis of transparent mesoporous calcium hydroxyapatite (HAp)

Since it has already been confirmed that phosphoric acid can be used as a solvent in the formation of stable mesophases, we thought that combining it with other solvents (salts) capable of assembling surfactant molecules could be useful in the synthesis of important phosphate-containing materials. In this section, we investigated the possibility of forming calcium hydroxyapatite through interfacial reaction between phosphoric acid and calcium nitrate.

In our study, we show for the first time that stable precursor-surfactant mesophases can be formed through the collective use of $Ca(NO_3)_2 \cdot 4H_2O$ salt (containing 4 water molecules) and phosphoric acid (containing 1 water molecule) as solvents in assembling oligo (ethylene oxide) type surfactant such as ($C_{12}EO_{10}$). The surfactant mimics the role of collagen proteins (responsible for directing the shape and size of the HAp crystals in natural systems) in our system.

We investigated this system within a wide range of composition in order to access the behavior of the phases with concentration. The compositions investigated range from 5.3/1 to 13.3/1, precursors to surfactant ratio. Despite the different concentrations, all the solutions remained clear even after 6 month of aging in the vials. The pH of the 5.3/1 ratio solution was measured and found to be 0.73. This high acidity in the vial (solution) is capable of preventing reactions between the precursors and hence inhibit the formation and precipitation of calcium phosphate species. This could perhaps be the reason why the samples could stay for more than months in the vials without precipitating salts in any form. The solutions can also be spin coated over substrates to form mesophases, through the evaporation of excess water. We assumed that, once the mesophases are formed, slow reaction between the confined phosphoric acid and calcium nitrate species in the hydrophilic domains of the mesophase, starts. **Figure 3-16** is a schematic representation of

the anticipated arrangement of the precursors, leading to the formation of HAp. In the next subsections, we will discuss in detail, the formations, stability, and properties of the mesophases. In addition to that, results from various characterization techniques confirming the production of HAp thin films upon calcination will also be fully discussed.

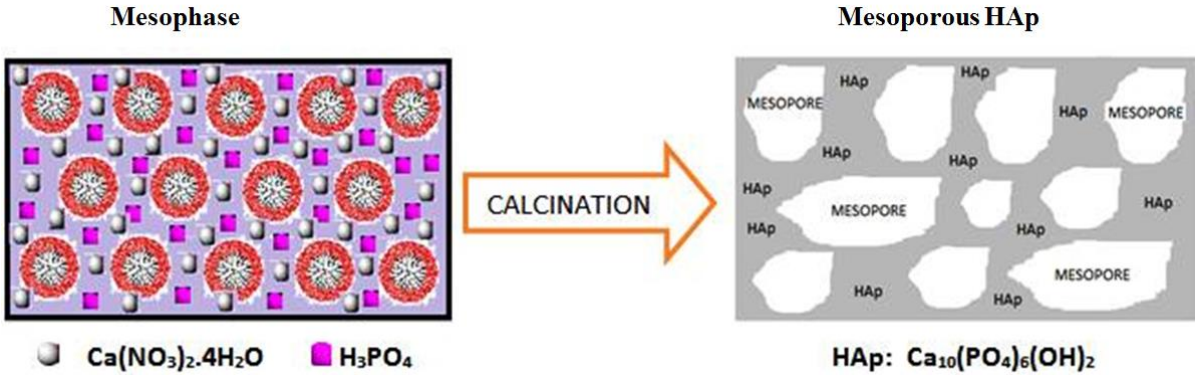

Figure 3-16. Schematic representation of mesoporous HAp formation in our system.

3.2.1. X-Ray diffraction measurements of the mesophases

All the compositions (clear solutions) were spin coated on ordinary glass substrates and transferred to our XRD instrument to identify their LLC phases. This was accurately done for both the fresh and the aged samples. The data from these investigations, as shown in **Figure 3-17,** revealed that all compositions gave one diffraction line at around 1.78, 2Θ values, showing the presence of mesophases in all of them. Lack of significant shifting of the diffraction lines with increasing concentrations (just as observed in the PA-surfactant case) supports our argument that the number of micellar units increases at the expense of decreasing aggregation numbers. In other words, as the concentration of the precursors increases, the number of surfactant molecules in the micelles (aggregation number) decreases in other to form new micellar units that can accommodate more amount of the precursors. In addition to the peak observed at 1.78^o, 2Θ values, another, less intense,

diffraction line was also observed at around 7.45°, 2 Θ. Using the PDF card 01-074-0566 as our reference, we came

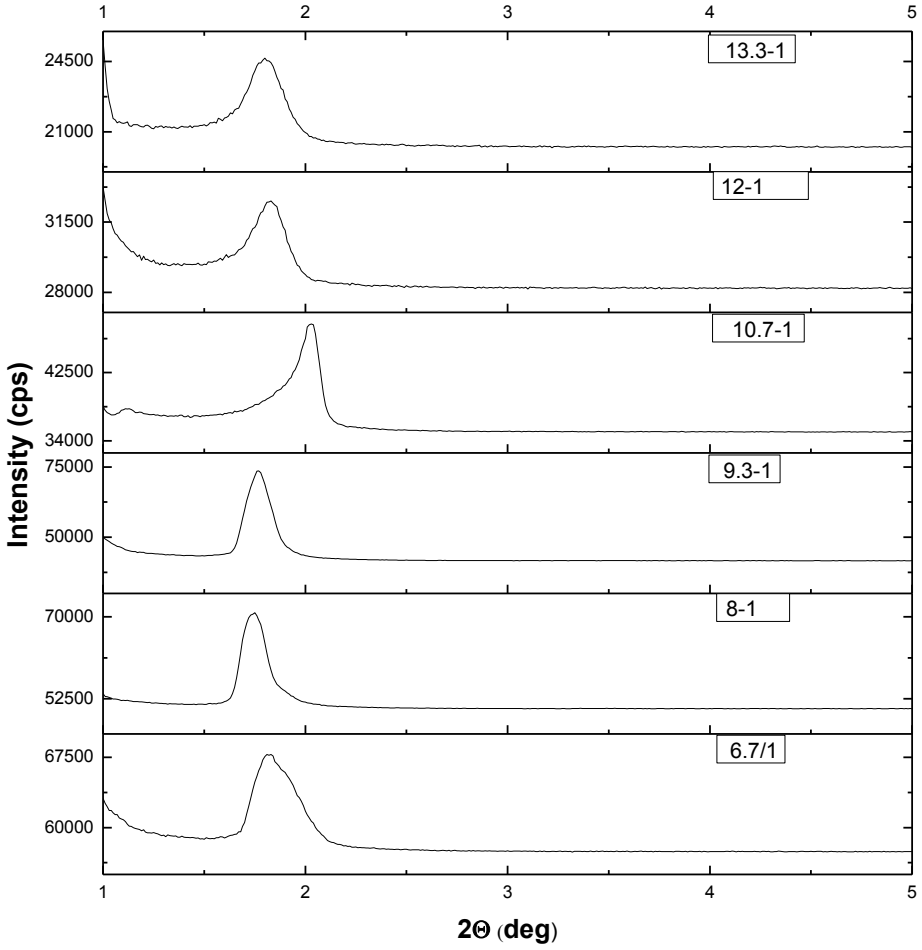

Figure 3-17. XRD data showing the mesophases of different precursor to surfactant ratio (compositions shown on the top left of the figure).

up with the assumption that this line could be due to the presence of $Ca(H_2PO_4)\cdot 2H_2O$ as an intermediate formed in the freshly spin coated samples.

The samples were then aged for a day, later for a week and even for months but they still remained stable. In **Figure 3-18,** we show the behavior of some selected number of compositions with time. From these data, it is clear that the intensity of the first diffraction line decreases with time, indicating a slight decrease of orientation in the aged samples.

The diffraction lines were also slightly shifted to higher 2Θ values, which means a decrease in the d-spacing values of the aged samples. Additionally, the intensity of the peak we assumed to be related to $Ca(H_2PO_4)\cdot 2H_2O$ also started decreasing after 24 hours

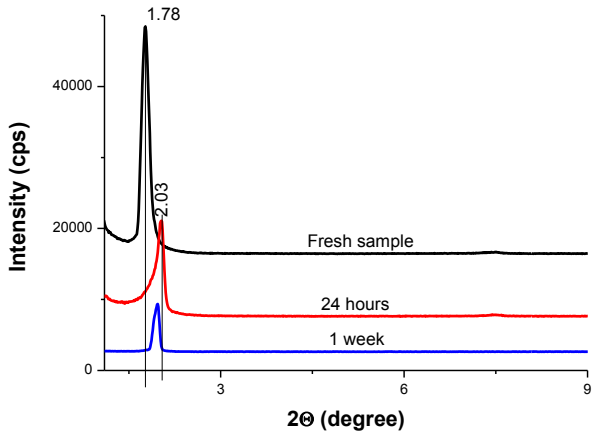

a)

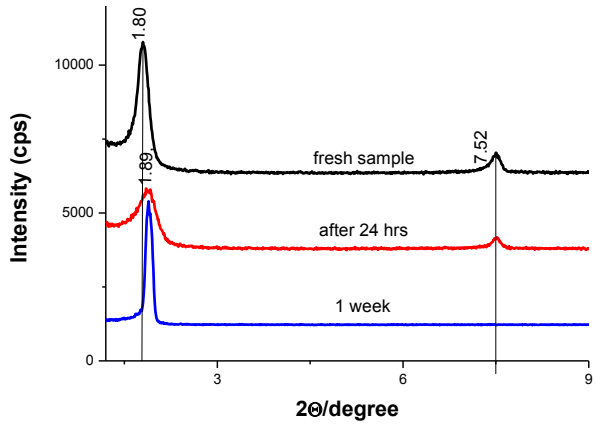

b)

Figure 3-18. XRD data of uncalcined HAp mesophases with precursor (Ca (II):H3PO4) mole ration of a) 9.3/ 1, and b) 13.3/1 10.

before finally disappearing after 1 week of aging. This can be explained by considering the high solubility of the calcium dihydrogenphosphate crystals. This high solubility makes them dissolve in between the hydrophilic domains of the mesophases and eventually causing their disappearance from the XRD pattern.

3.2.2. FT-IR investigations of the mesophases and calcined films

To further elucidate the nature of the species in the LLC media, the LLC mesophases were also monitored by collecting their FT-IR spectra. Solutions of different concentrations were homogeneously spin coated on silicon wafers and monitored in time. In some case, instead of spin coating, small quantities of the samples were placed on glass substrates and left under ambient weather condition for gelation to occur. This was followed by smearing

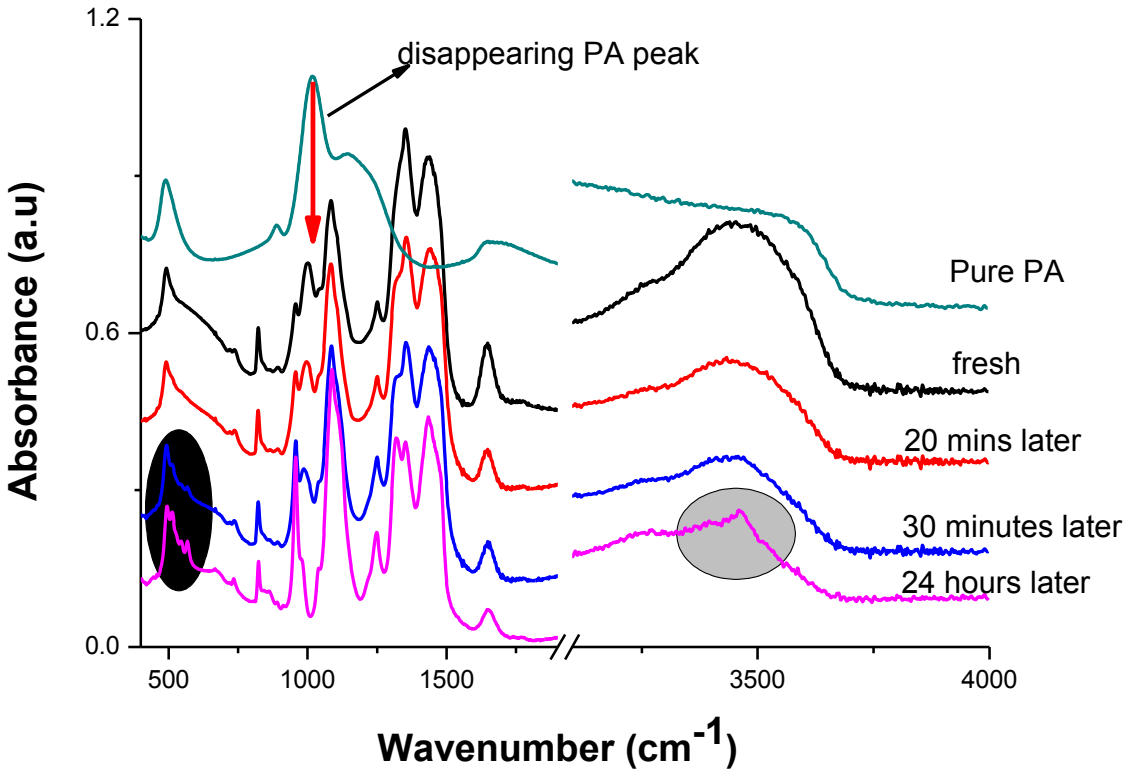

Figure 3-19. Time-dependent FT-IR spectra of the 5.3/1 composition

small quantities of the gels on the surface of the silicon wafers. The thickness of the gels on the silicon wafers were controlled in such a way that the amplitude of the light source was never compromised.

Figure 3-19 shows the behavior of the 5.335 precursor/surfactant mole with aging. From these spectra, the peaks around 2340 and 2930 cm^{-1} are characteristic peaks of H_3PO_4 and

are due to the symmetric and antisymmetric υ-OH modes of phosphoric acid. The high frequency broad peak at around 3560 cm^{-1} is a characteristic peak of non-hydrogen bonded OH sites of H_3PO_4. The other broad features around 3200-3500 cm^{-1} are due to free and coordinated water molecules around the Ca^{2+} ions. The peak at around 1003 cm^{-1} and high frequency shoulder in the pure H_3PO_4 shifts to 956 cm^{-1}, see the difference spectra over time in **Figure 3-20**. This behavior was similarly observed for all the freshly spin coated samples of this composition. It therefore, confirmed that no reaction occurs in the vial; all reactions start immediately after the evaporation of excess water from the spin coated samples to form the mesophases. In the mesophases, pure phosphoric acid, $H_2PO_4^-$, nitrates, and some free and coordinated water molecules are well arranged in between the micellar domains.

In moving from the spectrum of the freshly formed mesophase to the last measured spectra, one can easily notice many changes in the spectra. For examples, the water peak at 1640 cm^{-1} and nitrate related peaks, at 1045, 1296, 1370, and 1490 cm^{-1}

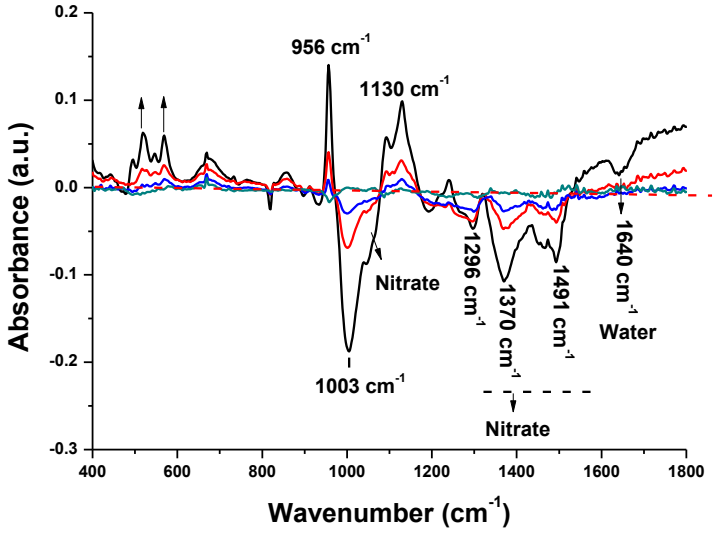

Figure 3-20. Difference in 5.33 precursor/surfactant mole ratio time-dependent FT-IR spectra.

lose intensity, while new peaks at 493, 520, 544, 568, 855, 956, and 1130 cm^{-1} start emerging. These spectral changes clearly show that some water and nitrates are continuously being eliminated from the mesophases in the form of water vapor and nitric acid respectively, as the media reaches equilibrium. Evaporation of both water and nitric acid enhances the formation of calcium phosphate type species. Again, the emergence of a sharp peak at 3641 cm^{-1} as already shown in **Figure 3-19** confirmed the presence of crystalline water in a crystal. This information combined with the newly emerging sharp peaks at 493, 520, 544, and 568 cm^{-1}, belonging to the bending modes of phosphate and coordinated water, confirmed the assumption made from the XRD data (**Figure 3-18)** regarding the formation of $Ca(H_2PO_4)\cdot 2H_2O$ as an intermediate in the mesophase. Just as the compound's diffraction lines disappeared after a week in the XRD data, here too, the sharp water peak disappeared after 1 week, while the peaks representing the bending mode of phosphate groups also became relatively broader and slightly blue shifted, showing the formation of another less crystalline phosphate compound (possibly, $CaHPO_4$) in the mesophase. However, the samples still remained as gel-like and stable for months without undergoing complete formation of calcium hydroxyapatite, possibly because of the high acidity of the media. This effect is more pronounced in the higher concentrated samples.

We also investigated the effect of high precursor to surfactant ratios using FT-IR spectroscopy. The motive behind increasing the concentration of the precursor at a constant mass of the surfactant was to build stronger HAp walls in between the mesopores. In **Figure 3-21** we show the FTIR spectra of two other compositions (one intermediate, 9.3/1 and the other high, 13.3/1 precursor to surfactant ratios) monitored over time. Other than the increased reaction kinetics in these higher concentrated samples, all other features observed in these investigations are more or less the same as the observations made in the 5.3/1 precursor to surfactant mole ratio. Clearly, the nitrate and phosphate related peaks increase

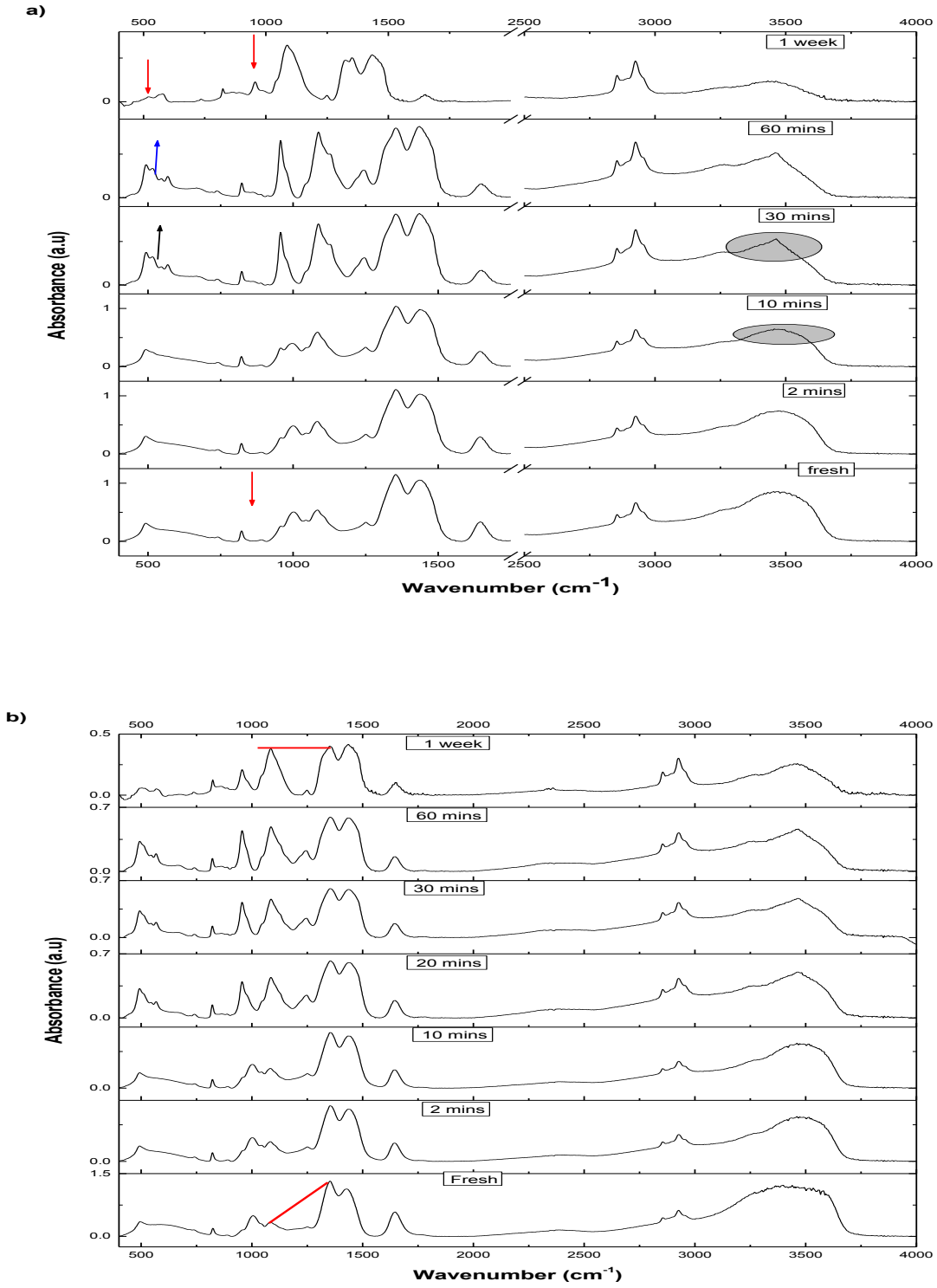

Figure 3-21. FTIR spectra of the freshly prepared samples of $Ca(NO_3)_2$-H_3PO_4-$C_{12}EO_{10}$ with different precursor to surfactant mole ratios a) 9.3/1 and b)13.3/1.

in intensity as compared to the 5.3/1 precursor to surfactant mole ratio, because of the increasing concentrations of the precursors. The formation of the dihydrogenphosphate specie in the 13.1/1 composition was also observed to start in the first 10 minutes of aging (faster than the case of 5.3/1) and continued to complete formation within 60 minutes, before transforming to a lesser crystalline phosphate-containing species within a time space of one week. However, the HAp formation was not still expedited by the high concentration of the precursors at RT. This showed that, the formation of HAp is temperature dependent and could not be enhanced by increasing the concentration of the precursors.

In order to ascertain the exact temperature of formation, a freshly prepared sample of the 5.33/1 mole ratio was spin coated on a silicon wafer and annealed at different temperatures starting from 100 ^{o}C to higher temperatures. The annealing stages which lasted for at least 1hr at all the investigated temperatures, were monitored using FTIR spectroscopy, **Figure 3-22**. From the figure, it can be seen that the surfactant related peaks kept decreasing in intensity with increasing temperatures. The same was also

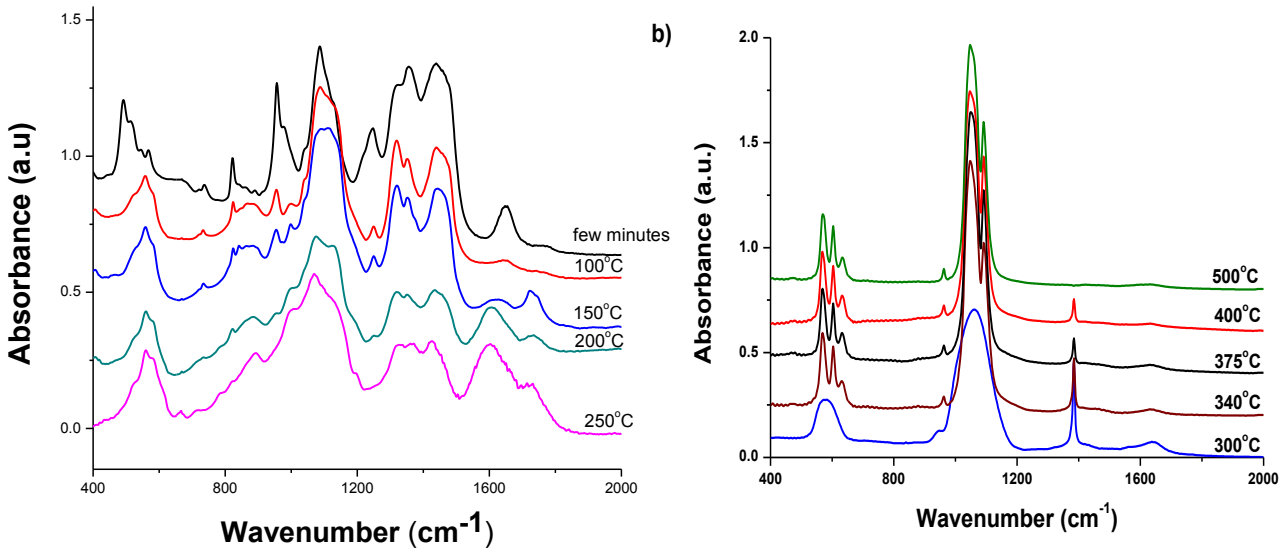

Figure 3-22. FTIR data of HAp samples annealed at different temperature a) low temperature regions showing incomplete formation b) higher temperatures.

observed for the nitrate related peaks observed at 1296 and 1370 cm^{-1}. However, both the surfactant and the nitrate related peaks remained visible even at 250 ^{o}C. On the contrary, the stretching modes of the phosphate related peaks continued increasing in intensity whilst the bending modes became broader and shifted to higher wavenumbers. This observations confirm the disappearance of one crystalline phosphate containing compound and the formation of a less crystalline one. Again, annealing at higher temperatures was also observed to speed up the transformation of calcium dihydrogenphosphate to calcium hydrogenphosphate as compared to the unheated samples. For example, annealing at 100^{o}C, showed features such as, the disappearance of the sharp water peaks, which could only be observed after one week in the uncalcined samples. Regardless of these many changes, it can still be observed that HAp, could not be formed even at temperatures as high as 250 ^{o}C.

Fresh samples of the same compositions were again spin coated on standard microscope glass substrate and then calcined at higher temperatures: 300, 340, 375, 400, 500 and 600 ^{o}C. The calcination was immediately done in a pre-heated oven, temperatures set at half of the required final temperature, in order to terminate the formation of side products that could inhibit the HAp synthesis as well as the transparency of the films. These temperatures were enough to burn off all surfactant species together with the decomposition of some of the nitrates and thus led to the formation of pure mesoporous HAp films. The films obtained after the calcination were absolutely transparent. However, the samples calcined at relatively lower temperatures; 300 to 500 ^{o}C were more transparent than those calcined at temperatures above 500 ^{o}C, **Figure 3-23**. Small portion of the calcined films of different compositions were scrapped off from the glass substrates and combined with KBr to form pallets for FT-IR measurements.

Their FT-IR data (shown in **Figure 3-22b)** showed that the formation of HAp in our system actually starts at 300 ^{o}C. At this temperature, the bending and the stretching modes of both the phosphate and OH formed broad peaks because of less crystallinity. However, as the annealing temperature increases to 340 ^{o}C and even higher, the HAp turned out to be more crystalline (shown by the sharper and more resolved peaks) as compared to the samples calcined at 300 ^{o}C. These results showed an enhanced crystallinity with increasing calcination temperatures. At 340 ^{o}C, the peaks at 567 and 604 cm^{-1} corresponding to the bending mode of the PO_4^{3-} group, [93] [94] became well distinct. The stretching modes of the phosphate groups were also clearly observed at 960, 1048 and 1091 cm^{-1}. [93] [94] The low intensity sharp peak observed at 636 cm^{-1} corresponds to the bending mode of the OH groups. [94]

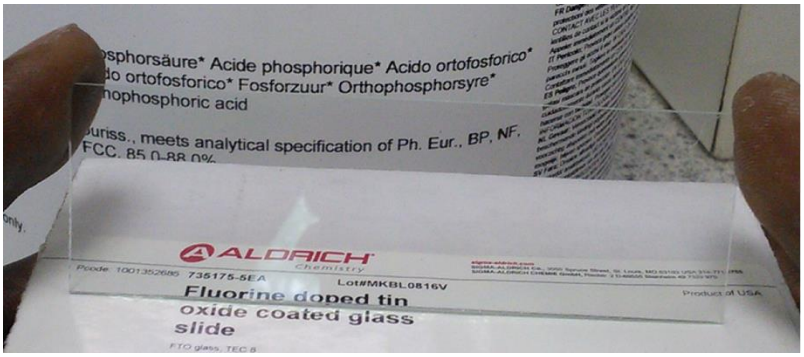

Figure 3-23. A photograph showing the transparency of a film calcined at 300^{o}C.

It was also realized that, an additional new sharp peak started emerging at 3573 cm^{-1}, which is due to the OH groups of HAp. [94] However, the nitrate peak at 1384 cm^{-1} remained in the sample even at 400 ^{o}C. It is observed as a sharp peaks in the spectra indicating that, the nitrate reacted with potassium from the KBr (used in making the pallet) to form well crystalline KNO_3. However, at temperatures above 400 ^{o}C, the nitrate band disappeared

leaving behind a well crystalline and pure HAp. Starting from 500 ºC, the only change observed in the spectra was increase in crystallinity.

The same thermal treatment was also done for samples of higher concentrations, **Figure 3-24.** Surprisingly, the behavior at specific temperatures was again the same for all the samples despite the difference in their concentrations. For example, the nitrate peak was observed to disappear at 500ºC in all the studied compositions. This further confirmed that HAp formation is highly independent of the concentration of the precursor.

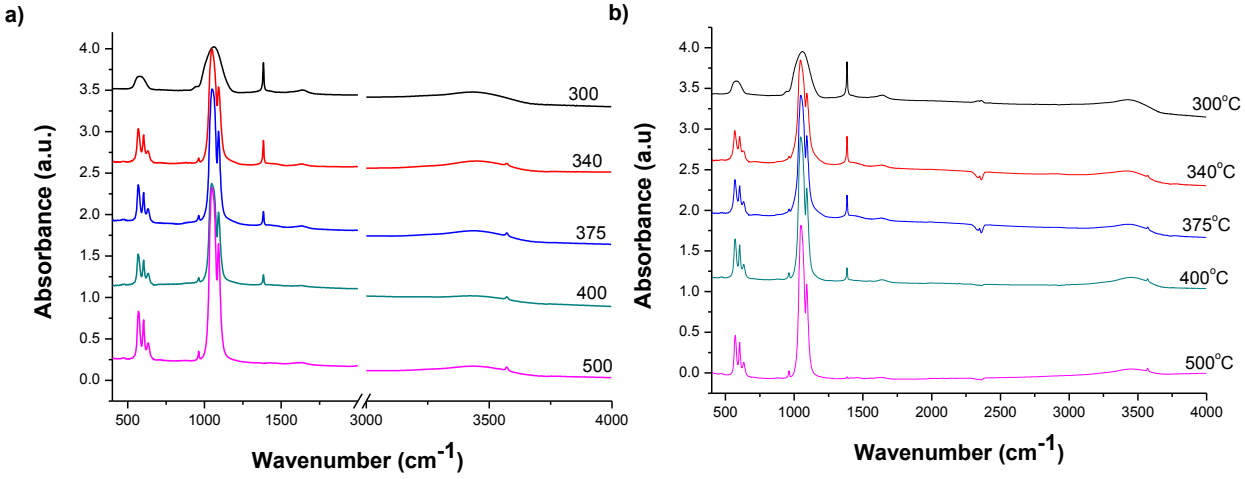

Figure 3-24. FT-IR spectra of higher concentrated samples calcined at different temperatures a) 9.3/1 mole ratio b) 13.3/1 mole ratio.

From the observations made in the XRD of the mesophases and the FT-IR of the fresh, aged, and calcined samples, we came up with a reaction pathway leading to the formation of HAp. In this pathway, we assumed that the formation does not take place in a straight forward manner, but involved the formation of intermediate products as shows in the equations below:

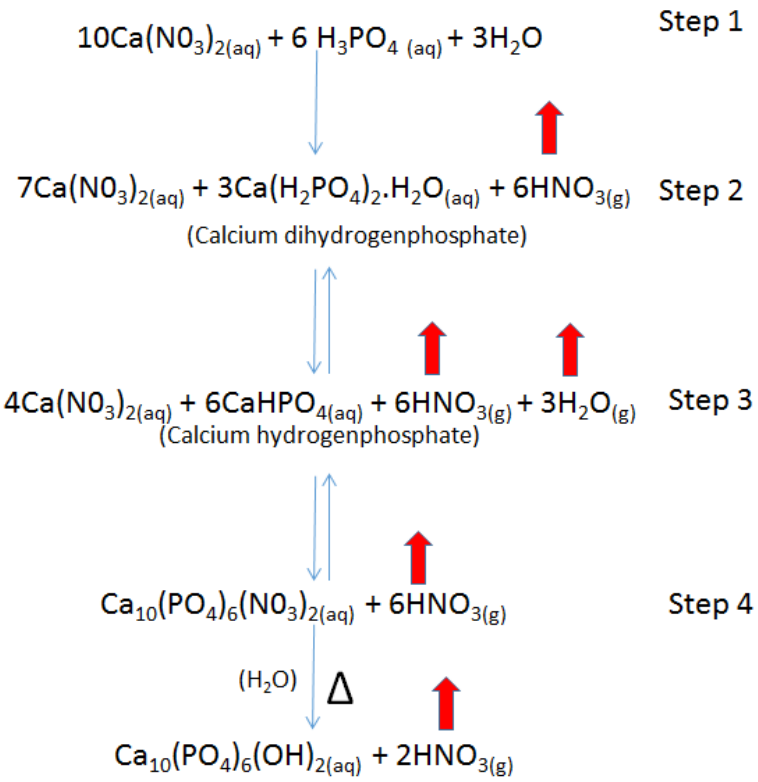

Step 1, which usually occurs in the mesophase (after spin coating), proceed in a straight forward manner. The driving force for the formation of calcium dihydrogenphosphate is the liberation of excess water. From the equation above, it can be seen that the presence of more than 3 moles of water (as in the vials) will make the reaction reversible. This explains why the mixtures were stable for months as clear solutions in the vial. The formation of calcium dihydrogenphosphate in the first stage of the reaction has already been proven by both, the XRD and the spectroscopic studies. It is assumed that it forms on the surfaces of the mesophase as large crystals within an hour after spin coating but later dissolves in between the micellar domains because of its high solubility. After dissolving (**step 2**), it slowly reacts with excess calcium nitrate to form minute quantity of lesser soluble calcium hydrogenphosphate species inside the mesostructure. For this reasons (forming inside the mesophase), the peaks of the $CaHPO_4$ are not very visible in the XRD data. However, the disappearance of the sharp water peak belonging to the calcium dihydrogenphosphate

species, the shifting of the peaks of phosphate bending mode (explained above) and the other phosphoric acid signals, confirmed the formation of a new phosphate-containing species. In **step 3,** we assumed that the $CaHPO_4$ species reacted with some more unreacted $Ca(NO_3)_2$ in the media to form calcium nitroapatite, which eventually leads to the formation of hydroxyapatite on heating (**step 4**). Note, starting from step 2, nitric acid had been spontaneously eliminated from the media. If it remains in the mesophase, it will direct the reaction to the reactant side rather than the opposite.

3.2.3. Powder XRD analysis of samples calcined at different temperatures

Since the calcined films were absolutely thin, it was almost impossible to collect their XRD pattern in a regular diffractometer. As such, hundreds of the 5.3/1 ratio transparent films, calcined at 300 ^oC were scraped off from glass surfaces in order to collect around 60 mg of sample for powder XRD (PXRD) analysis. The results from the PXRD **(Figure 3-25)** showed broad diffraction lines, indicating a semi-crystalline and/or a porous material. When the data from the PXRD was compared with 01-074-0566 PDF card of bulk HAp, it was confirmed that all the observed peaks corresponded to HAp. However, some HAp diffraction lines were not very visible in the data of the samples calcined at 300 ^oC because of the broadness of the diffraction lines, which overshadowed some of the other lines. The same powder was later annealed to 400^oC for 2 hours and the XRD data retaken. This time around, most of the lines which could not be clearly seen from the PXRD of the sample calcined at 300 ^oC, started becoming more visible. This showed growth and/or further crystallization of the calcium hydroxyapatite pore walls. This increasing crystallinity at higher temperatures is consistent with our observation in the FT-IR spectra. The sample was further annealed at 500 and 600^oC respectively but the result obtained from all of those

XRD measurements were almost identical. The only differences being that, as the line width

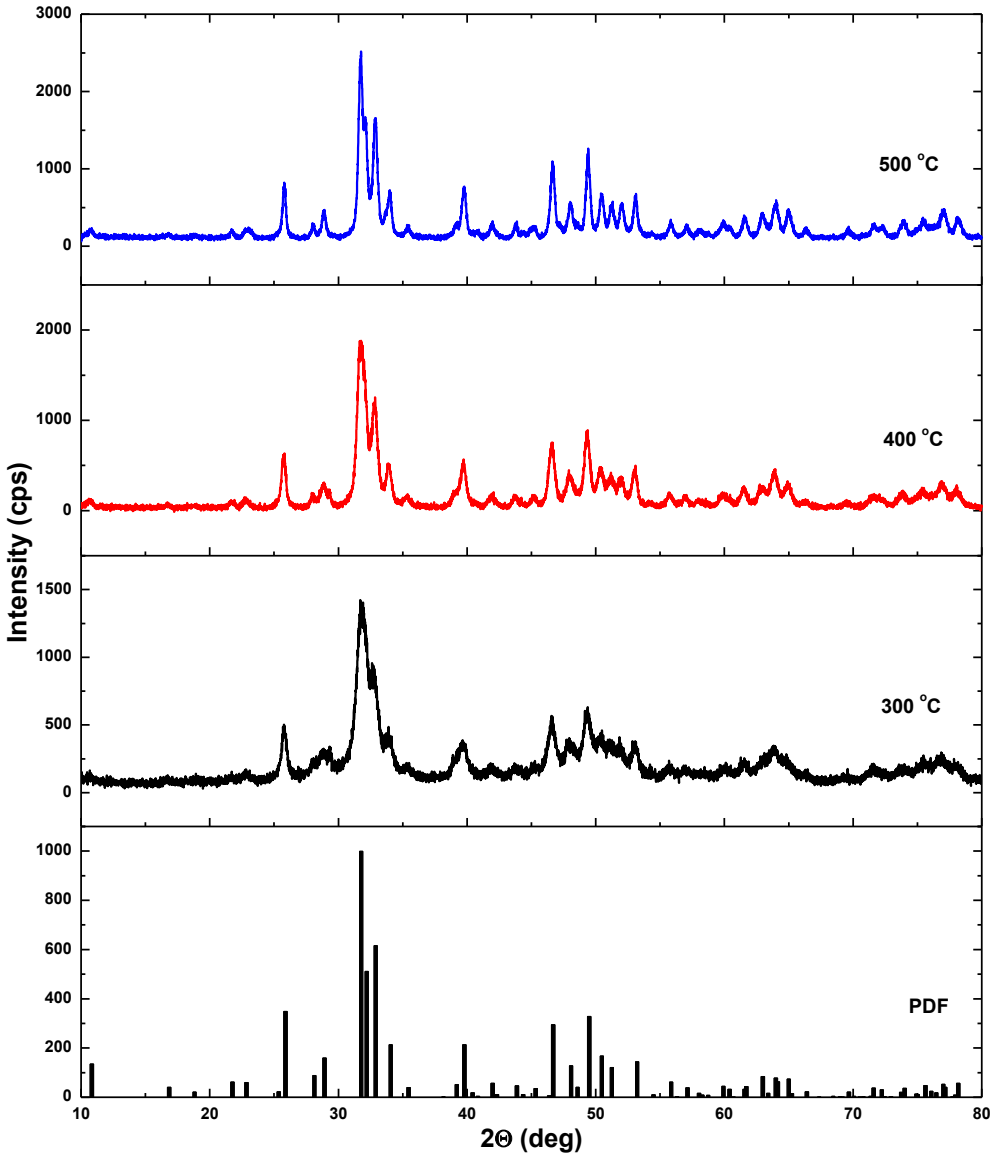

Figure 3-25. PXRD of HAp samples calcined at different temperatures; 300, 400, and 500 ºC and the PDF card of bulk HAp.

decreased, the diffraction lines got sharper, and many other lines became more distinct as compared to the data from the previous temperatures.To authenticate the accuracy of the

data, we also applied the same heat treatments to higher concentrated samples. The behaviour, shown in **Figure 3-26** was again similar to the 5.3/1 mole ratio. However, in the 13.3/1 mole ratio, the sample calcined at 300 ºC showed relatively broader diffraction lines as compared to the less concentrated samples calcined at the same temperature. This could be because of the relatively thicker films in the 13.3/1 mole ratio. Although all the samples were spin coated with the same RPM, the higher concentrated compositions will no doubt form thicker films because of less viscosity of the solution. Note, one way to obtain thicker

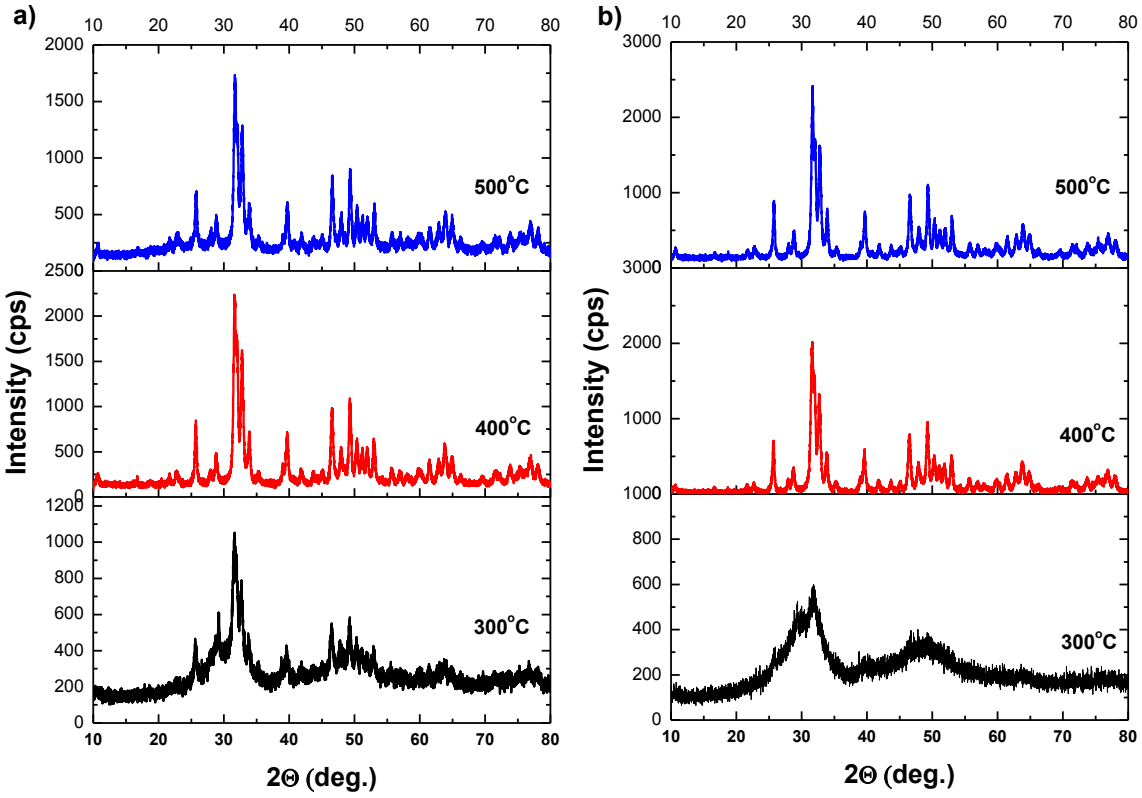

Figure 3-26. PXRD data of higher concentrated samples calcined at three different temperatures: 300, 400 and 500 ºC. A) 9.3/1 mole ratio and B) 13.3/1 mole ratio.

films through spin coating, is by using less viscous samples.

3.2.4. N_2 adsorption-desorption measurements

This technique was used to analyze the pore sizes, pore volume, and pore size distribution of the different compositions. In using this analysis technique, the mass of sample that can be used should be indirectly proportional to the surface area of the sample i.e.; the smaller the surface area, the more sample needed to obtain an accurate result. Therefore, since the approach used in our synthesis was completely new and the porosity of our HAp could only be estimated from the SEM and TEM result, 60 mg, obtained after scraping 150 HAp glasses (the same sample used for PXRD measurement), was used in order to obtain a justifiable N_2-sorption data. The 5.3/1 composition was first weighed and later put inside of a ½ inch BET P_0-tube. This was followed by firstly degassing under room temperature condition for ten minutes, and then later degassing at 250 ^{0}C for three hours under a vacuum chamber (~ 10^{-2} torr). After all the degassing treatments were done, the sample was later re-weighed to confirm its exact mass before been finally transferred to the sorption instrument for the measurement. During the whole process of the measurement, isothermal jacket was used to maintain the level of liquid nitrogen in the tube. The sample was evacuated at a pressure of 10 mmHg under a vacuum set point of 150 μmHg for 1hours. Both leak test and out-gas test were done at 120 s and 180 s respectively. The whole period of the measurements lasted for about 9 hours, after which the sample was removed from the tube and then annealed at higher temperatures (400 and 500 ^{o}C) in order to monitor the temperature-dependent changes of the pores in HAp. **Figure 3-27** shows the N_2 sorption isotherms at those different temperatures. It can be easily seen from the figure that the isotherms are type IV (characteristic of mesoporous materials) with hysteresis. The BET surface area changes from 96 m^2/g to 61 m^2/g and to 24 m^2/g upon heating at 300, 400, and 500 ^{o}C, respectively. The decreased in the surface area of the sample with increasing temperatures was attributed to the excessive crystal growth at higher temperatures (shown

in the PXRD and FT-IR sections). The desorption BJH pore size also increased with temperature and were determined to be 19.5, 26.4, and 15.7 nm at 300, 400 and 500 ^{o}C, respectively. The changes in the pore volume accords with the pore size, as 0.58, 0.40, and 0.07 cm^3/g at 300, 400, and 500 ^{o}C, respectively. This further confirmed the consistency of the XRD data with the N_2 sorption data and also proved that the mesoporous walls grow in size and further crystallized by heating and finally collapses at around 600 ^{o}C. Pore size increases from 19.5 to 26.4 nm with increasing temperatures from 300 to 400 ^{o}C, but the pore volume decreases from 0.58 to 0.40 nm, respectively. This is a clear indication that while pore sizes are expanding, the pore walls are also becoming thicker. The largest drop on the pore volume occurred at 500 ^{o}C corresponding to the further growth of the pore-walls (this will be discussed in the TEM data below).

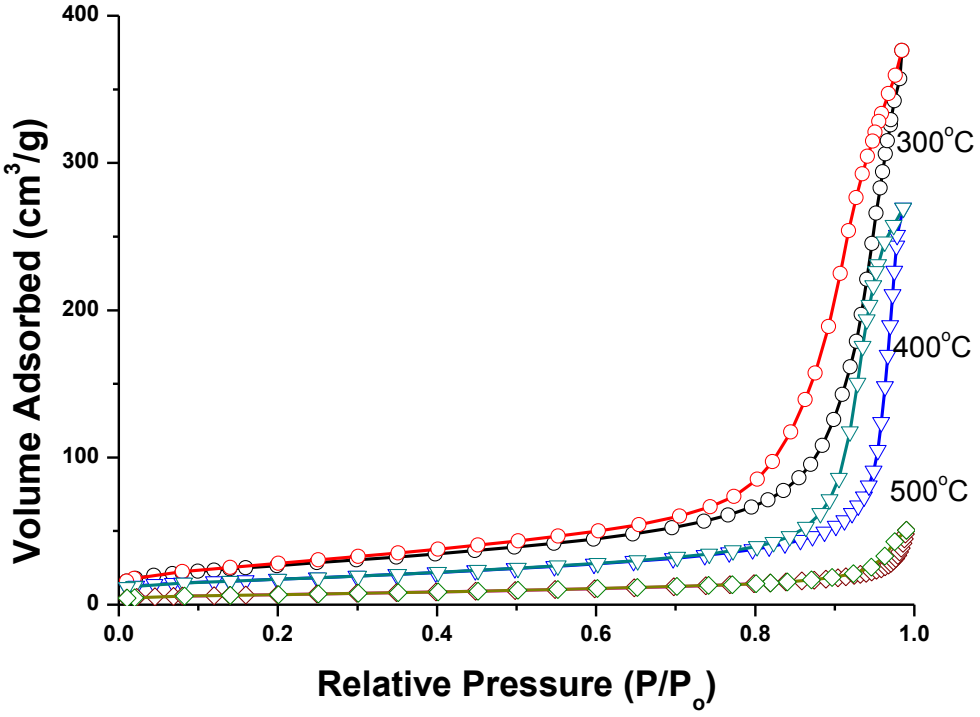

Figure 3-27. 77.4 K N_2- sorption measurements of samples calinced at different temperatures showing the decreasing surface areas with temperature.

The trend of decreasing surface area with volume was also the same for the higher concentrated samples, **Figure 3-28**. Their isotherms are all similar but the isotherms of the higher concentrated samples show a more uniform distribution. Additionally, for samples calcined at the same temperatures, the 5.3/1 mole ratio always turn out to have the largest surface area. For example, the 5.3/1, 9.3/1 and 13.3/1 calcined at 300°C have surface areas of 96, 86, and 78m^2/g, respectively. This shows that, increase in concentration leads to decrease in surface area. The reason for this could be due to the relatively thicker walls in the higher concentrated samples. Increasing thicknesses of the pore walls with

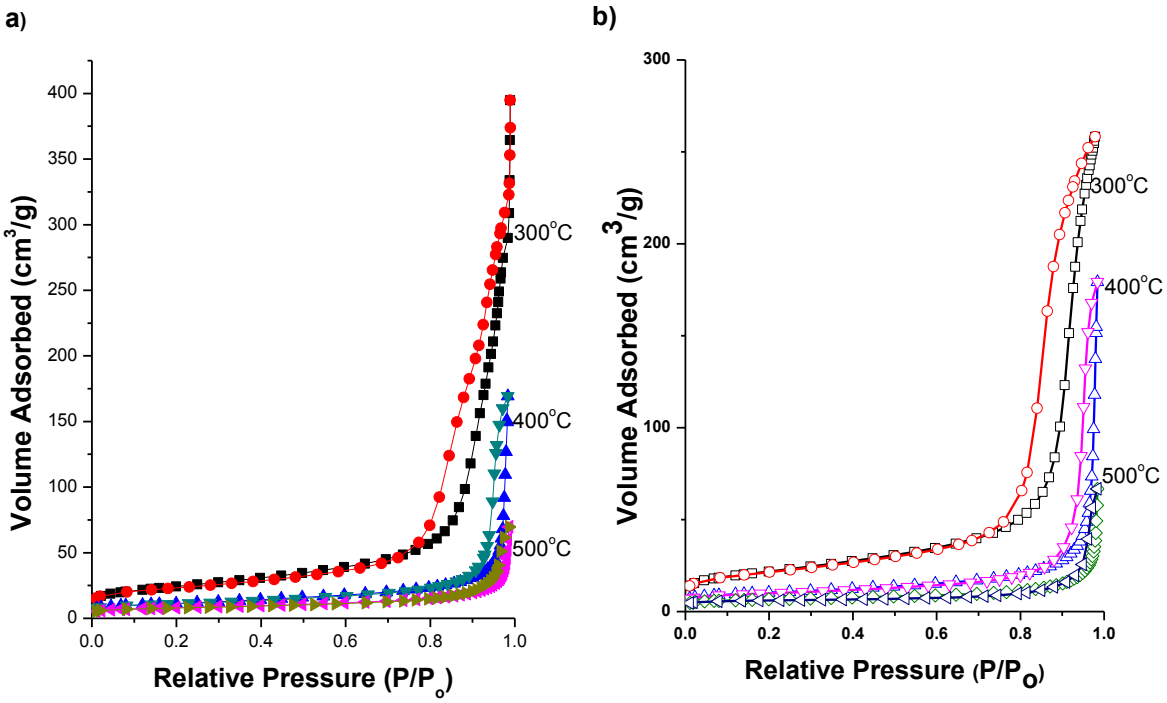

Figure 3-28. 77.4 K N_2-Sorption Isotherms of samples higher than 5.3/1 mole ratio

concentration decreases the mesopores and hence, a lesser surface area. This effect can be clearly seen in the pore size distribution plots in **Figure 3-29**. From this data (**Figure 3-29 (a to c**), one sees that increase in temperature leads to decrease in the pore size distribution

and at the same time leading to the formation of larger pores. In other words, the pores get larger and more uniform as one increases the annealing temperature. On the other hand, **Figure 3-29(d)**, where comparison was made on different compositions calcined at 300^{o}C, showed that, the concentration has opposite effect on the pore sizes as temperature. The pore sizes in these plots can be seen to be getting more uniform in the lower pore region of the plot, when the concentration increases. This, as explained above, is basically based on the fact that higher quantity of precursors leads to the reduction of the pore sizes due to the thickening of the pore walls caused by the excessive infiltration of the hydrophilic domains. The charts in **Figure 3-30,** are a summary of all the observations explained above. Note: since we could not determine the exact pore sizes and pore volumes of the dominating pores, the charts were plotted using averages of desorption branch. In these charts, the decreasing surface area with concentration and temperature can be clearly observed. Additionally one sees that, the average desorption pore sizes of the samples increase from 300 ^{o}C to 500 ^{o}C for all compositions. The trend of change in the pore volumes with respect to temperature can also be observed to have direct correlation with changing surface area.

In terms of compositions, one observes that the pore sizes and pore volumes of the three compositions calcined at the same temperature did not change much. The representation on the charts might be misleading, since they are only based on average values. The explanation for the slightly responding pore sizes and pore volumes with concentration is based on the AN concept, explained above.

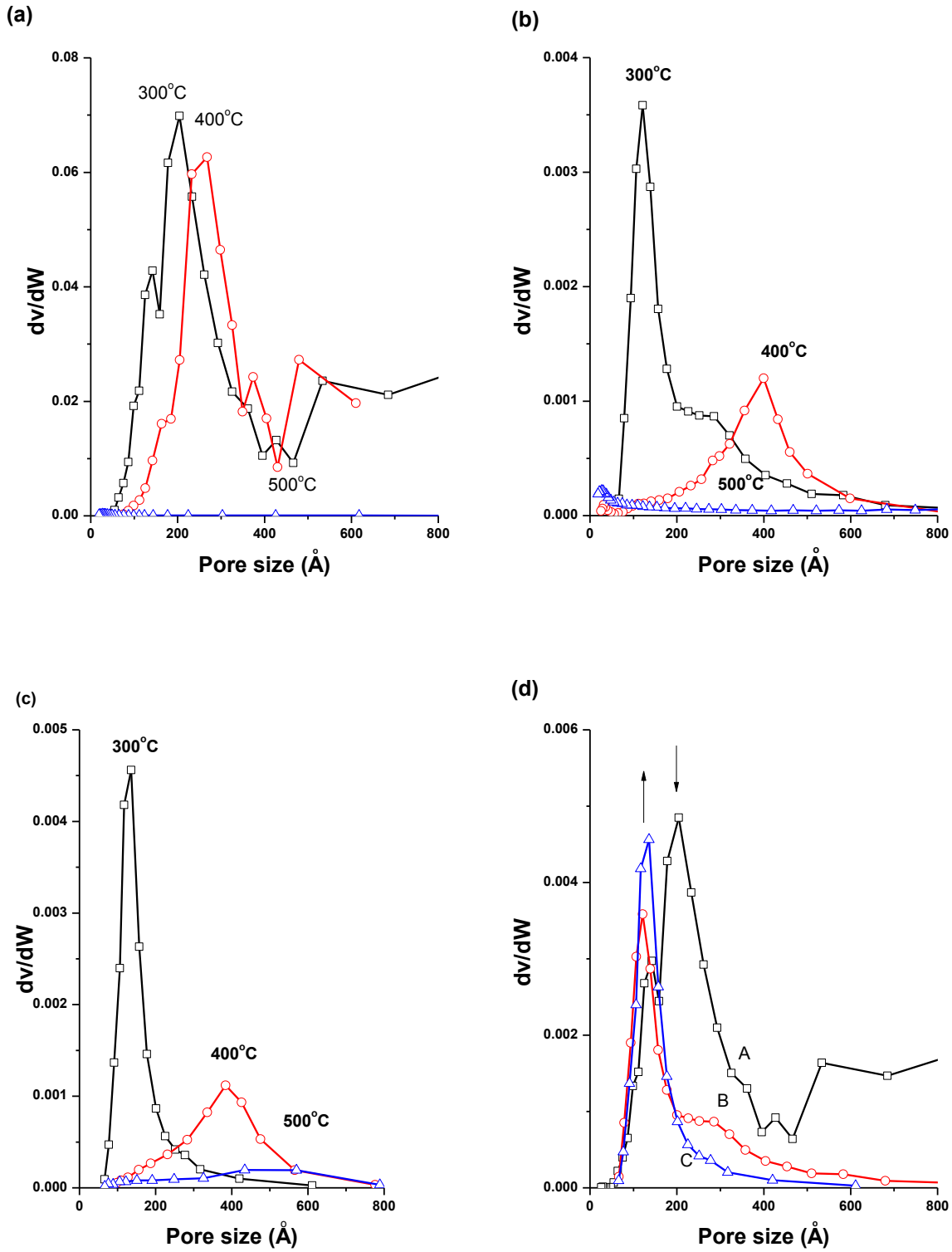

Figure 3-29. Pore size distribution plots at different temperatures and compositions a) 5.3/1, b) 9.3/1, c) 13.3/1 and d) comparison of all the compositions calcined at 300 ºC.

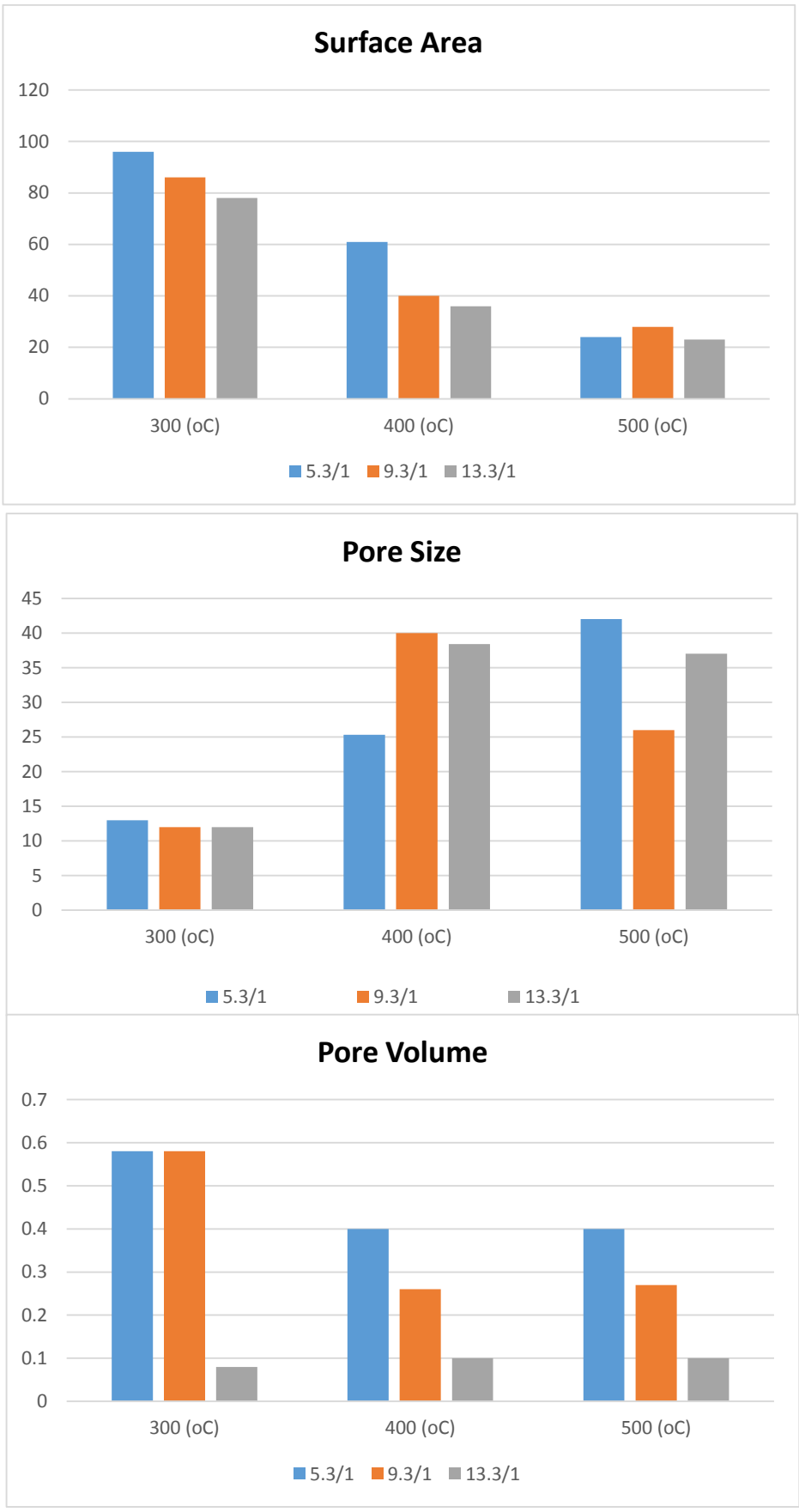

Figure 3-30. Summary of the results obtained from the gas sorption measurements.

3.2.5. Transition Electron Microscopy Analysis

Part of the 5.3/1 HAp transparent films, calcined at different temperatures were careful scrapped using well-cleaned glasses. The scrapped samples were transferred to a mortar and grinded to smaller film particles for about 20 minutes. During the process of grinding, small quantity of ethanol was added to the mortar in order to facilitate the dispersion of the HAp particles. The mixtures were then transferred to vials and absolute ethanol added, for ultrasonication. This step lasted for 30 minutes and caused the further dispersion of the particles. The well-dispersed samples were then drop casted onto a carbon supported films for TEM analysis.

Although the samples were all grinded for about 20 minutes during the preparation step, their images showed the presence of well homogenous films with uniform pore sizes and pore distribution. The increasing crystal size with temperature is also quite noticeable, **Figure 3-31**. The TEM images of the film at 300 ^{o}C, **Figure 3-31(a),** clearly show a sponge like porosity, with a wall thickness of 6.0 nm. However, the sizes of the crystals increases roughly to about 15-20 nm nanometres for samples calcined at higher temperatures. Above 500 ^{o}C, the crystals grow too large that the films start becoming opaque. This, therefore, further confirmed the validity of the temperature-dependent data observed in the FTIR, PXRD, and BET. The insets at the top right of the images calcined at different temperatures, show the atomic fringes in the HAp crystals. In this comparison, one clearly sees a noticeable difference in the number of atomic fringes with increasing calcination temperature. The fringes from the samples calcined at 300 ^{o}C are not very visible when compared to those observed from the samples calcined at 500 ^{o}C. To understand the effect of temperature in more detail, selective area electron diffraction (SAED) patterns were also taken (shown in the bottom right of the main images) and analysed. The SAED patterns images show transition from semi-crystalline particles for samples calcined at 300 ^{o}C to

crystalline particles for samples calcined at higher temperatures. Therefore, with these TEM images, we provide additional details to support the decrease of the surface area of HAp with increasing temperature. High resolution images of the crystalline pore-walls were further analyzed to prove that the walls are calcium hydroxyapatite.

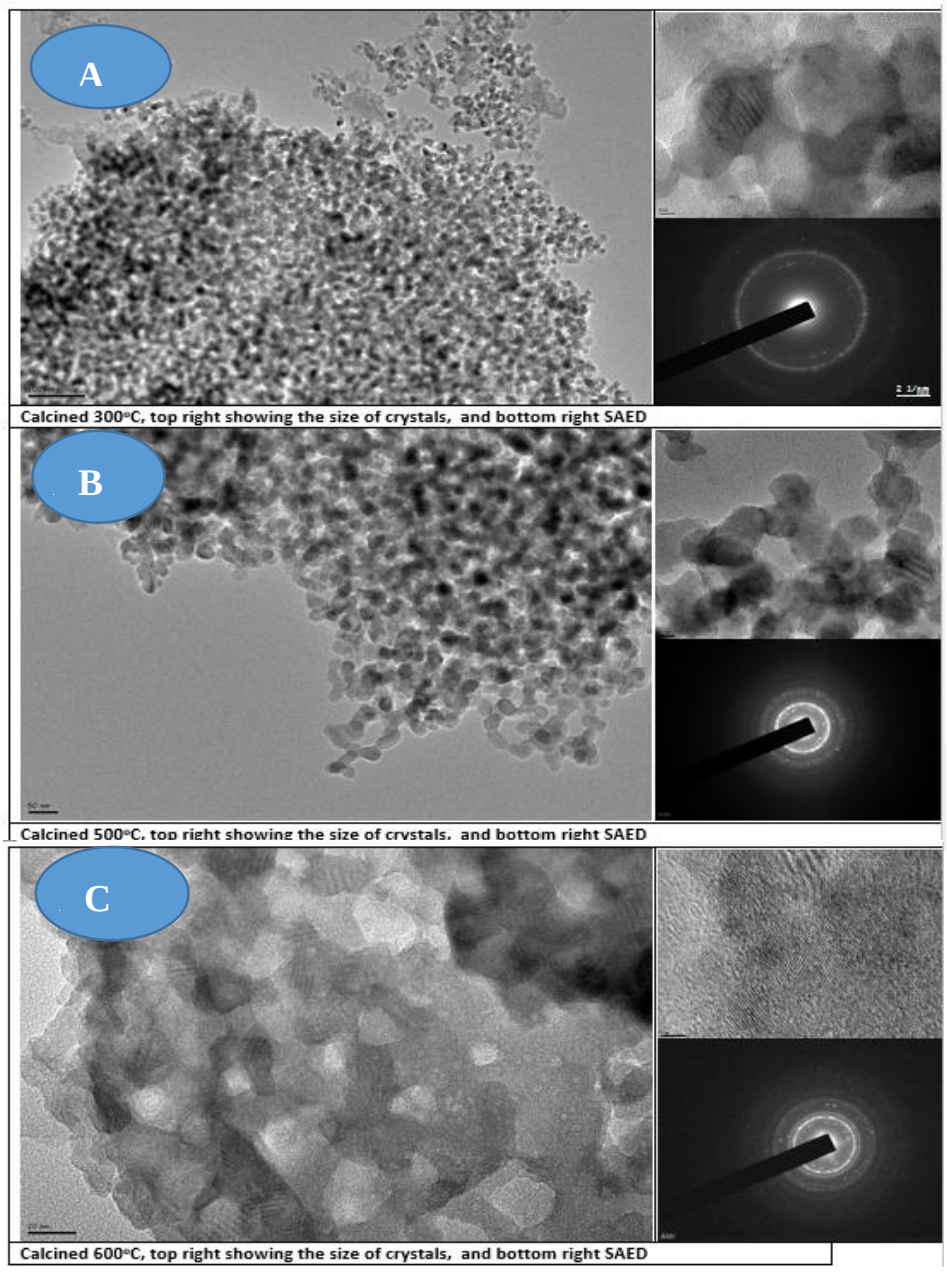

Figure 3-31. TEM images of mesoporous $Ca_{10}(PO_4)_6(OH)_2$ calcined at 300, 400 and 500 ºC with identical magnifications. Atomic fringes shown on the top right of the main images and SAED in the inset at the bottom right of the images image.

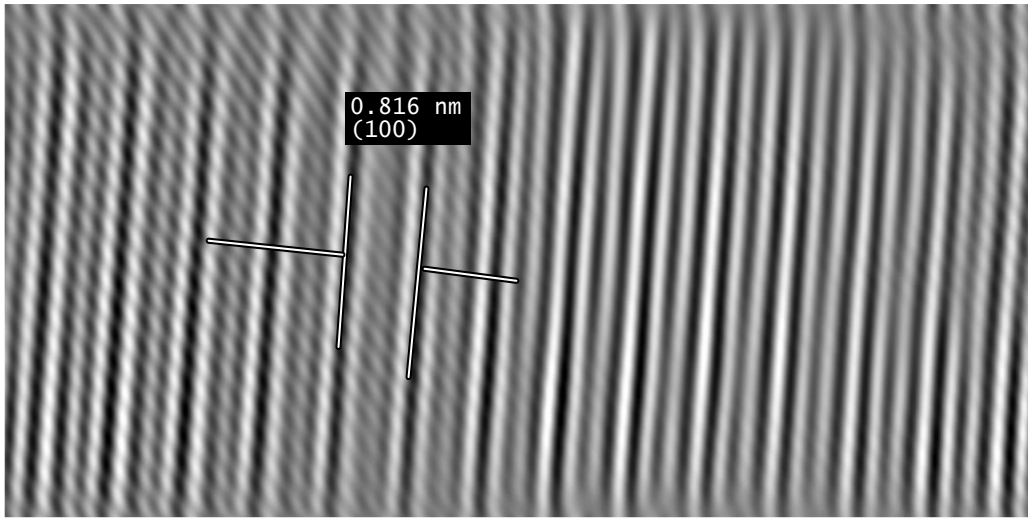

Figure 3-32. High resolution TEM images obtained by FFT analysis.

Figure 3-32 displays processed images (inverse fast fourier transform (FFT) of a selected area, masked and back FFT) that clearly display lattice fringes with spacing of 0.816 nm corresponding to the main plane (100) of hexagonal $Ca_{10}(PO_4)_6(OH)_2$. Other HAp planes not shown in the figure can also be evaluated from these high resolution TEM images with careful analysis.

3.2.6. Investigation of HAp shapes using Scanning Electron Microscopy (SEM)

The morphology of 5.3/2 samples calcined at different temperatures were again investigated by taking series of SEM images. In preparing the samples for the SEM imaging, small portion of the films were scrapped off the glass substrates and placed on an aluminum SEM-sample holders. Because of the low conductivity of the samples, Carbon tape was often used to enhance the conductivity and hence leads to better resolution SEM images. The images as indicted in **Figure 3-33**, also proved the existence of film rather than powder. High uniformity of the pores can also be observed in both compositions. Under the same scale, the images of the sample calcined at 500 ^{o}C were observed to have

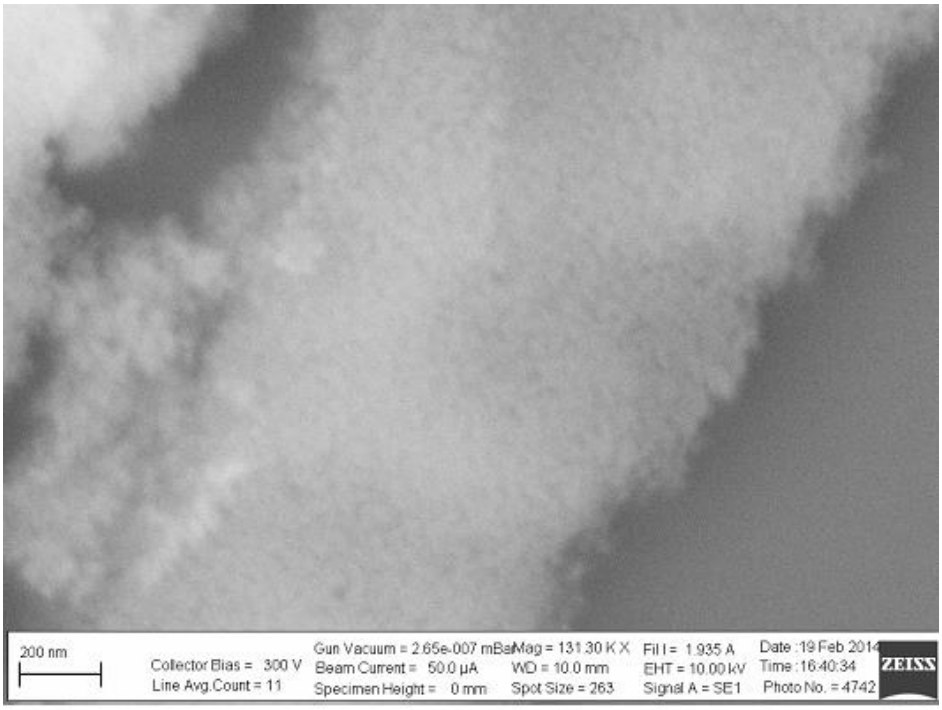

Image of sample calcined at 300°C

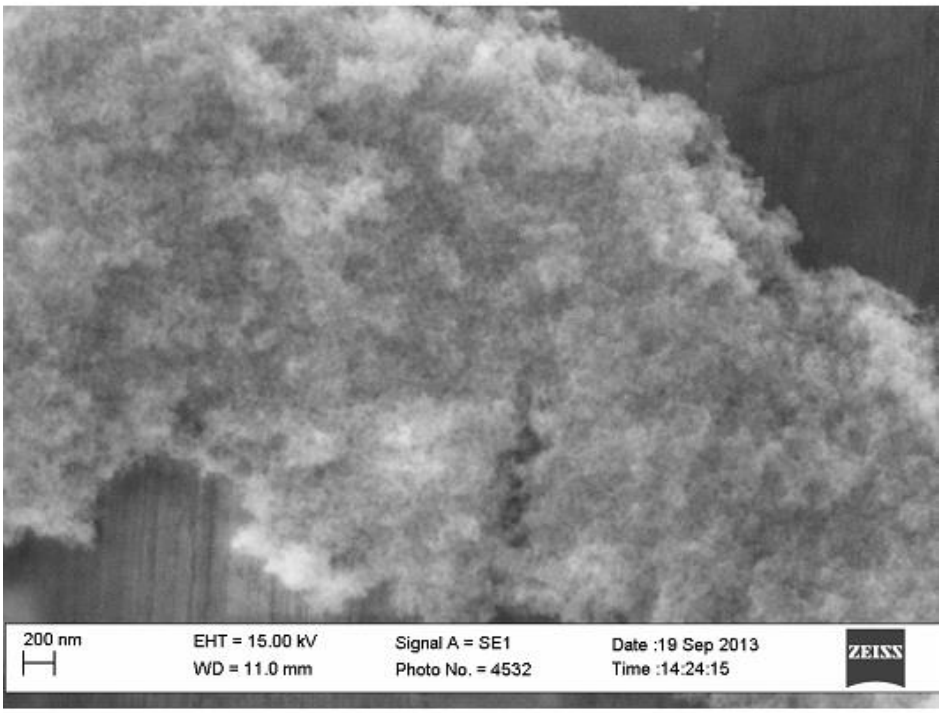

SEM image of 5.3/1 calcined at 500°C.

Figure 3-33. SEM images of the 5.3/1 composition calcined at different temperatures.

relatively bigger particles due to the effect of temperature on the size of crystals.

4. CONCLUSION

With this research work, we brought new expansions to the formation and application of lyotropic liquid crystalline materials. Since the discovery of lyotropic liquid crystalline materials, water, transition metal salt, supercritical CO_2, oil and some other organic liquids were the only solvents used in assembling surfactant molecules. Recently, it was discovered that some salts of main group elements with low DRH values can also be used as solvent in the salt-surfactant system. This is based on their hygroscopic nature, which enables salts to absorb moisture from the atmosphere and effectively assemble surfactant molecules.

Although the importance of deliquescence in the formation of lyotropic liquid crystals was earlier known, the concept of acid or deliquescent liquids as solvents in assembling surfactant molecules have never been reported, even though many acids have low DRH values. Therefore, we take pride for being the first to thoroughly investigate the possibility of using acid as a solvent in self-assembling surfactant. The mesophases of the acid were found to exhibit high thermal stability, proton conductivity, and also useful in the synthesis of mesoporous materials. The isotropization temperatures (melting point) of our gels (more than 120 ^{o}C for some compositions) are so far the highest in the solvent-surfactant system. The acid-surfactant mesophases were studied and found to be stable within a wide range of acid to surfactant concentration (from 2/1 to 20/1 mole ratio). This concentration is again the highest composition in this system. Different phases such as 2D & 3D hexagonal phases, cubic etc. were observed by varying the concentration. The phases were also found to be stable as gel for more than months. Most importantly, it was realized that the confined acid species have high intrinsic proton conductivity values of up to 20 mS/cm, depending on the concentration of the acid. The reason for this high conductivity was understood to be due to confinement effect. This high conductivities make such materials attractive candidates as gel electrolytes in electrochemical applications. Additionally, we monitored

the conductivity of the mesophases within a broad range of temperature (-70 ^{o}C to 150 ^{o}C) and the conductivity results obtained at low temperatures were still reasonable.

In addition to the high proton conductivity and stability of the mesophases, the confined acid species can also be reacted with other precursors such as calcium nitrate tetrahydrate to form mesoporous HAp thin films with high surface area. In this aspect of the research, different precursor to surfactant ratios were investigated ranging from 5.3/1 to 13.3/1. The largest surface area, 96 m^2/g, was obtained in the least concentrated samples, while the smallest surface area, 77 m^2/g was observed in the highest concentrated sample, 13.3/1 mole ratio. The HAp films were absolutely transparent, making them quite applicable in cell proliferation/growth. However, the transparency of the films was largely affected by the calcination temperature and concentration. For example, high salt to surfactant ratio was observed to result in the formation of thicker films with thicker pore walls, faster crystal growth, and hence cloudy films, while extremely low concentrations lead to the formation of very transparent films with thinner pore walls. In this method of synthesizing HAp, no precipitator (basic compound) is required in the synthetic procedure, thus making the method absolutely neat. All the techniques employed in this investigation; ED, XRD, SEM, TEM, N_2-sorption, and FT-IR, collectively show that the films are mesoporous and the pore-walls are made up of pure and crystalline calcium hydroxyapatite.

Since phosphate-containing compounds are important in almost all aspects of life, living or non-living things, we believe that, this new development can be very useful to not only proton conductive membranes and synthesis of hydroxyapatite, but also in the synthesis of materials for application in lithium ion batteries (mesoporous metal phosphates) and many more.

REFERENCES:

[1] I. Tadwee, S. Shahi, V. Ramteke, and I. Syed, "Liquid Crystals pharmaceutical application: A Review," *Int. J. of Pharm. Res. & All. Sci,* vol. 1, no. 2, pp. 06-11, 2012.

[2] A. Bubnov, M. Kaspar, V. Haplova, U. Dawin, and F. Giesselmann, "Thermotropic and Lyotropic behaviour of new liquid-crystalline materials with different hydrophilic groups: Synthesis and Mesomorphic properties," *Beilstein J. Org. Chem,* no. 9, pp. 425-436, 2013.

[3] P. Collins, "In Liquid crystals: nature's delicate state of mater," Princeton University Press, NJ, 1990.

[4] S. Reekmans, D. Bernik, M. Gehlen, J. V. Stam, M. V. D. Auweraer and F. C. D. Schryver, "Change in the Micellar Aggregation Number or in the Size Distribution: A Dynamic Fluorescence Quenching Study of Aqueous Cetyltrimet hylammonium Chloride," *Langmuir,* no. 9, pp. 2289-2296, 1993.

[5] J. M. Seddon, and R. H. Templer, "Polymorphism of Lipid-Water Systems," in *Handbook of Biological Physics*, Elsevier Science B.V., 1995, pp. 97-160.

[6] D. L. Gin, W. Gu, B. A. Pindzola, and W. J. Zhou, "Polymerized Lyotropic Liquid crystal assemblies for materials applications," *Acc. Chem. Res.,*vol. 34 no. 12, pp. 973-980, 2001.

[7] R. Dong and J. Hao "Complex fluids of poly (oxythylene) monoalkyls ether nonionic surfactants.," *Chem. Rev.,* vol. 110, pp. 4978-5022, 2010.

[8] J. Liu, B. Han, G. Li, Z. Liu, J. He, and G. Yang "Solubility of the non-ionic surfacactant tetraethylene glycol n-laurel in supercritical CO2 with n-pentanol," *Fluid Phase Equilibria*, vol. 187, pp. 247- 254, 2001.

[9] C. Seguin, J. Eastoe, R. Clapperton, R. K. Heenan, and I. Grillo, "Alternative non-aqueous water- miscible solvents for surfactant.," *Colloids and Surfaces A: Physicochem. Eng. Aspects*, vol. 282, pp. 134-142, 2006.

[10] M. U. Araos and G. G. Warr "Self-Assembly of Nonionic Surfactants into Lyotropic Liquid Crystals in Ethylammonium Nitrate, a Room-Temperature Ionic Liquid," *J. Phys. Chem. B,* vol. 109, no. 30 , pp. 14275-14277, 2005.

[11] Ö. Çelik, and Ö. Dag, "A new lyotropic liquid crystalline system: Oligo (ethylene oxide) surfactants with (M(H2O)n)Xm transition metal complexes," *Angew. Chemie. Ed.*, vol. 40, no. 20, pp. 3800-3803, 2001.

[12] C. Karakaya, Y. Turker, C. Albayrak, and Ö. Dağ, "Assembly of Molten Transition Metal Salt-Surfactant in a Confined Space for the Synthesis of Mesoporous Metal Oxide-Rich Metal Oxide-Silica Thin Films," *Chem. Mater.* vol. 23, no. 12, pp. 3062-3100, 2011.

[13] K. Holmberg, B. Jönsson, and B. Lindman, Surfactants and ploymers in aqueous solutions, John Wiley & sons, 2003.

[14] M. J. Hollamby, K. Trickett, A. Mohamed, and J. Eastoe, "Surfactant aggregation in CO_2/Heptane solvent mixture," *Langmuir*, vol. 25, no. 22, pp. 12909- 12913, 2009.

[15] Y. Nibu and T. Inoue, "Phase behavior of aqueous mixtures of some polyethylene glycol decyl ethers revealed by DSC and FT-IR measurements," *J. Colloid and Interface sci.*, vol. 205, no.2, pp. 305-315, 1998.

[16] D. J. Mitchell, G. J. T. Tiddy, L. Waring, T. Bostock, and M. P. McDonal, "Phase transition of polyoxyethylene surfactants with water. Mesophase, structure and partial miscibility (cloud point)," *J. Chem. Soc. Faraday Trans.1*, no. 79, pp. 975-1000, 1983.

[17] G. Cevc, "Isothermal lipid phase transitions," *Chem. Phys. Lipids.*, vol. 57, no.2-3, p. 293–307, *1991*

[18] T. Inoue, T. Takasago, and T. Ushifusa, "Effect of hydrphilic additives on mesophase regions of Aqueous nonionic surfactant mixture," vol. 43, no. 1, pp. 39-50, 2012.

[19] L. Q. Zheng, H. Minamikawa, K. Harada, T. Inoune, and G. G. Cernik, "Effect of inorganic salts on the phase behaviour of an aqueous mixture of heptaethylene glycol dodecyl ether," *Langmuir*, vol. 19, no. 25, pp. 10487-10494, 2005.

[20] T. Inoue, Y. Yokoyama, and L. Q. Zheng, "Hofmeister anion effect on aqueous phase behavior of heptaethylene," *Journal of Colloid and Interface Science*, vol. 274, no. 1, p. 349–353, 2004 .

[21] L. M. Wang, F. He and, R. Richert, "Intramicellar glass transition and liquid dynamics in soft confinement," *Phys. Rev. Lett*, vol. 92, no. 9, pp. 095701, 2004.

[22] A. F. Demirörs, Bekir E. Eser and Ömer Dağ, "Liquid crystalline mesophases of pluronics (L64, P65, and P123) and Transition Metal Nitrate salts ($M(H_2O)_6(NO_3)_2$)," *Langmuir*, vol. 21, no. 9, pp. 4256-4162, 2005.

[23] G. S Attard, J. C. Glyde, and C. G. Göltner, "Liquid-crystalline phases as templates for the synthesis of mesporous silica," *Nature*, vol. 378, pp. 366-368, 1995.

[24] Ö. Dag, S. Alayoğlu, and İ. Uysal, "Effects of ions on the Liquid Crystalline Mesophases of transition-Metal salt: Surfactant (C_nEO_m)," *J. Phys. Chem. B*, vol. 108, pp. 8439-8446, 2004.

[25] C. Albayrak, N. Özkan, and Ö. Dag, "Lyotropic Liquid Crystalline Mesophases of $[Zn(H_2O)_6](NO_3)_2$-$C_{12}EO_{10}$-CTAB-H_2O and $[Zn(H_2O)_6](NO_3)_2$-$C_{12}EO_{10}$-SDS-H_2O Systems" *Langmuir*, vol. 24, no. 19, p. 10592, 2008.

[26] C. Albayrak, N. Özkan, and Ö. Dag, "Origin of Lyotropic Liquid crystalline Mesophase Formation and Liquid Crystalline to Mesostructured solid transformation in the Metal Nitrate salt-Surfactant Systems," *Langmuir*, vol. 27, no. 3, pp. 870-873, 2010.

[27] C. Albayrak, G. Barım, and Ömer Dag, "Effect of Hygroscopicity of the Metal Salt on the Formation and Air Stability of Lyotropic Liquid Crystalline Mesophases in Hydrated Salt-Surfactant Systems," *Unpblished work*

[28] K. Kishimoto, M. Yoshio, T. Mukai, M. Yoshizawa, H. Ohno, and T. Kato, "Nanostructured Anisotropic Ion-Conductive Films," *J. Am. Chem. Soc.* , vol. 125, no. 11, pp. 3196-3197, 2003 .

[29] M. Yoshio, T. Mukai, H. Ohno, and T. Kato, "One-Dimensional Ion Transport in Self-Organized Columnar Ionic Liquids," *J. Am. Chem. Soc.* , vol. 126, no. 4, pp. 994-995, 2004.

[30] T. Ikeda, T. Sasaki, and K. Ichimura, “Photochemical switching of polarization in photoelectric Liquid crystal films,” *Nature*, vol. 361, pp. 428-430, 1993.

[31] D. Umeyama, S. Horike, M. Inukai, Y. Hijikata, and S. Kitagawa, “Confinement of mobile histamine in coordination nanochannels for fast proton transfer,” *Angew. Chem. Int. Ed.* , vol. 50, no. 49, p. 11706 –11709, 2011.

[32] H. Tang, J. Li, Z. Wang, H. Zhang, M. Pan and S. P. Jiang, “Self-Assemble of nanostructed proton exchange membranes for fuel cells,” Washington DC, American Chemical Society, 2013, pp. 243-263.

[33] R. Negrini and R. Mezzenga, “pH-Responsive lyotropic Liquid Crystals for Controlled Drug Delivery,” *Langmuir*, vol. 27, no. 9, pp. 5296-5303, 2011.

[34] C. Albayrak, A. Cihaner, and Ö. Dag, “A new, highly conductive. lithium salt/ nanionic surfactant, lyotropic Liquid-crystalline Mesophase and its application,” *Chem.Eur. J*, vol. 18, no. 14, pp. 4190-4194, 2012.

[35] O. Ikkala, and G. T. Brinke, "Hierarchical self-assembly in polymeric complexes: Towards functional materials" *Chem. Commun*, pp. 2131-2137, 2004.

[36] P. L. Kerr, S. A. Miller, R. K. Shoemaker, B. J Elliott, and D.L. Gin, "New type of Li ion conductor with 3D Interconnected nanochannels via polymerization of a liquid organic electrolyte-filled lyotropic liquid-crystal assembly", *J. Am. Chem. Soc*, vol. 131 no. 44, pp. 1592-1593, 2009.

[37] C. Albayrak, N. Özkan, Ö. Dag, Origin of lyotropic liquid crystalline mesophase formation and liquid crystalline to mesostructured solid transformation in the

metal nitrate salt-surfactant systems" *Langmuir,* vol. 27, no. 3, pp. 870-873, 2011.

[38] L. Carrette, K. A Friedrih, and U. Stimming, “Fuel Cells- Fundamentals and applications,” *fuel cells*, vol. 1, no. 1, pp. 5-39, 2001.

[39] C. C. Araujo, K. D kreuer, M. Schuster, G. Portale, H. Mendil-jekani, G. Gebel, and M. Maier, "poly (p-phenylene sulfone)s with high ion exchange capacity: ionomers with unique microstructural and transport features", *J. Phys. Chem.* , vol. 11, no. 17, pp. 3305-3312, 2009.

[40] C. Ke, J. Li, X. Li, Z. Shao, and B. Yi, "Protic ionic liquids: an alternative proton-conducting electrolyes for high temperature proton exchange membrane fuel cells", *RSC Adv*, no. 2, p. 8953-8956, 2012.

[41] S. Ueda, J. Kagimoto, T. Ichikawa, T, Kato, and H. Ohno, " Anisotropic proton-conductive materials formed by the self-organization of phosphonium-type zwitterions", *Adv. mater,* vol. 23, no. 27, pp. 3071-3074, 2011.

[42] T. Ichikawa, T. Kato, and H. Ohno, " 3D continuous water nanosheet as a gyroid minimal surface formed by bicontinuous cubic liquid-crystalline zwitterions" *J. Am. Chem. soc,* no. 134, pp. 11354-11357, 2012.

[43] S. Horike, D. Umeyama, and S Kitagawa, " Ion conductivity and transport by porous coordination polymers and metal-organic frameworks" *Acc. Chem. Res.* vol. 46, no. 11, pp. 2374-2384, 2013.

[44] K. A. Mauritz, and R. B. Moore, " State of understanding of Nafion", *Chem. Rev*, no. 104, pp. 4535-4585, 2004.

[45] S. S. Nagarkar, S. M. Unni, A. Shrama, S. Kurungot, and S. K. Ghosh, "Two-in-One: inherent Anhydrous and water-assisted high proton conduction in a 3D Metal-Organic Framewok," *Angewandte,* vol. 126, no. 10, pp. 1-6, 2013.

[46] B. Soberats, M. Yoshio, T. Ichikawa, S. Taguchi, H. Ohno, and T. Kato, "3D Anhydrous Proton- Transporting Nanochannels Formed by Self- Assembly of LC composed of a sulfobetaine and a sulfonic Acid," *J. Am. Chem. Soc,* vol. 135, no. 41, pp. 15286-15289, 2013.

[47] Q. Tang, G. Qian, and K. Huang, "Hydrophobic hydrogel caged H_3PO_4 as a new class of high-tempearture proton exchange membranes with enhanced acid retention," *RSC. Adv.,* no. 3, pp. 3520-3525, 2013.

[48] J. Zeng, B. He, K. Lamb, R. D. Marco, P. K. Shen and S. P. Jihang, "Phophoric acid functionalized pre-sintered meso-silica for high temperature proton exchange membrane fuel cells," *Chem. Commun,* no. 49, pp. 4655-4657, 2013.

[49] L. Xiao, H. Zhang, E. Scanlon, L.S. Ramanathan, E. W. Chow, D. Rogers, T. Apple, and B. C. Benicewicz, "High-Temperature Polybenzimidazole Fuek Cell Membranes via a Sol-Gel Process," *Chem. Mater,* vol. 17, no. 21, pp. 5328-5333, 2005.

[50] K. A. Perry,, K. L. More, E. A. Payzant, R. A. Meisner, B. G. Sumpter, and B. C. Benicewicz., "A comparative study of phophoric Acid-Doped m-PBI membranes," *Polymer Physics,* vol. 52, no. 1, pp. 26-35, 2014.

[51] J. A Asensio, E.M Sanchez, and P. Gomez-Romero, "Proton-conducting membranes based on benzimidazole polymers for high-temperature PEM fuel cells. A chemical quest" *Chem. Soc. Rev,* vol. 39, no. 8, p. 3210, 2010.

[52] N. Agmon, "The Grotthuss Mechanism," *Chem. Phys. Lett,* Vol. 244, no. 5-6, pp. 456-462, 1995.

[53] R. A. Rodinson, and R. H. Sokes, Electrolyte soltuins, 2nd Ed, London: Butterworths, 1959.

[54] M. Tuckerman, K. Leasonen, M. Sprik, and M. Parrinello, "Ab *initio* Molecular dynamic simulation of the solvation and transport of H_3O+ and OH^- ions in water," *J. Phys. Chem,* vol. 99, pp. 5749-5752, 1995.

[55] D. Marx, M. E. Tuckerman, and M. Parinello, "The nature of the hydrated excess proton in water," *Nature,* no. 397, pp. 601-604, 1999.

[56] R. H. Fowler, and J. D. Bernal, A theory of water and ionic solution, with particular reference to hydrogen and hydroxyl ions, *J. Chem. Phys*, vol. 1, no. 8, p. 515, 1933.

[57] B. E. Conway, Modern aspect of Electrochemistry, vol 3, London: Butterworths, 1964.

[58] X. Liang, F. Zhang, W. Feng, X. Zou, C. Zhao, H. Na, C. Liu, F. Sun and G. Zhu, "From metal–organic framework (MOF) to MOF–polymer composite membrane: enhancement of low-humidity proton conductivity," *Chem. Sci.,* no. 4, pp. 983-992, 2013.

[59] K. D. Kreuer, A. Rabenau, and W. Weppner, "Vehicle Mechanism, A New Model for the Interpretation of the Conductivity of Fast Proton Conductor," *Angew. Chem. Int. Ed. Engl*, vol. 21, no. 3, pp. 208-209, 1982 .

[60] T. Ueki and M. Watanabe, “Macromolecules in Ionic Liquids: Progress, Challenges, and Opportunities,” *Macromolecules*, vol. 41, no. 11, pp. 3739-3749, 2008.

[61] L. Vilciauskas, M. E. Tuckerman, G. Bester, S. J. Paddison and K. D. Kreuer, “The mechanism of proton conduction in phosphoric acid,” *NCHEM*, vol. 4, pp. 461-466, 2012.

[62] Y. Aihara, A. Sonai, M. Hattoti, and K. Hayamizu, “Ion cnductivity mechanism and thermal propertis of hydrated and anhydrous phosphoric acid studied with 1H,2H, and 31P NMR,” *J. Phys. Chem. B*, vol. 110, no. 49, pp. 24999-25006, 2006.

[63] R. K. Brundavanam, G. Eddy, J. Poinern, and D. Fawcett, “modelling the crystal structure of a 30 nm sized particle based hydroxyapatite powder synthesized under the influenced ofultrasound irradiation from X-ray powder diffraction data.,” *Am. J. Mater. Science*, no. 3, pp. 84-90, 2013.

[64] M. Bilton, A. P. Brown and S. J. Milne, “sol-gel synthesis and characterization of nano-scale hydroxyapatite,” *J. Phys. Conf. Ser.* vol. 241, no. 1, 012052, 2010.

[65] J. C. ELliott, "Stucture and Chemistry of the apatites and other calcium orthophosphate", Amsterdam: Elsevier, 1994.

[66] N. Szabo, "The structure of Apatite (CaF) $Ca_4(PO_4)_3$", *Zeits.Krisht*, vol. 75, pp. 387-398, 1930.

[67] M. Mehmel, "Über die Strucktur des Apatits I", *Zeit Krist*, vol. 75, pp. 323-331, 1930.

[68] T. A. Taton, “Attempts to tailor nanometer-scale objects to mimic and interact wirth natural materials raise the question of how to predict the biological response to these tiny creations,” *Nature,* vol. 412, pp. 491-492, 2001.

[69] X. Lu, H. Zhang, Y. Guo, Y. Wang, X. Ge, Y. Leng and F. Watari, “Hexagoanl hydroxyapatite formation on TiO_2 nanotubes under urea modulation,” *Cryst.Eng.Comm.*, no. 13, pp. 3741-3749, 2011.

[70] H. Wang, L. Zhai, Y. Li, and T. Shi, " Preparation of irregular mesoporous hydroxyapatite" *Mater Res Bull,* vol. 43, no. 6, p. 1607, 2008.

[71] T. Matsumoto, M. okazaki, A Nakahira, J. Sasaki. H. Egusa and T. Sohmura. Matsumoto, *Curr. Med. Chem,* no. 14, pp. 2726-2733, 2007.

[72] Y.T Huang, M. Imura, Y. Nemoto, C.H Cheng and Y. Yamauchi, "Block-copolymer synthesis of hydroxyapatite nanoparticle with high surface area and uniform size", *Sci. Technol. Adv. Mater,* no. 12, pp. 045005-045010, 2011.

[73] T. Matsumoto, M . Okazaki, M. Inoue, S. Yamaguchi, T. Kusunose, T. Toyonaga, Y. Hamada, and J. Takahashi “Hydroxyapatite particles as a controlled release carrier of protein,” *Biomaterials,* vol. 25, no. 17, p. 3807–3812, 2004.

[74] P. A. Williamson, P. J. Blower and Mark A. Green, “Synthesis of porous hollow silica nanostructures using hydroxyapatite nanoparticle templates,” *Chem. commun.*, no. 47, pp. 1568-1570, 2011.

[75] M. A. Rauschmann, T. A Wichelhaus, V. Stirnal, E. Dingeldein, L. Zichner, R. Schnettler, V. Alt, “Nanocrystalline hydroxyapatite and calcium sulphate as

biodegradable composite carrier material for local delivery of antibiotics in bone infections.," *Biomaterials*, vol. 26, no. 15, p. 2677, 2005.

[76] A. Barroug and M. J. Glimcher, "Hydroxyapatite crystals as a local delivery system for cisplatin: adsorption and release of cisplatin in vitro" *J. Orthop. Res.*, vol. 20, no. 20, p. 274, 2002.

[77] E. M. Rivera-Munoz,, "Hydroxyapatite-based materials: synthesis and characterization," in *Biomedical Engineering- Fronterier and Challenges*, Mexico, pp. 75-98.

[78] X. Ye, G. Xu, S. Cai, and Y. Dou, "Presentation, Surface properties, and MC3T3-E1 cell response of mesoporous hydrozyapatite thin films," *J Mater Sci*, no. 47, pp. 3763-3769, 2012.

[79] S. M. Best, A. E. Porter, E. S. Thian, and J. Huang, "Bioceramics: past, present and for the future," *Journal of the European Ceramic Society,* vol. *28,* no. 7, pp. 1319-1327, 2008.

[80] D. M. Liu, T. Troczynski, and W. J. Tseng "Water-based sol-gel syntehsis of hydroxyapatite: process development," *Biomaterials*, vol. 22, no. 13, pp. 1721-1730, 2001.

[81] T. M. Ishikawa, and S. Kinko, *Fundamental of absorption,* p. 321, 1991.

[82] Q. Huo, D. I. Margolese, U. Ciesla, D. G. Demuth, P. Y. Feng, T. E. Gier, P. Sieger, A. Firouzi, B. F. Chmelka, F. Schuth, and G. D. Stucky, " Organization of Organic Molecules with Inorganic Molecular Species into Nanocomposite Biphase Arrays" *Chem Mater,* vol. 6, no. 6, p. 1176, 1994.

[83] S. Bose and S. K. Saha, “synthesis and characterizayion of hydroxyapatite nanopowders by emulsion technique,” *Chem. Mater.*, vol. 15, no. 23, pp. 4464-4469, 2003.

[84] M. Uota, H. Arakawa, N. Kitamure, T. Yoshiramura, T. Tanaka, and T. Kijia, “Synthesis of high surface area hydroxyapatite nanoparticles by mixed surfactant-mediated aproach,” *Langmuir,* no. 21, pp. 4724-4728, 2005.

[85] K. Lin, and Y. Zhou, “Biomimetic hydroxyapatite porous microsheres with co-subsmitted trace elements: surfactant-free hydrothermal sythesis, enhanced degradation and drug release,” *Journal of Materials Chemistry,* vol. 21, no. 41, pp. 16558-16565, 2011.

[86] T. Liang, J. Qian, Y. Yuan, and C. Liu, “Synthesis of Mesoporous hydroxyapatite nanoparticles using a template-free sonchemistry-assisted microwave method,” *J Mater Sci,* vol. 48, no. 15, pp. 5334-4341, 2013 .

[87] C. T. Kresge, M. E. Leonowicz, W. J. Roth, J. C. Vartuli and J. S. Beck, "Ordered mesoporous molecular sieves synthesized mechanism", *Nature,* vol. 359, p. 710, 1992.

[88] M. Uota, H. Arakawa, N. Kitamure, T. Yoshiramura, T. Tanaka, and T. Kijia, “ Synthesis of high surface area hydroxyapatite nanoparticles by mixed surfactant-mediated approached.,” *Langmuir* , vol. 21, no. 10 , pp. 4724-4728, 2005.

[89] M. J. Olszta, X. Cheng, S.S Jee. R. Kumar, Y. Y Kim, M. J. Kaufman, E. P. Douglas and L. B. Gower, *mater.Sci. Eng., R,* no. 58, p. 77, 2007.

[90] W. Chen, T. Long, Y. Y. Guo, Z. A. Zhu and Y. P. Guo, “Magnetic hydroxyapatite coatings with oriented nanorod arrays: hydrothermal synthesis,

struture and biocompartibility," *J. Mater. Chem,* vol. 2, no. 12, pp. 1653-1660, 2014.

[91] Y. Wang, N. A. Lan, C. N Sun, F. Fan, T. A. Zawodzinski and A. P. Sokolov, "Ionic conductivity and glass transition of phosphoric acids," *J. Phys. Chem B,* vol. 117, no. 26, pp. 8003-8009, 2013.

[92] W. W. Rudolph, "Raman- and infrared spectroscopic investigation of dilute aqueous phosphoric acid solutions," *Dalton Trans,* no. 20, pp. 9642-9653, 2010.

[93] J. D. Chen, Y. J. Wang, K. Wei, S. H. Zhang , X. T. Shi, "Self-organization of hydroxyapatite nanorods through oriented attachment" *biomaterials,* vol. 28, no. 14, pp. 2275-2280, 2007.

[94] J. Yao, W. Tjandra, Y. Z. Chen, K. C. Tam, J. Ma and B. Soh, "Hydroxyapatite nanostructure materials derived using cationic surfactant as a template", *J. Meter.Chem..*, no. 13, p. 3053-3057, 2003.

[95] C. Albayrak, G. Barım, and Ö. Dag, "Effect of hygroscopıcıty of salts on the formation of lyotropic liquid crystalline mesophases," *Langmuir,* 2014 (unpublished work).

[96] X. Qian, N. Gu. Z. Cheng, X. Yang. E. Wang, S. Dong, "Methods to study the ionic conductivity of polymeric electrolytes using a.c impedance spectroscopy," *J Solid Sate Electrochem,* vol. 6, no. 1, pp. 8-15, 2001.

[97] C. Zhong, Y. Deng, A. F. Roudsari, A. Kapetanovic. M.P Anantram and M. Rolandi, "A polysaccharide bioprotonic field-effect transistor," *ncomms,* vol. 476, no. 2, pp. 1-5, 2011.

[98] N. Agmon,."The Grotthuss Mechanism." *Chem. Phy. Lett,* Vol. *244*, no. 5-6, pp. 456-462, 1995.

[99] L. Vilciauskas, M. E. Tuckerman, G. Bester, S. J. Paddison and K. D. Kreuer, "The Mechanism of proton conduction in phosphoric acid," *nchem,* vol. 4, pp. 461-466, 2012.

[100] Z. Zuo, Y. Fu and A. Manthiram, "Novel Blend Membranes Based on Acid-Base Interactions for," *Polymers* , no. 4, pp. 1627-1644, 2012.

[101] G. H. Brown, "Liquid Crystal- The Chameleon Chemicals," *Journal of Chemical Education,* vol. 60, no. 10, pp. 900-905, 1983.

[102] D. F. Evans, and H. Wennerström, The colloidal Domain: Where Physics, Chemistry, and Technology meet, New York: VCH Publisher, 1994.

[103] B., Lindman., and H. Wannerstöm, "Amphiphile aggregation in aqueous solution" *Top. Curr. Chem.,* vol. 87, no. 1, 1980.

[104] R. G. Laughlin, "The aqueous phase behavior of surfactants," in *Academic Press*, London, 1994.